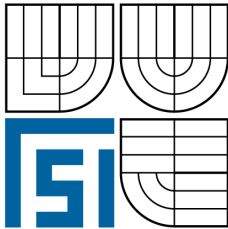


VYSOKÉ UČENÍ TECHNICKÉ V BRNĚ
BRNO UNIVERSITY OF TECHNOLOGY



FAKULTA STROJNÍHO INŽENÝRSTVÍ
ÚSTAV FYZIKÁLNÍHO INŽENÝRSTVÍ
FACULTY OF MECHANICAL ENGINEERING
INSTITUTE OF PHYSICAL ENGINEERING

TOLERANCE A VADY SEŘÍZENÍ PRO ELEKTRONOVĚ OPTICKÉ PRVKY A SYSTÉMY

TOLERANCES AND MISALIGNMENT ABERRATIONS FOR ELECTRON OPTICAL ELEMENTS
AND SYSTEMS

DISERTAČNÍ PRÁCE
DOCTORAL THESIS

AUTOR PRÁCE
AUTHOR

Ing. ONDŘEJ SHÁNĚL

VEDOUCÍ PRÁCE
SUPERVISOR

Ing. JAKUB ZLÁMAL, Ph. D.

Abstrakt

Nepřesnosti při výrobě a sestavení rotačně souměrné čočky a deflektoru a jejich přesného zařazení do elektronově optického systému se projeví jako dodatečné pole příslušné symetrie, které deformuje ideální zobrazení. Tato dodatečná pole dokážeme spočítat pomocí metody konečných prvků v programu EOD. Toleranční analýza spočívá ve stanovení požadavků na rozměry a sestavení jednotlivých prvků a jejich částí. Korekce vad seřízení pak spočívá v určení typu a polohy korekčních vychylovacích cívek a multipólů tak, aby se tyto dodatečné vady odstranily, nebo aby se minimalizoval jejich vliv. Cílem dizertační práce je analýza projevů vad seřízení a chování neseřízených systémů prozařovacích elektronových mikroskopů.

Summary

Inaccuracies in the production and assembling of rotationally symmetric lenses and deflectors and their accurate positioning in the electron optical system can be treated as an additional field with specific type of symmetry. The additional fields can be evaluated with the help of the finite element method in the program EOD. Tolerance analysis allows evaluation of the requirements on the dimensions and position of individual elements and their parts. Elimination of misalignment aberrations consists in determining the type and position of correcting deflection coils and multipoles so that these additional aberrations are removed or their effect is minimized. The aim of the dissertation is the analysis of the effect of misalignment aberrations and behavior of misaligned systems of transmission electron microscopes.

Klíčová slova

TEM, astigmatismus, korekce vad, mechanické tolerance

Keywords

TEM, astigmatism, aberrations correction, mechanical tolerances

SHÁNĚL, O. *Tolerance a vady seřízení pro elektronově optické prvky a systémy*. Brno: Vysoké učení technické v Brně, Fakulta strojního inženýrství, 2014. 87 s. Vedoucí doktorské práce Ing. Jakub Zlámal, Ph. D.

Prohlášení

Prohlašuji, že jsem toto pojednání ke státní doktorské zkoušce vypracoval samostatně, pouze pod odborným vedením Ing. Jakuba Zlámala, Ph. D. a s použitím uvedené literatury.

V Brně 31. prosince 2013

Acknowledgments

I would like to thank Ing. Jakub Zlámal, Ph. D. for supervising of my project and the support.

I would like to thank my wife Marcela for her support during my studies at Brno University of Technology.

The great word of thanks belongs to Mgr. Milada Húsková , my teacher of mathematics at the grammar school, for opening my mind towards mathematics and physics.

Contents

1	Introduction	3
1.1	Objective of doctoral work	3
2	Theory of Transmission Electron Microscopy	5
2.1	Introduction	5
2.2	Electron in the static electric or magnetic field	5
2.3	Parasitic aberrations	7
2.4	TEM construction	9
2.4.1	Lens design	10
2.4.2	Deflection coil design	11
2.4.3	Stigmator design	12
2.5	Geometrical tolerances	13
2.6	Simulation of mechanical imperfections	14
2.7	EOD plugin Tolerancing	17
3	Spot optimization	21
3.1	Evaluation of aberration coefficients	21
3.2	Evaluation of current density profile	22
3.2.1	Calculation of diffraction integral	22
3.3	Optimization method	22
3.3.1	Minimization of the spot size	23
3.3.2	Minimization of the coma	23
3.3.3	Optimization of the wavefront error	23
4	Study of condenser astigmatism	27
4.1	Analysis of the upper objective pole piece	27
4.2	Calculation	28
4.3	Influence of individual regions	31
4.3.1	Calculation of Region A	32
4.3.2	Calculation of Region B	32
4.3.3	Calculation of Region C	33
4.3.4	Calculation of Region D	34
4.4	Combinations of imperfections in different regions	35
4.4.1	Mechanical vs. optical mutual region rotation	36
4.4.2	Combined influence of Region A and D	36
4.4.3	Combined influence of Region A and C	37
4.4.4	Combined influence of Regions A, C and D	40
4.5	Measurements on prototype pole pieces	40

4.5.1	Optical measurement	40
4.5.2	Mechanical tolerance measurement	40
4.6	Comparison of calculated and measured values	42
4.7	Influence of other mechanical imperfections	43
5	Conclusion	47
5.1	Publication	48
6	Appendix I	51
6.1	Simulation results	51
7	Appendix II	87
7.1	Measured data	87

List of abbreviations

AT	Ampere turn
$C_{1,2}$	2-fold astigmatism coefficient
EOD	Electron optical design software
ETEM	Environmental transmission electron microscopy
HR-STEM	High resolution scanning transmission electron microscopy
HR-TEM	High resolution transmission electron microscopy
SEM	Scanning electron microscopy
STEM	Scanning transmission electron microscopy
TEM	Transmission electron microscopy

Chapter 1

Introduction

Transmission electron microscopes are universal systems providing both main techniques of nowadays - HR - TEM and HR - STEM.

Nowadays electron microscopes are close to the edge of limits given by charged particle optics theory. Any imperfection in the manufacturing has critical influence on the system performance, especially in high resolution techniques as HR - TEM and HR - STEM.

Increasing number of HR - STEM applications is the driving motivation to investigate the design of all components that can lead to a better performance. HR - STEM requirements are ultimate (small spot with high current density, minimal spot and specimen drift, coils power supplies and accelerating voltage stabilities, . . .) and only deep knowledge help us to make systems on even a higher level pushing the envelope regarding to the resolution and system stability.

1.1. Objective of doctoral work

This study discusses an influence of mechanical imperfections of various regions of pole pieces that can cause a condenser astigmatism of 200 keV TEM objective lens. Condenser astigmatism is a well known term used to describe astigmatism of optical column part which have an influence on the beam spot shape. The objective upper pole piece has the biggest influence on the condenser astigmatism within TEM systems based on the practical experience. Mechanical imperfections were studied introducing tilt, misalignment and ellipticity in different pole piece regions.

The results are mainly valid for the system with non-corrected spherical aberration where 2 - fold astigmatism is the dominant effect limiting the resolution. 2 - fold astigmatism (in this case an axial astigmatism arising from mechanical imperfections rather than an astigmatism caused by off axis object position) is mostly dependent on ellipticity of the lens pole pieces and on their material homogeneity.

The methodology to design a pole piece within the required optical performance with respect to the pole piece's mechanical accuracy is developed.

Higher order aberrations (3 - fold astigmatism, 4 - fold astigmatism and star aberration) are not studied in this work because of their negligible influence on image quality compared with 2 - fold astigmatism.

The theory of TEM microscope is discussed in the chapter 2 together with mechanical desing, including general system overview and detailed description of key elements such as magnetic lenses, deflection coils, stigmators and their expression in the trajectory

1.1. OBJECTIVE OF DOCTORAL WORK

equation. Attention is focused to parasitic aberrations and simulation of mechanical imperfections. Geometrical tolerances used for mechanical description of pole pieces are explained in this chapter as well.

Chapter 3 discusses the used simulation methods. Calculations of the objective lens field and particle trajectories were done in EOD 4.001 software [1]. Calculated trajectories were evaluated in Matlab to obtain the aberration coefficients. The final spot shape including diffraction addition was then calculated to check the spot size.

Methodology of the 2-fold astigmatism study with measured results on prototype pole pieces are discussed in chapter 4. The pole piece is analyzed to determine the regions of the interest. Mechanical imperfections in the individual regions are studied separately to find out their particular influence. Combined influence of mechanical imperfection in different regions are studied later on. Comparison of optical and mechanical measured data with calculation outputs are done to verify the method.

Chapter 2

Theory of Transmission Electron Microscopy

2.1. Introduction

Transmission electron microscope (TEM) is a device using a focused beam of electrons to investigate a specimen at micro- and nanometric scale. In 1924 de Broglie formulated his hypothesis that any particle has wave-like character. It was experimentally proved for electrons by Davisson and Germer in 1927 [2]. These properties enable to reach better resolution than any standard light microscope. Magnetic or electrostatic field can be used to act on electrons as lenses [5]. Ernst Ruska and Max Knoll designed and assembled the first prototype of an electron microscope in 1931. Two years later in 1933 the first image acquired with TEM was presented by Max Knoll. The first commercial transmission electron microscope was produced by Siemens in 1936 [3].

The work in this area was stopped in 40's of 20th century. After that main research and development took place in the Netherlands, Czechoslovakia, Germany, Great Britain and Japan. In 60s' and 70s' of the 20th century many pioneer works were done on the theory of charged particle optics, interaction of electron beam with the specimen, detectors, etc. [3].

Modern TEM is used for an investigation in many various fields such as material science, semiconductor industry, surface science, food industry, mineralogy, biology, medicine, etc.

Today's TEM can achieve resolution up to 50 pm [4]. A special type of TEM can work in low vacuum which is used for real-time investigation of growing nano-structures, for example carbon nanotubes. The residual atmosphere can avoid a charging and a dewatering of a specimen as well.

2.2. Electron in the static electric or magnetic field

Electron in the electric or magnetic field is affected by the Lorentz force

$$\vec{F}_{\text{Lor}} = -e(\vec{E} + \vec{v} \times \vec{B}), \quad (2.1)$$

where e is the elementary charge, \vec{v} is the speed of the electron, \vec{E} is the electric field, \vec{B} is the magnetic flux density.

2.2. ELECTRON IN THE STATIC ELECTRIC OR MAGNETIC FIELD

The equation of motion can be expressed as [12]

$$\frac{d}{dt}(\gamma m_0 \vec{v}) = -e(\vec{E} + \vec{v} \times \vec{B}), \quad (2.2)$$

where m_0 is the rest mass of the electron and γ is defined as

$$\gamma = \frac{1}{\sqrt{1 - \frac{v^2}{c^2}}}, \quad (2.3)$$

where c is the speed of the light in vacuum.

It is necessary to use the relativistic modification of the Newton's equation of motion due to the small mass of the electron and the high energies used in TEM in the order of 60 - 300 keV (in special design 5 keV or 2 MeV). The dependence of the electron wavelength and mass on its acceleration voltage is in Tab. 2.1.

U [V]	λ [m]	$\frac{v}{c}$	$\frac{m}{m_0}$
10^0	$1.22 \cdot 10^{-9}$	0.002	1.00000
10^1	$3.87 \cdot 10^{-10}$	0.006	1.00002
$6 \cdot 10^3$	$4.88 \cdot 10^{-12}$	0.446	1.11723
$2 \cdot 10^5$	$2.51 \cdot 10^{-12}$	0.648	1.39078
$3 \cdot 10^5$	$1.97 \cdot 10^{-12}$	0.776	1.58641

Tab. 2.1: Parameters of an electron as a function of its acceleration voltage U (λ is the wavelength, v is the speed, c the speed of the light, m is the mass and $m_0 = 0.511 \text{ MeV}c^{-2}$ is the rest mass of the electron).

Instead of solving the equation of motion, the trajectory equation is computed which is more relevant for static electric and magnetic fields. This equation is derived from equation (2.2) [12, 13] and it is expressed as

$$\frac{d}{dz} \left(w' \sqrt{\frac{U^*}{1 + w' \bar{w}'}} \right) = -\frac{\gamma}{2} \sqrt{\frac{1 + w' \bar{w}'}{U^*}} E_w - i\eta (B_w - w' B_z), \quad (2.4)$$

where U^* is a so-called relativistic corrected potential, which is defined as

$$U^* = U \left(1 + \frac{e}{2mc^2} U \right), \quad (2.5)$$

where U is the accelerating voltage, the w , E_w and B_w are the complex variables defined as

$$w(z) = x(z) + iy(z), \quad (2.6)$$

$$E_w(z) = E_x(z) + iE_y(z), \quad (2.7)$$

$$B_w(z) = B_x(z) + iB_y(z) \quad (2.8)$$

where i is the imaginary unit. The symbol \bar{w} denotes the complex conjugated variable and the symbol w' represents the derivative with respect to z

$$w' = \frac{dw}{dz} \quad (2.9)$$

and η is defined as

$$\eta = \sqrt{\frac{e}{2m}}. \quad (2.10)$$

The primary electron beam is located close to the optical axis of the system. Equation 2.4 can be rewritten into the so-called paraxial equation [13]:

$$w'' + \left(\frac{\gamma U'}{2U^*} - \frac{i\eta}{U^{*\frac{1}{2}}} B \right) w' + \left(\frac{\gamma U''}{4U^*} - \frac{i\eta}{2U^{*\frac{1}{2}}} B' \right) w = 0, \quad (2.11)$$

where $U = U(z)$ is the electrostatic potential, $B = B(z)$ is the magnetic flux density. All fields are axial.

2.3. Parasitic aberrations

Equation 2.11 is derived under the consideration of the perfect system without any non-symmetry and mechanical imperfection. The aberrations of the objective lens have a crucial influence on the final spot size and aberrations contributions of other lenses can be neglected for the most of the calculations with reasonable good results.

If we want to see influence of a system imperfection on the beam trajectory we have to add the aberrations contribution to the equation 2.11 as follows:

$$w'' + \left(\frac{\gamma U'}{2U^*} - \frac{i\eta}{U^{*\frac{1}{2}}} B \right) w' + \left(\frac{\gamma U''}{4U^*} - \frac{i\eta}{2U^{*\frac{1}{2}}} B' \right) w = P(z), \quad (2.12)$$

where $P(z)$ is part which contains parasitic aberrations [9,11,16].

Contribution of $P(z)$ can be calculated with using two approaches - geometrical and wave. We used the wave approach because it enables us to add the diffraction contribution to obtain the final spot shape and size as it is seen in the real microscope.

Term $P(z)$ causes the phase shift of the ideal spherical wave which can be expressed using Krivanek notation [16] as follows:

$$\begin{aligned} \chi(\theta, \phi, r) = \sum_p \sum_q \sum_n \sum_m \frac{r^p \theta^{(n+1)}}{n+1} \{ & C_{n,m,a}^{p,q,a} \cos(q\omega) \cos(m\phi) + \\ & + C_{n,m,a}^{p,q,b} \sin(q\omega) \cos(m\phi) + C_{n,m,b}^{p,q,a} \cos(q\omega) \sin(m\phi) + C_{n,m,b}^{p,q,b} \sin(q\omega) \sin(m\phi) \}, \end{aligned} \quad (2.13)$$

where $r = |w|$ is a distance from optical axis, θ is a complex slope coordinate (see Fig.2.1 and Eq. (2.14)), $n, m, p, q \in \mathbf{Z}_0^+$, $C_{n,m,(a,b)}^{p,q,(a,b)} \in \mathbf{C}$ is an aberration coefficient of the order $n+p$ and multiplicity m which defines the number of maximums of $\chi_{\theta,\phi}$ in the range of ϕ from 0 to 2π , q is the field multiplicity index (value from 0 to p), a and b are used to separate orthogonal contributions to the same aberration in case they are present (see Eq. (2.18)), ω is the azimuthal angle in the field (see Eq. 2.16).

$$\vec{\theta} = \theta e^{i\phi} = \theta_x + i\theta_y = w', \quad (2.14)$$

where ϕ and ω are defined as:

$$\phi = \text{atan}(\theta_y, \theta_x), \quad (2.15)$$

$$\omega = \text{atan}(y, x). \quad (2.16)$$

Eq. 2.13 describes axial and non-axial aberrations. HR-STEM system is investigated in the following parts of this work so the equation (2.13) can be simplified using only axial aberrations. The isoplanatic approximation fits acceptable well for a system with very

2.3. PARASITIC ABERRATIONS

small field of view (typically in order of 10 nm) which the HR-STEM system fulfills in general. Eq. (2.13) then simplifies to:

$$\chi(\theta, \phi) = \text{Re} \left\{ \sum_n \sum_m \frac{C_{n,m}}{n+1} \theta^{(n+1)} e^{-im\phi} \right\}, \quad (2.17)$$

where $C_{n,m} \in \mathbf{C}$ is an axial aberration coefficient.

Aberrations having $m = 0$ are real ($C_{n,0} \in \mathbf{R}$). Aberrations having $m \neq 0$ are complex numbers and they can be expressed as:

$$C_{n,m} = C_{n,m,a} + iC_{n,m,b}, \quad (2.18)$$

where $C_{n,m,a}$ and $C_{n,m,b} \in \mathbf{R}$.

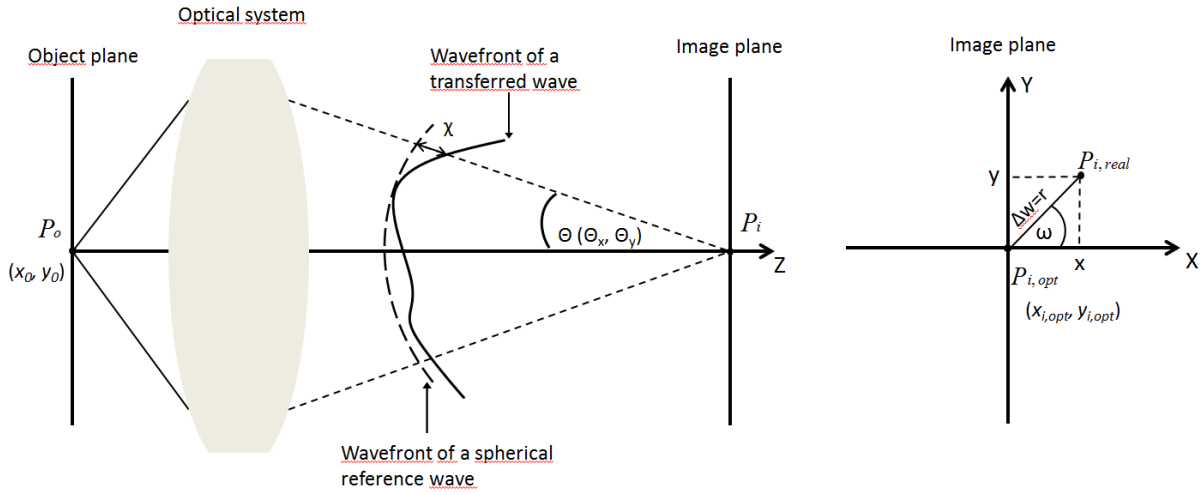


Fig. 2.1: Definition of the wave phase shift χ and image shift Δw caused by parasitic aberrations - P_o is a point in the object, $P_{i,opt}$ is its image without any aberrations in the image plane, $P_{i,real}$ is its image with aberrations in the image plane.

The wavefront phase shift is translated to the shift in the real space Δw as follows [17]:

$$\Delta w = \left(-\frac{\partial \chi_\theta}{\partial \theta_x}, -\frac{\partial \chi_\theta}{\partial \theta_y} \right). \quad (2.19)$$

Using formula (2.19) we can write the final position of particle $w_{i,real}$ in the image plane as:

$$w_{i,real} = w + \Delta w, \quad (2.20)$$

where w is the particle position for the perfect system calculated from Eq. (2.11) and Δw is the additional shift caused by parasitic aberrations calculated from Eq. (2.19).

The image position of a particle can be expressed with using only 3rd order aberration terms, reasonably well for a non-spherical aberration corrected system as:

$$w_{i,real} = w + C_{1,0}\theta + C_{1,2}\bar{\theta} + \frac{1}{3}\theta \left(2C_{2,1}\bar{\theta} + \bar{C}_{2,1}\theta \right) + C_{2,3}\bar{\theta}^2 + C_{3,0}\theta^2\bar{\theta} + \theta \left(C_{3,2}\theta^2 + 3\bar{C}_{3,2}\bar{\theta}^2 \right) + C_{3,4}\bar{\theta}^3, \quad (2.21)$$

where the meaning of coefficients is: $C_{1,0}$ - defocus, $C_{1,2}$ - 2-fold axial astigmatism, $C_{2,1}$ - axial coma, $C_{2,3}$ - three-fold axial astigmatism, $C_{3,0}$ - spherical aberration, $C_{3,2}$ - axial star aberration, $C_{3,4}$ - four-fold axial astigmatism.

2.4. TEM construction

TEM microscope design can vary depending on the machine type and the producer but the main building blocks of the construction are the same for any TEM (see Fig. 2.2) as follows:

- **Electron gun:** It is used to generate electrons. There are three main types of electron sources - thermionic, Schottky field emitter and cold field emitter.
- **Accelerator:** It is used to accelerate electrons generated in electron gun to the required energy in the range from 60 kV to 300 kV typically.
- **Electrostatic or magnetic lenses:** They are used to illuminate a specimen by the required beam shape and to transfer the specimen image on a camera or on a detector (condenser lenses, objective lens, projective lenses).
- **Apertures:** They are located along the optical axis of TEM and change the diameter of the primary beam. They are used to limit aberrations and stray electrons.
- **Deflection coils:** They are used to align optical axes of mechanical units to each other to minimize influence of misalignment or to allow to scan over the specimen in STEM.
- **Stigmators:** These correction elements are used to suppress the influence of 2-fold or 3-fold astigmatism mainly emerging from condenser and objective (projective) parts of the microscope.
- **Specimen chamber (region):** This area is evacuated under high vacuum conditions (pressure better than 10^{-5} Pa) or to the low vacuum conditions (order of 100 Pa) in special modes (ETEM).
- **Specimen stage:** It is used to manipulate the specimen via specimen holder typically in the range of ± 1 mm in x , y direction, $\pm 0,5$ mm in z direction (optical axis). Tilt of the specimen is possible in one or two axes up to ± 70 degrees typically.
- **Projection chamber:** It is used for placing most of the detectors and cameras and it is evacuated to the high vacuum in the order of 10^{-4} Pa.
- **Detectors:** Interaction of the primary beam electrons with the specimen generates signals such as: elastic and non-elastic scattered electrons, secondary electrons or X-rays. Detectors register these signals and convert them to information displayed to the user.
- **Coil current supplies:** They provide currents for lenses and the electron gun with stability typically better than 10 ppm (1 ppm in state of art) of the maximum design value.
- **Personal computer:** It is used to manage all microscope functions like aligning optical performance, processing image or data.

2.4. TEM CONSTRUCTION

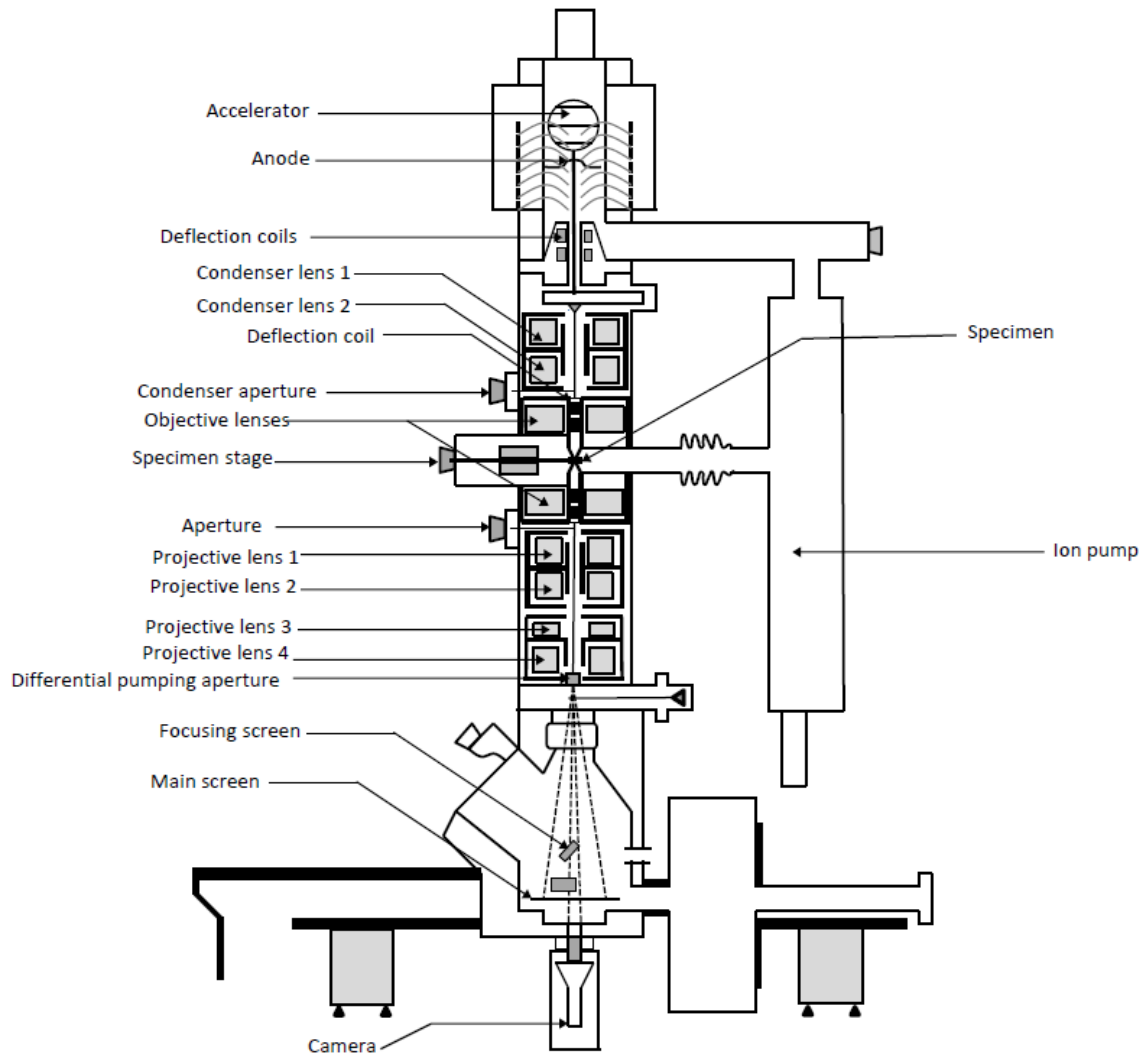


Fig. 2.2: Construction of the TEM microscope.

2.4.1. Lens design

All magnetic lenses used in regular TEM microscopes have the cylindrical symmetry. There are two good reasons to keep this type of the construction. The first one - cylindrical symmetry system does not suffer from even order aberrations in general when an ideal cylindrical shape is kept.

The second one which has the same importance, mainly at the beginning of electron microscopy age, is well handled machining process using lathes which guarantee the best machining accuracy from any regular used machine under an acceptable cost. Unfortunately even the best today machining technology cannot guarantee the ideal cylindrical symmetry, so some residual mechanical imperfections are always present - namely non-cylindricity often so-called ellipticity causing even order aberration - 2-fold astigmatism.

The particular design of any lens is a secret of TEM producer. But in general the lens consists of coil generating the magnetic flux, a housing used to transfer the magnetic flux and two pole pieces creating the magnetic gap shape (see Fig. 2.3). The pole pieces and the housing are produced from a special material which has required properties with

respect to the designed usage. The most often used materials are soft iron, nickel-iron alloys often called permalloys and cobalt-iron alloys called permendurs.

Electron trajectory modified by the magnetic lens can be expressed with using only terms connected to magnetic flux density as [13]:

$$w'' - \frac{i\eta}{U^{*1/2}} B w' - \frac{i\eta}{2U^{*1/2}} B' w = 0. \quad (2.22)$$

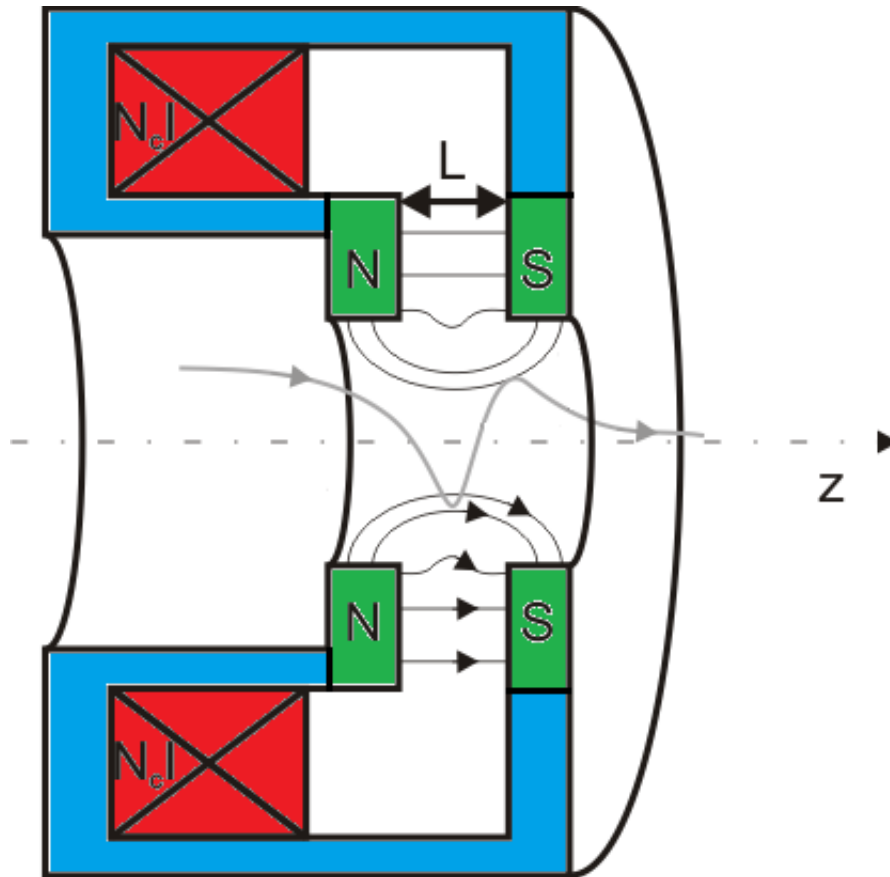


Fig. 2.3: General construction of the magnetic lens (blue - housing, green - pole pieces, red - coil) and grey curve represents the electron trajectory.

2.4.2. Deflection coil design

Each microscope is assembled from non-ideally machined parts. To suppress the influence of this non-ideal optical-mechanical system, deflection coils are used. They tilt or shift the electron beam to find its optimal trajectory where parasitic aberrations of the system are minimal from the optical point of view. They allow us to find the optimal system performance within machined mechanical imperfections.

Deflection coils can correct the mechanical shift and tilt of two parts with respect to each other. They allow us to limit the influence of aberrations like coma, field curvature and the distortion.

The second usage of deflection coils is a manipulation with the electron beam to scan over the specimen in HR-STEM or to change the illuminated region on the specimen.

Nowadays there are used two main types of deflection coils different by design:

- Helmholtz (straight) coils - easy and cheap to produce,

2.4. TEM CONSTRUCTION

- saddle coils - bent shape of the coil winding (typically in opening angle $\alpha = 120$ degrees), better homogeneity of the magnetic flux in the center (better linear deflection behavior), complex production and higher cost,

and two types different by the acting force:

- electrostatic - used in SEM and ion particle columns,
- magnetic - used mainly in TEM.

In general the principle of function of electrostatic and magnetic deflection coils is the same. For magnetic deflectors the pair of coils generates the magnetic flux density \vec{B} which is used to deflect the electron beam (see Fig. 2.4).

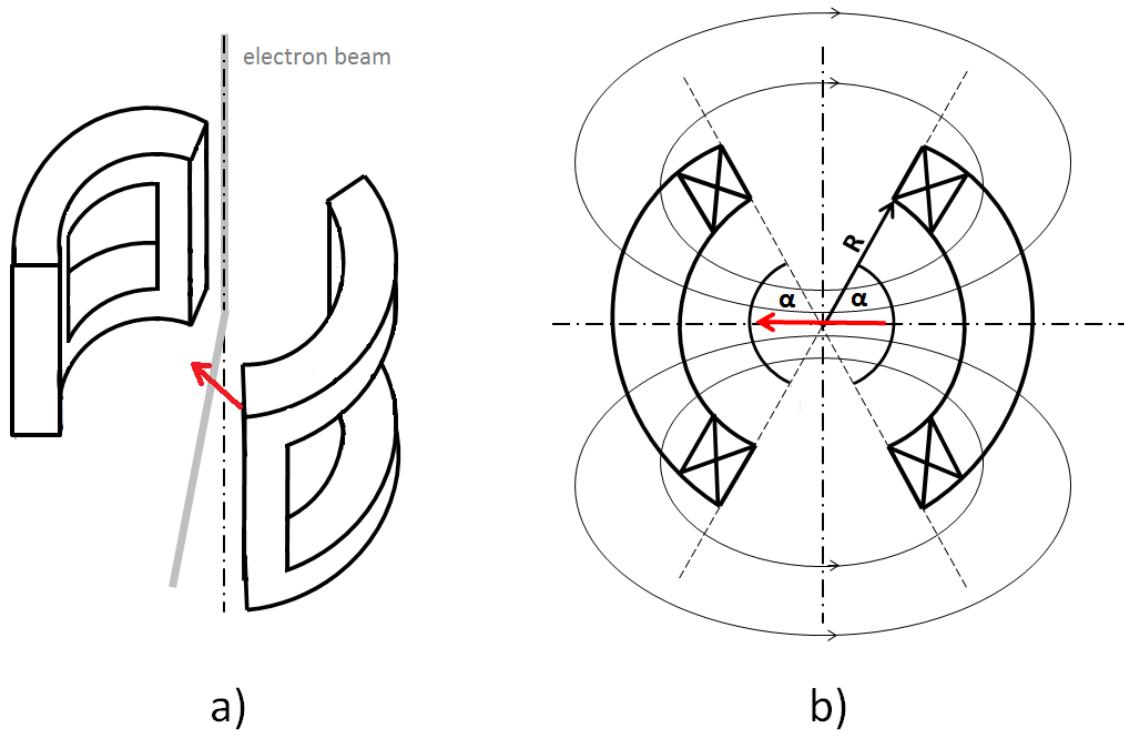


Fig. 2.4: Construction of the saddle deflection coil (red arrow represents the magnetic flux \vec{B} generated by the deflection coil).

The effect of the deflection coils in the paraxial equation (2.21) can be expressed introducing axial field function $F_1 = F_1(z)$ for an electrostatic deflector or $D_1 = D_1(z)$ for a magnetic deflector as [13]:

$$w'' + \left(\frac{\gamma U'}{2U^*} - \frac{i\eta}{U^{*\frac{1}{2}}} B \right) w' + \left(\frac{\gamma U''}{4U^*} - \frac{i\eta}{2U^{*\frac{1}{2}}} B' \right) w = -\frac{\gamma F_1}{2U^*} + \frac{\eta}{U^{*\frac{1}{2}}} D_1, \quad (2.23)$$

2.4.3. Stigmator design

Shift and tilt are not only mechanical imperfections in the real system. The second most often imperfection is non-cylindricity of part - usually called ellipticity. To correct this imperfection with 2-fold symmetry a quadrupole field must be generated. To do that

quadrupole stigmator is introduced to the optical system by four coils alternately excited (see Fig. 2.5). This setup generates a quadrupole field making possible to correct of ellipticity impact - 2-fold astigmatism.

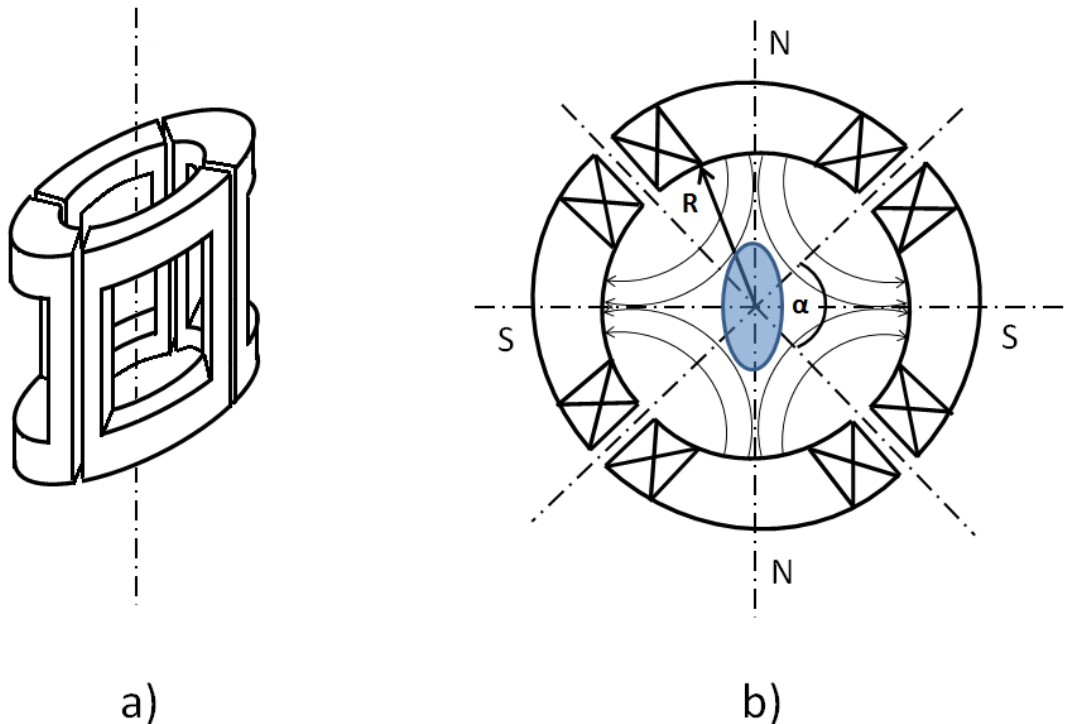


Fig. 2.5: Construction of the quadrupole stigmator.

Influence of stigmators on the electron trajectory can be expressed introducing the quadrupole electrostatic $f_2 = f_2(z)$ or magnetic $d_2 = d_2(z)$ field functions into Eq. 2.11 as [16]:

$$w'' + \left(\frac{\gamma U'}{2U^*} - \frac{i\eta}{U^{*\frac{1}{2}}} B \right) w' + \left(\frac{\gamma U''}{4U^*} - \frac{i\eta}{2U^{*\frac{1}{2}}} B' \right) w + \left(\frac{\gamma f_2}{2U^*} + \frac{\eta}{U^{*\frac{1}{2}}} d_2 \right) \bar{w} = 0, \quad (2.24)$$

2.5. Geometrical tolerances

Precision of product is affected by machine instabilities and random human errors during a production process creating deviations from the ideal shape. Dimensional and geometrical tolerances have been introduced in machinery to define allowable differences to the ideal shape. This thesis deals only with the geometrical tolerances which have the influence to the beam spot shape.

The nature of these deviations are more or less specific for each machining technology (turning, milling, drilling, ...) is machine (new one, before re-calibration, ...) but when large numbers of parts are considered, these deviations can be regarded as randomly distributed.

The pole pieces have a cylindrical symmetry. Geometrical tolerances used for description of the shape quality demands are cylindricity, circularity, total runout, runout, concentricity and perpendicularity. Their definition is as follows [21]:

2.6. SIMULATION OF MECHANICAL IMPERFECTIONS

- **Cylindricity:** It is a distance x between concentrically inscribed and a circumscribed cylinder of a part real shape over the length of measured region (see Fig. 2.6 a)).
- **Circularity:** It is a distance x between concentrically inscribed and a circumscribed circle of a part real shape (see Fig. 2.6 b)).
- **Total runout:** It is a distance x between concentrically inscribed and a circumscribed cylinder of a real shape of the part having the datum axis A over the length of measured region (see Fig. 2.7 a)).
- **Runout:** It is a distance x between concentrically inscribed and a circumscribed circle of a measured shape of the part having the datum axis A (see Fig. 2.7 b)).
- **Concentricity:** It is a diameter x of cylinder circumscribing a measured part axis with respect to datum axis A (see Fig. 2.8 a)).
- **Perpendicularity:** It is a distance x between two planes perpendicular to the datum plane A and circumscribing the measured plane (see Fig. 2.8 b)).

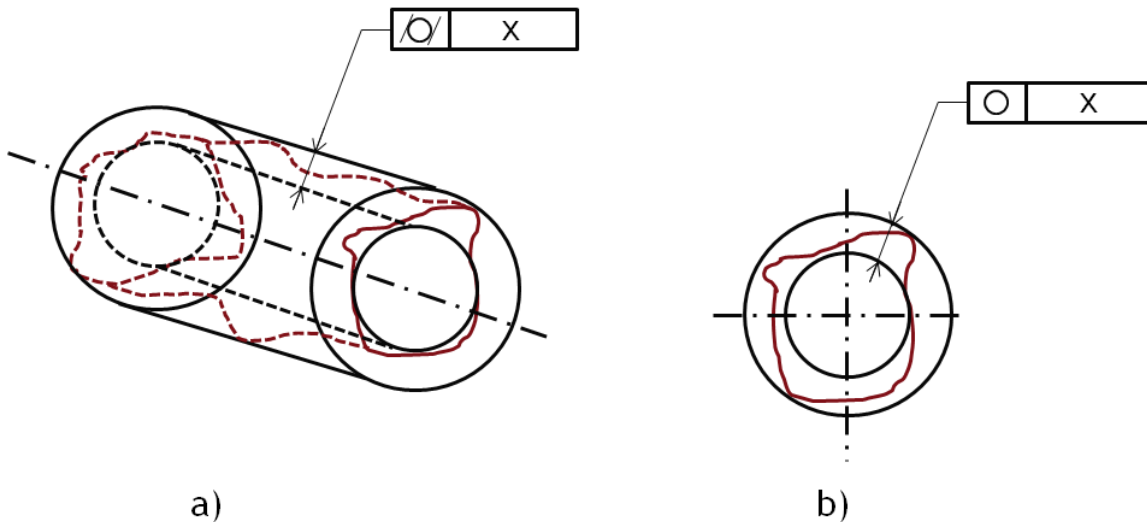


Fig. 2.6: Definition of a) cylindricity and b) circularity (red outline demonstrates the real part shape).

2.6. Simulation of mechanical imperfections

The standard treatment of the electron optics assumes an ideal optical system free of any mechanical imperfections. This condition cannot be realized using current manufacturing techniques. The highest mechanical precision which is reproducible and cost-effective is in the order of micrometers magnitude, and only high-end machining tools can produce parts with precision up to a half of micrometer. This requires sophisticated equipment with a tightly controlled environment (air-conditioned rooms with temperature stability better than $\pm 1^\circ\text{C}$, humidity from 60% to 80%, vibration dumped floor), operated by appropriately trained personnel. Additionally, strict final inspection of the machined parts is necessary to further select those fulfilling the requirements.

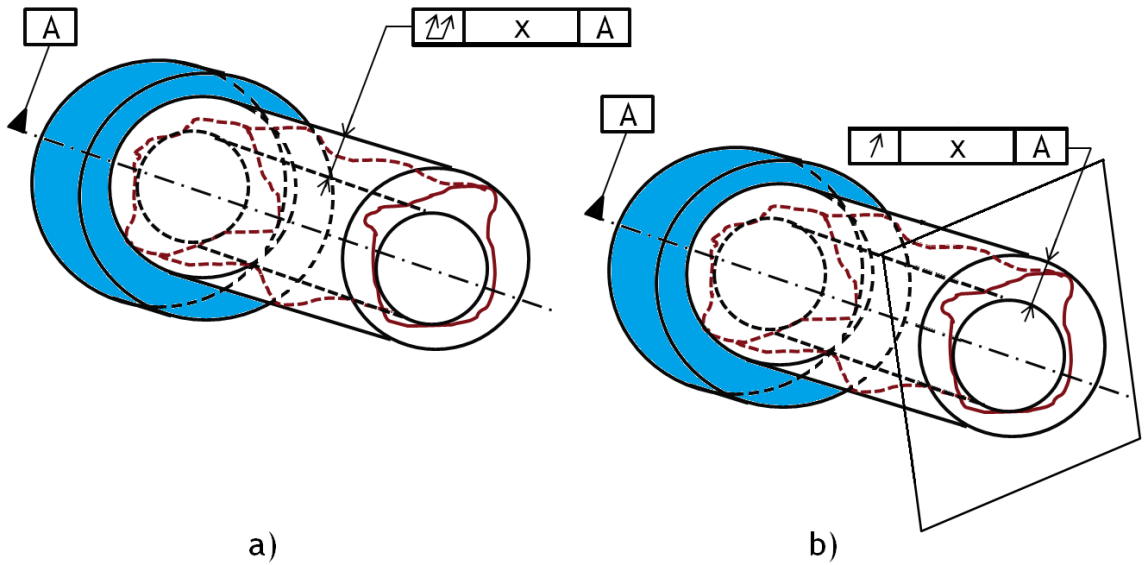


Fig. 2.7: Definition of a) total runout and b) runout with respect to the datum axis of the blue cylinder (red outline demonstrates the real part shape).

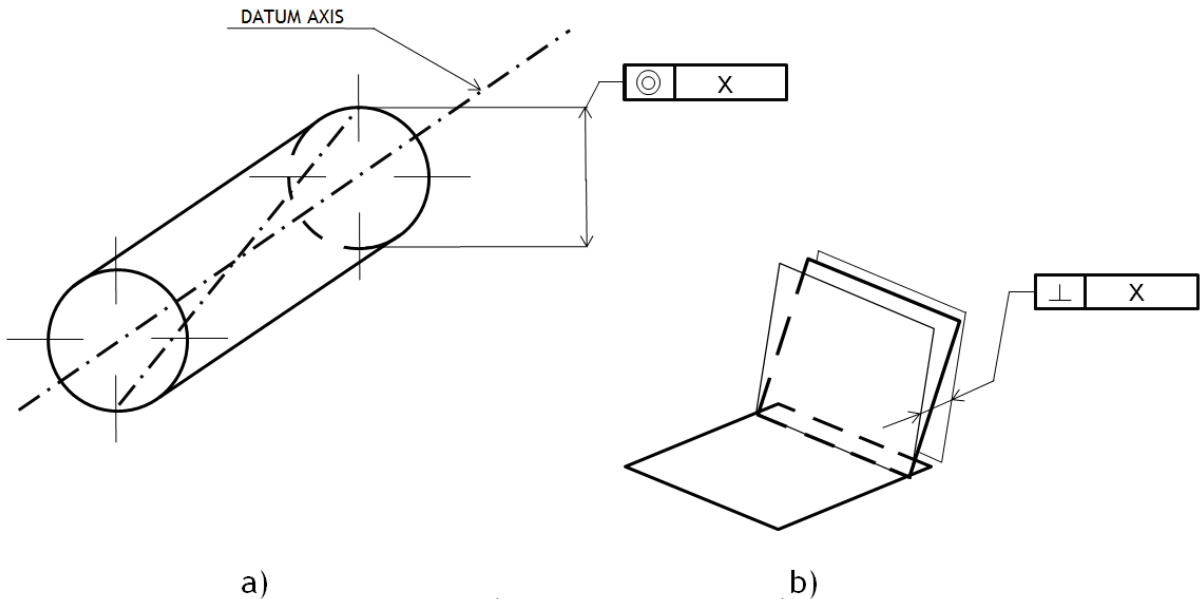


Fig. 2.8: Definition of a) concentricity and b) perpendicularity.

The material has an influence on the optical performance as well. Composition inhomogeneities in material having different magnetic properties cause various parasitic fields with different symmetry and consequently particular optical aberrations. These imperfections are very random over the pole piece and nowadays material production process can guarantee very high material homogeneity not having any significant influence on optical performance. Material imperfections are not studied in this work for this reason.

To determine the minimum precision of a pole piece for a given purpose, one needs to model the perturbations of the field, resulting from mechanical imperfections, acting on the electrons. That has been published by Munro for electrostatic lenses [18]. Using the same technique for magnetic lenses published by Sturrock [19], boundary conditions

2.6. SIMULATION OF MECHANICAL IMPERFECTIONS

of the reduced magnetic potential of the m -th multipole component on pole pieces can be defined as:

$$\Psi_m = \frac{\Phi_m}{r^m}, \quad (2.25)$$

where Φ_m is the scalar magnetic potential [1, 19].

The boundary conditions caused by ellipticity are

$$\Psi_2 = -H_r E, \quad (2.26)$$

where $E = \epsilon e^{i\beta}$ is a complex parameter characterizing the size of the ellipticity and its rotation (see Fig. 2.9). On material surfaces without ellipticity, $\Psi_2 = 0$.

The boundary conditions caused by misalignment are

$$\Psi_1 = -H_r S, \quad (2.27)$$

where $S = s e^{i\beta}$ is a complex parameter characterizing a misalignment shift in the plane perpendicular to the axis (see Fig. 2.9).

For tilt of a pole piece around the point z_c , the following boundary condition holds:

$$\Psi_1 = [r H_z - (z - z_c) H_r] T, \quad (2.28)$$

where $T = t e^{i\beta}$ is a complex parameter characterizing the tilt and its rotation around z axis (see Fig. 2.9) and $\vec{H}(r, \omega, z) = (H_r, 0, H_z)$ is the magnetic field of the lens.

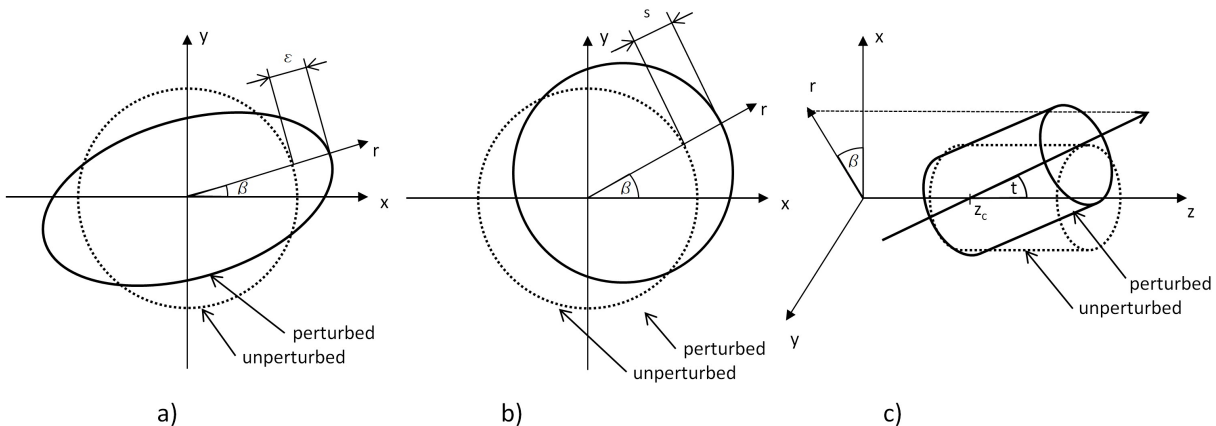


Fig. 2.9: Definition of mechanical imperfections — a) ellipticity, b) misalignment and c) tilt.

On the axis of symmetry and outer boundaries of the calculation region, $\Phi_m = 0$. Reduced potential is then calculated using the first order Finite Element Method for the Laplace equation for the m -th multipole component [15]:

$$\frac{\partial^2 \Psi_m}{\partial r^2} + \frac{2m+1}{r} \frac{\partial \Psi_m}{\partial r} + \frac{\partial^2 \Psi_m}{\partial z^2} = 0.$$

It is important to highlight that this is a physical simplification of a real situation coming from random machining errors and their directions. This approach used to describe real shape of pole pieces simulates the worst possible situation with respect to expected parasitic aberrations.

Generally it can be claimed that these mathematical terms can be translated to geometrical tolerances used in mechanics as:

- **ellipticity** as circularity, cylindricity, runout or total runout,
- **misalignment** as concentricity,
- **tilt** as perpendicularity.

As it was mentioned the best agreement between geometrical tolerances and mathematical representations has to be found for each application specifically.

2.7. EOD plugin Tolerancing

Calculation of the fields of lenses, deflectors and stigmators was performed in the software Electron Optical Design (EOD) [1]. Additional parasitic field of misalignment, tilt and ellipticity of the poles of the objective lens was calculated using Tolerancing plugin of EOD.

Tolerancing plugin was introduced in EOD 4.001 as a new feature enabling to calculate an influence of misalignment, tilt and ellipticity.

Using this feature is very user - friendly and intuitive. Regions which should be affected by an imperfection are selected as a region in the coarse mesh of the pole piece in Input file window (see Fig. 2.10) and marked with a letter T (meaning True) in the Material window of Input file (see Fig. 2.11). Z tilt [mm] defines the position of a tilt pivot point in case of tilt is present.

Calculation of lens input file with defined tolerances generates a standard axial field and axial field caused by the defined imperfections (Ψ_1 for misalignment and tilt or Ψ_2 for ellipticity) for 1 mm of misalignment and ellipticity and 1 mrad of tilt. This axial field is multiplied with the required imperfection size later on.

Trace settings and its tab Tolerancing is used to introduce required value of an imperfection in mm or in degrees (see Fig 2.12). Parameter **dx**, **dalpha** or **de** determines imperfection size and **dx rot**, **dalpha rot** and **de rot** defines the angle of its rotation in x, y plane of global coordinate system. Other work with EOD is the same as without Tolerancing plugin.

Detailed description of Tolerancing plugin is in Manual of EOD 4.001.

2.7. EOD PLUGIN TOLERANCING

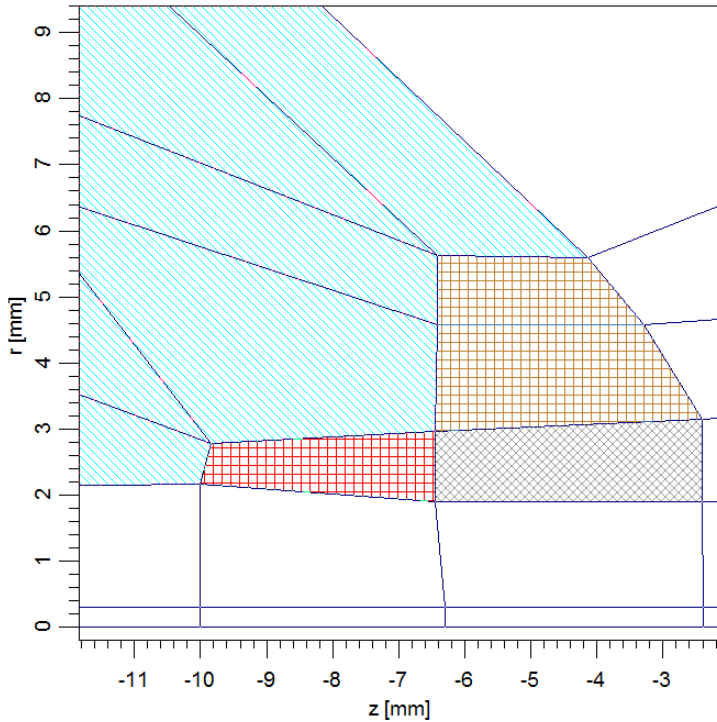


Fig. 2.10: Definition of regions affected by an imperfection in Input file - for material description see Fig. 2.11. Only the edge of magnetic material adjacent to vacuum is assumed to be imperfect.









Edit materials		H	C	Name	Misalig.	Tilt	z tilt [mm]	Elipt.
				Magnetic 1	F	F	0.00000	F
				Region C	T	T	-10.00000	T
				Region A	T	T	-6.00000	T
				Region D	T	T	0.00000	T

Fig. 2.11: Definition of regions affected by an imperfection (letter T) in Edit materials window.

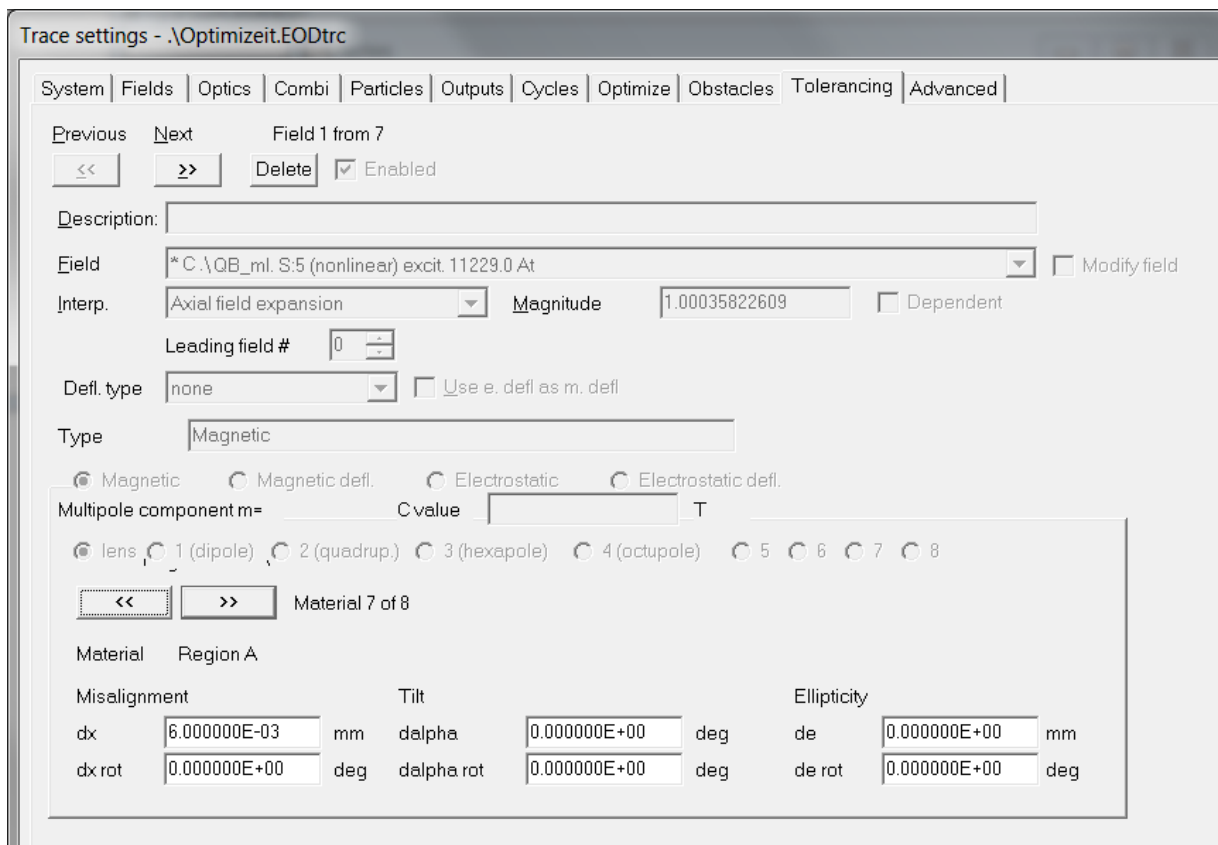


Fig. 2.12: Definition of imperfections values in Trace settings and its tab Tolerancing (a shift of $6\mu\text{m}$ is introduced in Region A of Material 7 with 0 degree rotation in x, y plane of global coordinate system).

2.7. EOD PLUGIN TOLERANCING

Chapter 3

Spot optimization

Influence of different mechanical imperfections of the pole pieces on the performance of the optical system was analysed by suppression of their effects on the final spot size by stigmators and deflection coils. Method used to find out excitations of stigmators and coils is described in this chapter.

Optimization is based on tracing set of one axial particle and N particles in n equidistant angles $\theta = \langle -\theta_{\text{omax}}/n, -\theta_{\text{omax}} \rangle$ and h polar angles $\omega = \langle 0, 2\pi(1 - 1/h) \rangle$ covering the whole aperture. Total number of test particles is $N + 1$ - the one is the axial particle. We obtain set of initial particle slopes in the object space

$$\theta_{o_j} = \theta_j e^{i\omega_j}, \quad j = 1, \dots, N$$

and the positions of particles in the image plane

$$w_{i_j} = x_{i_j} + iy_{i_j}, \quad j = 1, \dots, N.$$

Paraxial properties of the lens like demagnification of the object M , angular magnification M_a and the beam rotation ϕ are evaluated using Optics module of EOD from paraxial equation Eq. (2.11).

3.1. Evaluation of aberration coefficients

The knowledge of aberration coefficients is important in the optimization procedure. Coefficients are evaluated using least squares fitting of the regression model arising from the equation (2.21) as:

$$w_{i_j} = \frac{1}{M e^{i\phi_j}} \left[C_{0,0} + C_{1,0}\theta_j + C_{1,2}\bar{\theta}_j + \frac{1}{3}\theta_j(2C_{2,1}\bar{\theta}_j + C_{2,1}\theta_j) + C_{2,3}\bar{\theta}_j^2 + C_{3,0}\theta_j^2\bar{\theta}_j + \frac{1}{4}\theta_j(C_{3,2}\theta_j^2 + 3\bar{C}_{3,2}\bar{\theta}_j^2) + C_{3,4}\bar{\theta}_j^3 \right] + \varepsilon_j, \quad (3.1)$$

where ε_j is the error of fit of the j^{th} point position.

The least squares method is then based on the minimization of the sum

$$S = \sum_{j=1}^N |\varepsilon_j|^2, \quad (3.2)$$

where N is equal or larger than number of coefficients to be fitted.

The procedure of minimization is described in details in [22]. As a result of optimization all coefficients $C_{m,n}$ are known.

3.2. Evaluation of current density profile

Analyzed optical system is diffraction limited. The current density profile must be evaluated using diffraction integral [10]. The optical system acts as a phase object. Ideal spherical wavefront in the image space is affected by the aberrations and the phase error is

$$\begin{aligned} \chi(\theta_i) = \operatorname{Re} \left(C_{0,0}\bar{\theta}_i + \frac{1}{2}C_{1,0}\theta_i\bar{\theta}_i + \frac{1}{2}C_{1,2}\bar{\theta}_i^2 + \frac{1}{3}C_{2,1}\theta_i^2\bar{\theta}_i \right. \\ \left. + \frac{1}{3}C_{2,3}\bar{\theta}_i^3 + \frac{1}{4}C_{3,0}\theta_i^2\bar{\theta}_i^2 + \frac{1}{4}C_{3,2}\theta_i^3\bar{\theta}_i + \frac{1}{4}C_{3,4}\bar{\theta}_i^4 \right), \end{aligned} \quad (3.3)$$

where $\theta_i = \theta_{i_x} + i\theta_{i_y}$ is particle slope in the image space which is limited by the aperture to the maximal slope in the image space $\theta_{i_{\max}} = M_a\theta_{o_{\max}}$.

The transmission function of the optical system [23] is

$$t(\theta_i) = \begin{cases} \exp \left[i\frac{2\pi}{\lambda}\chi(\theta_i) \right] & \text{where } |\theta_i| \leq \theta_{i_{\max}}, \\ 0 & \text{otherwise.} \end{cases} \quad (3.4)$$

The object is assumed to be a point generating spherical wave. The wave function $\psi(x, y)$ in the image space can be expressed in Fraunhofer approximation as [23, 10]

$$\psi(x, y) = A \int_{-\infty}^{\infty} \int_{-\infty}^{\infty} t(\theta_i) \exp \left(-i\frac{2\pi}{\lambda}(\theta_{i_x}x + \theta_{i_y}y) \right) d\theta_{i_x} d\theta_{i_y} \quad (3.5)$$

where A is a normalization constant.

The current density is then evaluated as

$$j(x, y) = |\psi(x, y)|^2. \quad (3.6)$$

3.2.1. Calculation of diffraction integral

Integral in equation (3.5) was calculated in MATLAB using built-in two dimensional Fast Fourier Transform of the transmission function (3.4). The calculation was inspired by the MATLAB script published in [24].

Transmission function was sampled using $N = 2^{11} = 2048$ samples in our calculation and the size of the θ_i domain was chosen to have 122 samples in the aperture diameter $2\theta_{i_{\max}}$. The size of the domain was then $\langle -16.78\theta_{i_{\max}}, 16.78\theta_{i_{\max}} \rangle^2$.

The size of the corresponding image was $25d_{\text{Airy}}$. The sampling in the image space was done by 50 samples in Airy disk diameter d_{Airy} which was sufficient to smoothly describe current density profile.

Current density profile was then normalized to contain the beam current.

3.3. Optimization method

Optimization of the spot size is performed as a user defined plugin of EOD. This plugin utilizes EOD functions to calculate trajectories of particles and optical properties. Plugin uses standard SIMPLEX method to minimize the spot size.

Optimization procedure consists of different steps. At the beginning all stigmators and deflectors are off and the spot size is quite big. The diameter is about 100 nm (depending on the tolerances used). The final spot size d_{50} is supposed to be below 0.2 nm in our case. This big difference in the spot sizes needs different definitions of the spot quality through the optimization process.

3.3.1. Minimization of the spot size

When the optimization starts and spot size is big the RMS value r_{RMS} of the positions of the test particles is used as measure of the spot quality

$$r_{\text{RMS}} = \sqrt{\frac{1}{N} \sum_{j=1}^N |w_{ij}|^2}. \quad (3.7)$$

Optimization routine varies excitations of stigmators to minimize r_{RMS} at first. Afterwards excitation of deflectors is set according to changes of excitation of stigmators to direct the axial trajectory back to the axis with zero angle to the axis in the image plane. This optimization is terminated when the $r_{\text{RMS}} < 0.1$ nm.

3.3.2. Minimization of the coma

The next step of the optimization is the minimization of the coma. The coma is minimized by a beam tilt. Only the excitation of the deflectors is changed in this step to achieve the smallest possible coma aberration coefficient. SIMPLEX method is used to minimize value C of the aberration coefficients $C_{2,1}$ of the coma and $C_{1,2}$ of the 2-fold astigmatism

$$C = |C_{2,1}| + \frac{1}{\theta_{\text{i,max}}} |C_{1,2}|. \quad (3.8)$$

The coefficient of the astigmatism is divided by the maximum particle slope in the image space to obtain comparable values according to equation (2.21).

These two optimization procedures give almost perfect spot. The final stage of optimization focus on the optimization of the wavefront error.

3.3.3. Optimization of the wavefront error

The simulation gives that the smallest spot size of the system with spherical aberration and defocus corresponds to the maximal wave error equal to $\lambda/4$ at approximately 70 % of maximal aperture as shown in fig. 3.1a). The wavefront error of the system with additional astigmatism is in fig. 3.1b) for comparison. The cross-section of the wavefront error in the axes θ_x and θ_y is shown in Fig. 3.2.

The simplest possible method describing wavefront error for the procedure of optimization of spot size was used. The wavefront errors $\chi_{0.7}$ and $\chi_{1.0}$ respectively were characterized by the error for the two different angles $0.7\theta_{\text{i,max}}$ and $\theta_{\text{i,max}}$. In the ideal case the dependence of the wavefront error on the polar coordinate ϕ characterizing position on the circle with radius given by angle θ in Fig. 3.1 is represented by constant because the wavefront is fully symmetrical as shown in Fig. 3.3a) for the system without astigmatism. This ideal state can be characterized by the $\chi(\phi)$ mean value equal to $\chi_{0.7} = -0.25\lambda$,

3.3. OPTIMIZATION METHOD

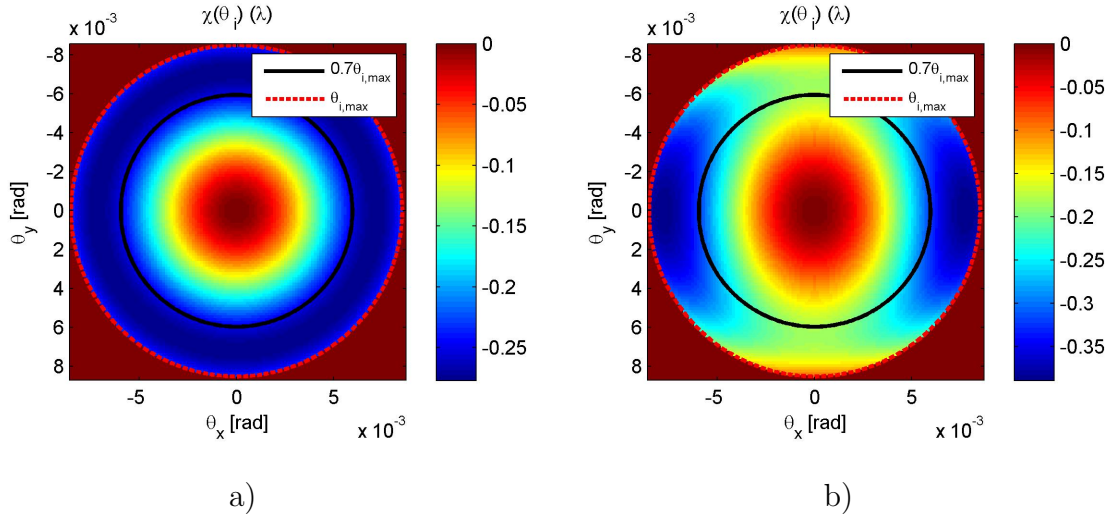


Fig. 3.1: The wavefront error. a) Spherical aberration $C_{3,0} = 1.05$ mm and defocus $C_{1,0} = -54$ nm; b) Spherical aberration $C_{3,0} = 1.05$ mm, defocus $C_{1,0} = -54$ nm and 2-fold astigmatism $C_{1,2} = 10$ nm

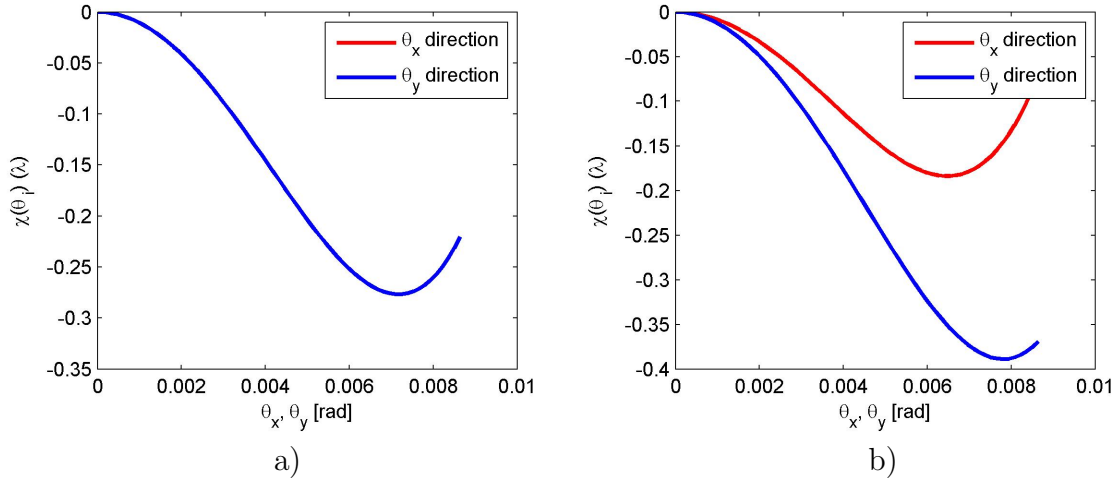


Fig. 3.2: The wavefront error as the function of θ_x and θ_y . a) Spherical aberration $C_{3,0} = 1.05$ mm and defocus $C_{1,0} = -54$ nm; b) Spherical aberration $C_{3,0} = 1.05$ mm, defocus $C_{1,0} = -54$ nm and 2-fold astigmatism $C_{1,2} = 10$ nm

$\chi_{1.0} = -0.23\lambda$ respectively. The standard deviations $s_{0.7}$ and $s_{1.0}$ are zero because the wavefront is symmetrical.

The situation is different for the system suffering from 2-fold astigmatism. Dependence of the wavefront error on the ϕ angle in Fig. 3.3b) shows loss of rotational symmetry of wavefront. This situation is characterized by

$$\chi_{0.7} = -0.25\lambda, \quad s_{0.7} = 0.05\lambda, \quad \chi_{1.0} = -0.23\lambda, \quad s_{1.0} = 0.10\lambda.$$

Mean values of wavefront error are identical with the ideal case but the standard deviation is nonzero.

As a measure of the wavefront error was chosen

$$\epsilon = (\chi_{0.7} - (-0.25\lambda))^2 + (\chi_{1.0} - (-0.23\lambda))^2 + (s_{0.7} + s_{1.0})^2.$$

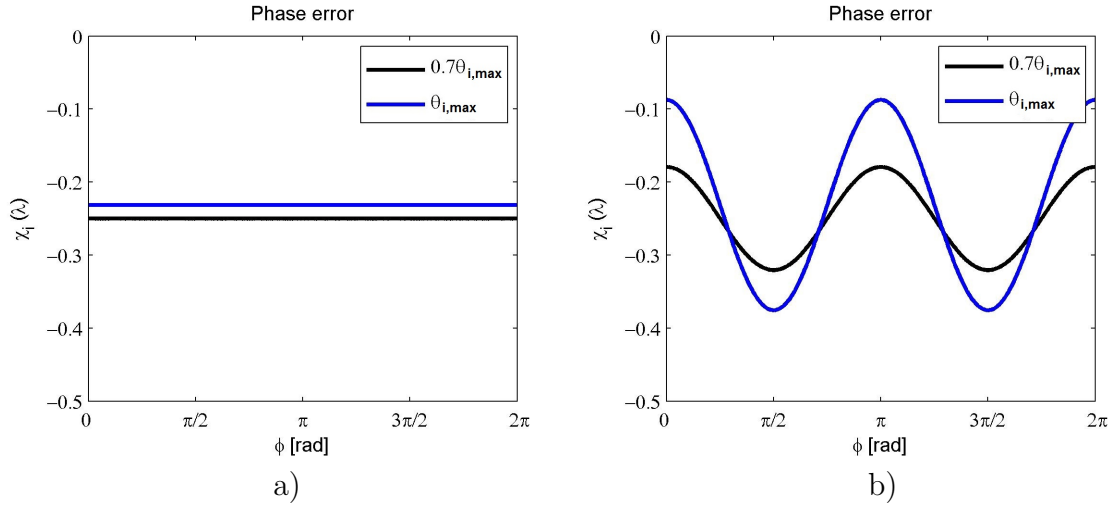


Fig. 3.3: The wavefront error as a function of polar angle ϕ for $\theta_i = 0.7\theta_{i,\max}$ and $\theta_i = \theta_{i,\max}$. a) Spherical aberration $C_{3,0} = 1.05$ mm and defocus $C_{1,0} = -54$ nm; b) Spherical aberration $C_{3,0} = 1.05$ mm, defocus $C_{1,0} = -54$ nm and 2-fold astigmatism $C_{1,2} = 10$ nm

The minimization of the error ϵ leads to spots with suppressed 2-fold astigmatism and as well as other axial aberrations.

3.3. OPTIMIZATION METHOD

Chapter 4

Study of condenser astigmatism

4.1. Analysis of the upper objective pole piece

Theoretical calculation was done in EOD 4.001 to see the magnetic saturation of the pole pieces to understand which regions are critical for optical performance. The magnetic saturation is shown in Fig. 4.1. The outline results with the assembly schematic design for HR-STEM mode are shown in Fig. 4.2 and 4.3. Tolerances of these regions are studied in this work.

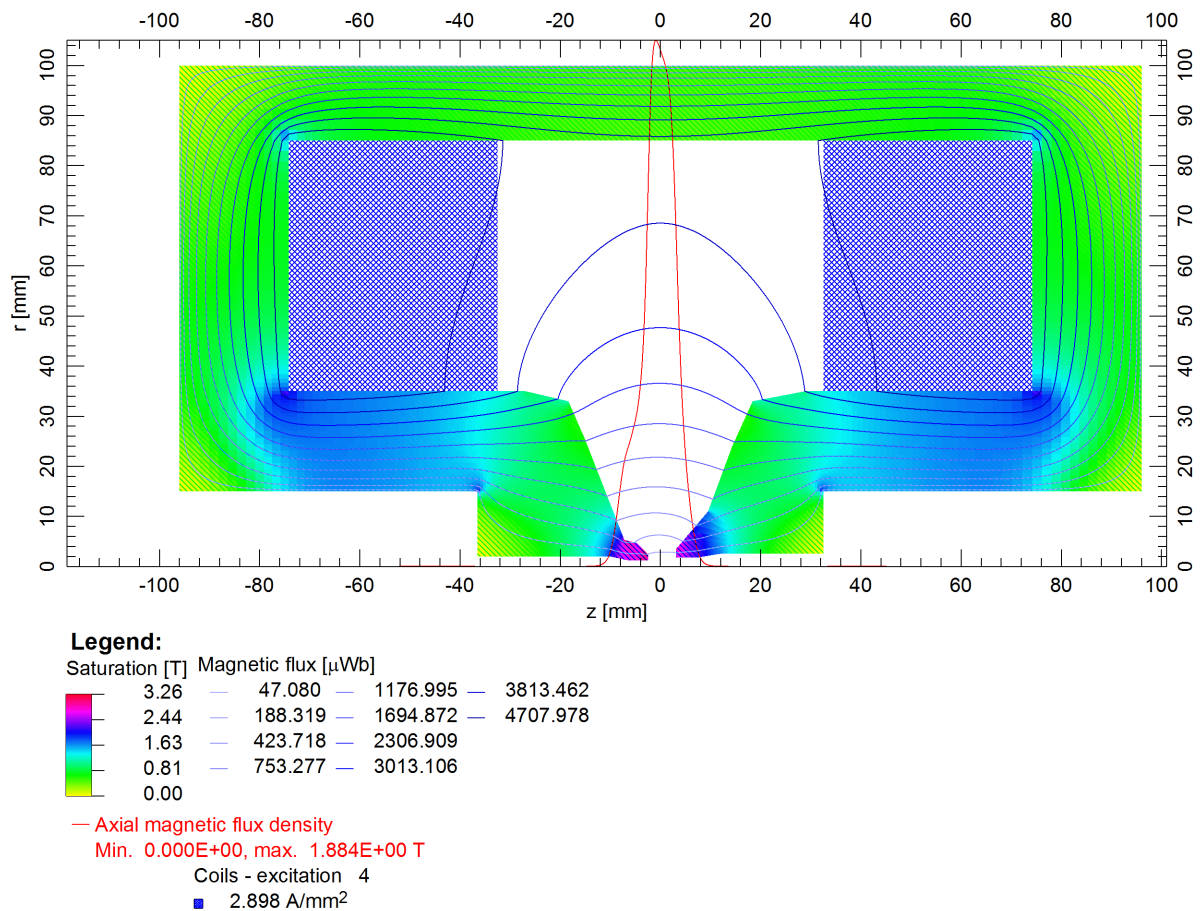


Fig. 4.1: Magnetic saturation of the objective lens.

4.2. CALCULATION

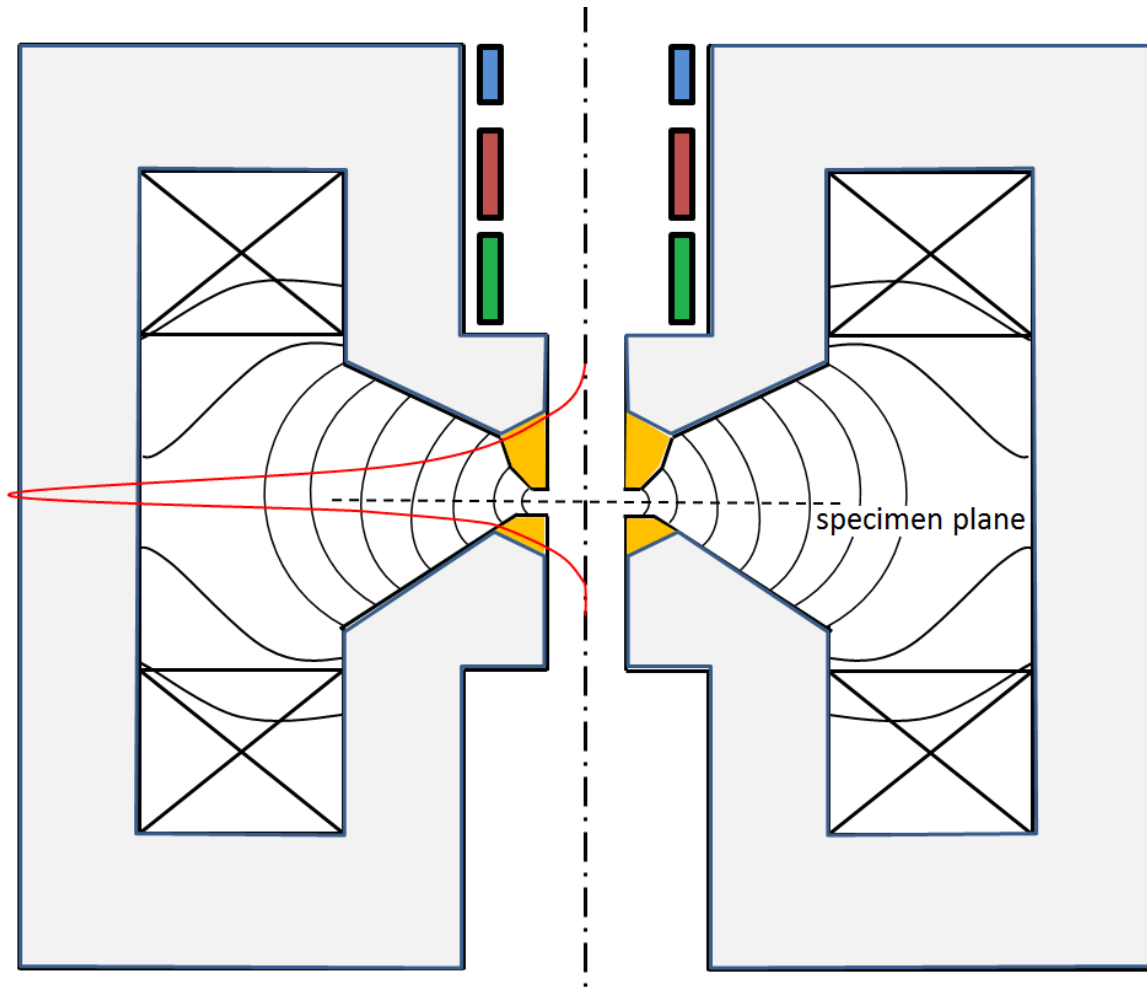


Fig. 4.2: General schematic of the design and the magnetic saturation of objective pole pieces in HR-STEM mode (red line represents the magnetic flux density generated by the lens, blue filled rectangles - condenser stigmators, red filled rectangles - upper deflection coils, green filled rectangles - lower deflection coils, yellow color highlights the magnetic oversaturation of the material, light grey filled area - magnetic material of the lens).

It is easily visible in Fig. 4.3 that the regions *A*, *B*, *C* and *D* are oversaturated and the magnetic field overflows from the material and modulates the lens acting region. The mechanical accuracy of these regions was put under investigation.

The quality of machining of regions *A*, *B*, *C* and *D* was measured on 26 objective upper pole pieces made specially for this study. The pole piece design was derived from the known HR-TEM pole pieces. The oversaturated area was split into three mechanical regions to study trends of the various saturations and imperfections effects coming from different regions. Pole pieces were manufactured in five batches of five and six pieces respectively from different rod of raw material to avoid any systematic error - neither in machining or in material inhomogeneity.

4.2. Calculation

The model consisting from the main objective lens, two quadrupole stigmators and four pairs of saddle deflection coils was created according the tested microscope design to verify

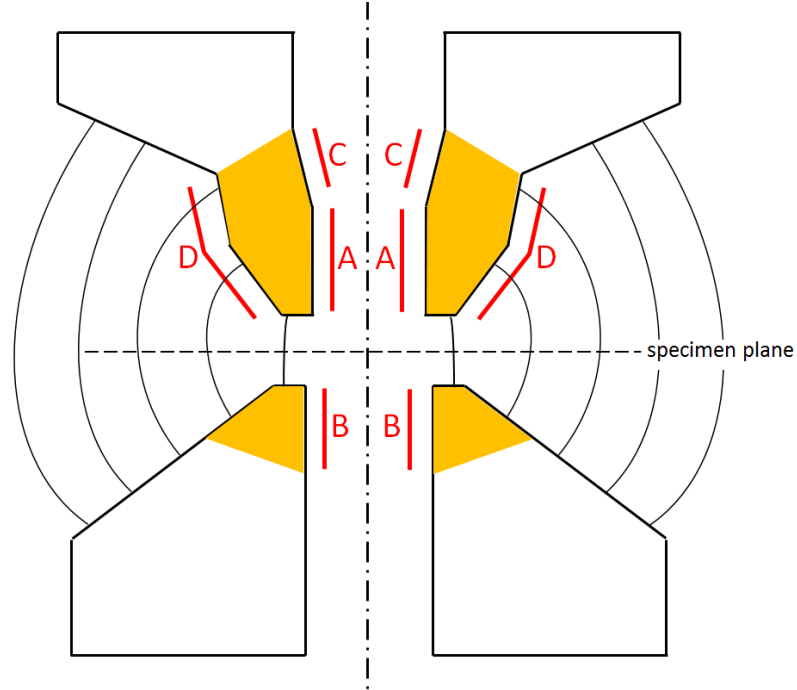


Fig. 4.3: General schematic of the tip design and the magnetic saturation of the upper objective pole piece. Regions A, B, C and D are oversaturated (yellow regions) and the magnetic field is overflowing from the material and it is modulating the lens acting region.

the assumption of the influences of regions A,B,C and D. Parameters of the elements shown in Fig. 4.2 are following:

- **Objective lens:** Bore diameter 2.4 mm, gap 5.5 mm, lens coil excitation 12086 AT, material is general permendur (Co-Fe alloy).
- **Deflectors** These are regular pairs of saddle coils with the open angle of 120 degrees, x and y coils are rotated by 90 degrees to each other. For details see Tab. 4.1.
- **Stigmators** Saddle coils are used with 30 degrees as open angle, x and y coils are rotated by 45 degrees to each other. For details see Tab. 4.1.

Coil	Length [mm]	Diameter [mm]	Pos. of coil center [mm]	Number of turns
Upper X	20	16	-70	24
Upper Y	20	20	-70	24
Lower X	20	20	-45	54
Lower Y	20	24	-45	54
Stigmator X	13	26	-90	200
Stigmator Y	13	26	-90	200

Tab. 4.1: Parameters of deflection coils and stigmators.

Simulations in EOD 4.001 were done under the following settings:

- 482587 mesh points (497 lines in horizontal fine mesh, 971 lines in vertical fine mesh) for calculation of magnetic field of the objective lens,
- non-linear accuracy of magnetic field distribution calculation 10^{-13} ,

4.2. CALCULATION

- relative accuracy of Runge-Kutta Fehlberg method of 7-8th order for tracing of particles 10^{-14} ,
- energy of particles 200 keV (an energy spread is neglected due to its low addition to the beam diameter around 30 pm - calculated with using formulas in [6] and typical energy spread for Shottky FEG 0.7 eV),
- 121 particles used for tracing and optimization of the axial aberrations, one particle on axis and 120 in 6 equidistant angles $\theta = \langle -18.7, -112.3 \rangle \mu\text{rad}$ and 20 polar angles $\omega = \langle 0, 2\pi \rangle$ covering whole aperture of diameter $70 \mu\text{m}$ placed in -120 mm. These settings correspond to semi-angle 8.5 mrad at the specimen plane.

The EOD uses quadruple-precision arithmetic to improve the solution accuracy if the relative accuracy of the integration of equation of motion is 10^{-14} . The field was interpolated using the radial series expansion about the axis using the axial field functions, which gives the correct field values near the axis and enables a fast computation with the precision of the particle position in the image plane of about 1 pm.

The particles are started at -120 mm which is the position of the aperture and the Gaussian image plane was set to $z = -77.9 \mu\text{m}$. The spot was observed and optimized at the Scherzer defocus plane $z_i = -63.1 \text{ nm}$ from the Gaussian image plane. The spherical aberration of the objective lens in this configuration was $C_S = 1.05 \text{ mm}$ and the angular magnification is $M_a = 75.68$. The optimal semi-angle of the beam limited by the spherical aberration and the diffraction in the image plane is $\theta = 8.5 \text{ mrad}$. The corresponding semi-angle at the object plane is $\theta_o = 0.112 \text{ mrad}$. This was calculated together with the theoretical beam spot size of 0.173 nm by means of the formulas of Barth and Kruit assuming the recommended parameters to reach the best fit of the spot size with the wave calculation [6].

Beam spot profile of the ideal system (without any mechanical imperfection) was calculated to obtain the optimal spot size and shape (see Fig 4.4) to compare the calculation model quality with the real system performance. It passes well (calculation stopped at $d_{50} \leq 0.2 \text{ nm}$).

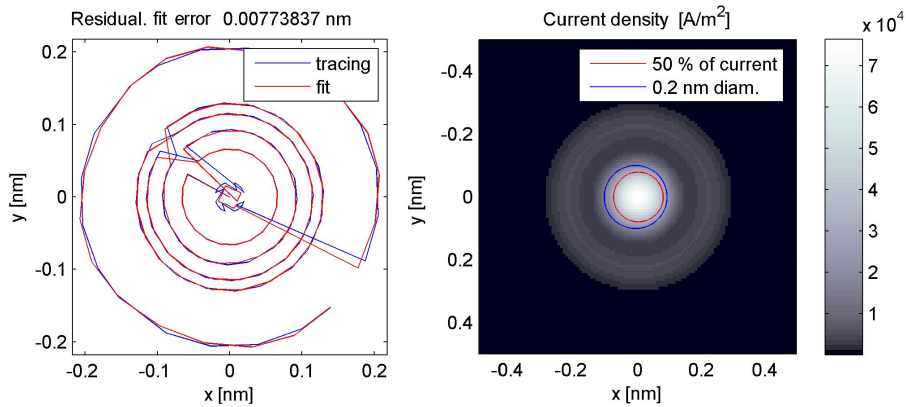


Fig. 4.4: Spot without any mechanical imperfection: a) geometrical shape, b) current density (the beam current 100 pA).

Machining errors were assumed to be on the pole pieces in regions A, B, C and D where the magnetic flux escapes from the material and moves towards the optical axis, influencing the electron beam. Axial field functions of dipole and quadrupole magnetic fields introduced by the imperfections are shown in Fig. 4.5.

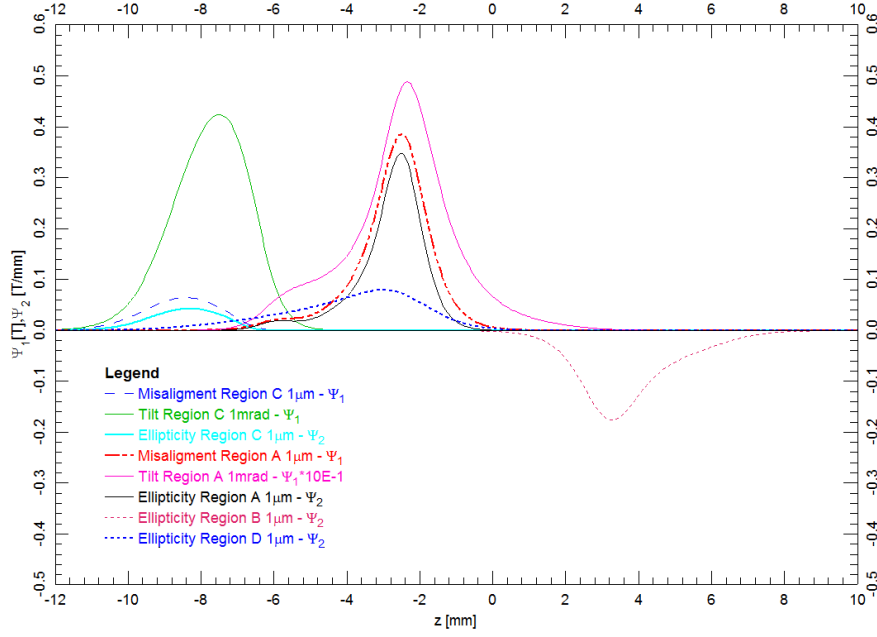


Fig. 4.5: Axial field functions of the imperfections in regions A, B, C and D of the pole pieces.

Spot optimization process is derived from the approach used in the common used HR-STEM alignment procedure as it is described in Chapter 3 in details.

To determine precision of lens, stigmators and deflection coils excitation adjustment to obtain the reproducible spot quality the influence of a change in lens elements was investigated. A change in the objective lens excitation of 1 ppm without the adjustment of the deflector excitation causes the axial trajectory shift of about 2 pm. Also a change in the stigmator excitation of 1 ppm causes the axial trajectory shift of about 0.5 pm because the stigmator and upper deflector fields overlap. Calculation is done with sufficient 1 pm accuracy for accuracy of the particle position in the image plane which is 200 times smaller than the required spot diameter.

4.3. Influence of individual regions

Calculation of influence of individual regions was done separately to see their particular contributions to the total 2-fold astigmatism $C_{1,2}$. The value of the stigmator current was calculated as well to enable a direct comparison with the result obtained on prototype objective lenses.

Mechanically reasonable values were applied - for ellipticity up to 5 μm in Region A and D, up to 10 μm in Region C, for misalignment up to 10 μm and up to 1 mrad for tilt.

This approach enables to understand which region has which influence on the total system 2-fold astigmatism. That helps to define reasonable values for particular region when their combined influence is investigated in the following section.

Tilt and misalignment are not assumed to be studied in this section. Their contribution causes mainly the axial coma which is corrected by the beam tilt and shift. This is done by deflection coils in our case. This is proven in subsection 4.3.1.

4.3. INFLUENCE OF INDIVIDUAL REGIONS

Aberrations created from combination of tilt, missalignment and ellipticity - mainly 3-fold astigmatism are not investigated because their influence is not comparable with the influence of 2-fold astigmatism within mentioned mechanical tolerances - see [16].

4.3.1. Calculation of Region A

As first only the influence of ellipticity on the 2-fold astigmatism was studied. Tilt and misalignment are not studied for Region A because they can be replaced as addition of tilt or misalignment of the other regions.

Spot size optimization procedure described in chapter 3 was used for ellipticities ϵ_A of Region A in the range $0 \mu\text{m}$ to $5 \mu\text{m}$ and coefficient $C_{1,2}^A$ of the 2-fold astigmatism was determined. The same method was used in further calculations. There is the dependance of the modulus of $|C_{1,2}^A|$ on ellipticity shown in Fig. 4.6. We can see that this is linear which was expected from Eq. (2.26). So, the linear trend line was plotted as follows with 95% confidence bands:

$$|C_{1,2}^A| = k_A \epsilon_A + K_A = ((2.205 \pm 0.021) \epsilon_A + (0.024 \pm 0.057)) \mu\text{m}, \quad (4.1)$$

where $|C_{1,2}^A|$ is the modulus of 2-fold astigmatism coefficient caused by ellipticity ϵ_A introduced in Region A, k_A is the slope of the line and K_A is the offset constant. K_A is supposed to be zero from the theory and it is because the error of the coefficient is greater than its value K_A is irrelevant.

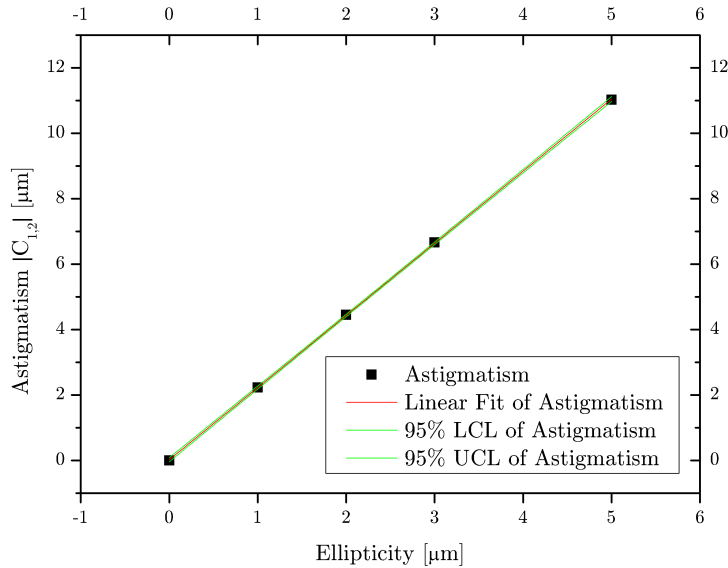


Fig. 4.6: Influence of ellipticity in Region A on the modulus of 2-fold astigmatism coefficient $|C_{1,2}^A|$.

4.3.2. Calculation of Region B

Axial fields caused by mechanical imperfections in Region B have only small part above the specimen plane in $-77 \mu\text{m}$ affecting beam focusing (see Fig. 4.5). Their influence was expected very small. To prove that ellipticity of $1 \mu\text{m}$ in Region B was calculated and

related 2-fold astigmatism coefficient $|C_{1,2}^B|$ was only $6.98 \cdot 10^{-4} \mu\text{m}$. This is more than 3000 times smaller than the influence of Region A with the same value of ellipticity.

Misalignment and tilt in Region B generate negligible 2-fold astigmatism created by optimization procedure to suppress coma influence on wavefront error.

The influence of Region B is not taken into account in further calculations because its negligible contribution with comparison to the other regions.

4.3.3. Calculation of Region C

Region C is assumed to be affected by all imperfections (ellipticity, misalignment, tilt) to see if the effect of misalignment and tilt on the 2-fold astigmatism is significant.

The modulus of astigmatism coefficient $|C_{1,2}^C|$ dependance on ellipticity of Region C is shown in Fig. 4.7. Linear trend line is plotted with the following parameters with 95% confidence bands:

$$|C_{1,2}^C| = k_C \epsilon_C + K_C = ((0.830 \pm 0.003)\epsilon_C + (0.012 \pm 0.015)) \mu\text{m}, \quad (4.2)$$

where $|C_{1,2}^C|$ is the absolute value of the astigmatism coefficient caused by ellipticity ϵ_C introduced in Region C, k_C is the slope of the line and K_C is the offset constant. K_C is supposed to be zero from the theory.

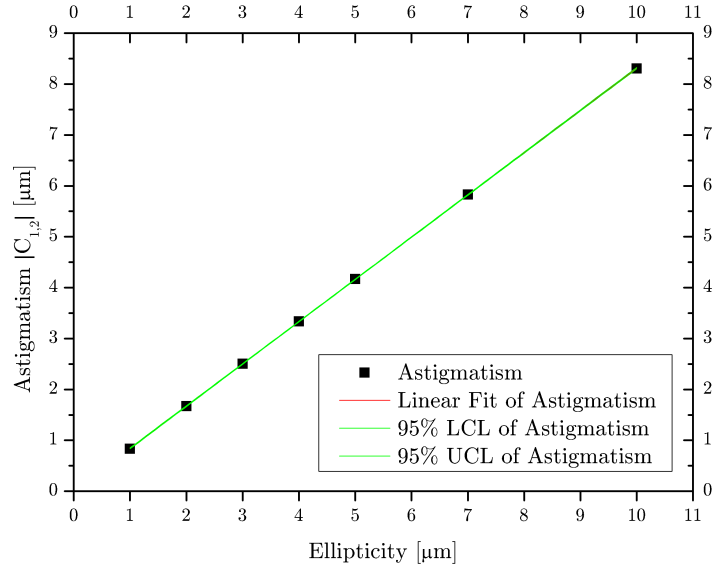


Fig. 4.7: Influence of ellipticity in Region C on the modulus of astigmatism coefficient $|C_{1,2}^C|$.

The influence of Region C and A can be compared by the ratio $g_{A,C}$ expressed from Eq. (4.1) and (4.2) as following:

$$g_{A,C} = \frac{k_A}{k_C} = 2.657. \quad (4.3)$$

The ratio can be explained by different magnitudes of the axial fields Ψ_2 caused by ellipticities in Region A and Region C (6:1) and different electron paths in these regions.

4.3. INFLUENCE OF INDIVIDUAL REGIONS

Calculation of a misalignment and a tilt influence on the 2-fold astigmatism coefficient does not add any significant value to $|C_{1,2}^A|$ - see Tab. 6.1 calculation 32-70 in tables in Appendix I section 6.1. These results are with good agreement with theory [10] because misalignment and tilt imperfections generate another aberrations than 2-fold astigmatism in general.

4.3.4. Calculation of Region D

Region D lies on the outer shape of oversaturated pole piece (see Fig. 4.3). It was the reason to take this region in the tolerancing calculation as well.

Ellipticity was assumed as only one mechanical imperfection in Region D knowing the negligible influence of a misalignment and a tilt in Region C to 2-fold astigmatism.

Unfortunately EOD 4.001 does not provide a correct and expected result of an axial field function (see Fig. 4.5) in this particular case. Current version of Tolerancing plugin of EOD assumes materials as unsaturated when it calculates tolerancing fields. This assumption causes smaller influence of the Region D than is observed.

The influence of ellipticity of Region D was calculated without help of Tolerancing plugin to overcome this issue. A small coil generating quadrupole field was placed on the interface of the pole material and air. Its excitation was tuned to obtain similar axial field function as it is given by the Tolerancing plugin with nonsaturated material. Then the saturated part of the pole was removed and the axial field function was calculated (see Fig. 4.8). This calculation is justifiable under assumption that the saturated magnetic material cannot transfer any other magnetic flux arising from ellipticity. Such calculated axial field function was used in further evaluation of ellipticity in Region D so it acts as an air with relative permeability equal to 1. From the shape of the axial field functions can be seen that the quadrupole field caused by ellipticity penetrates to the optical axis through the saturated part of the pole piece much more than through nonsaturated material.

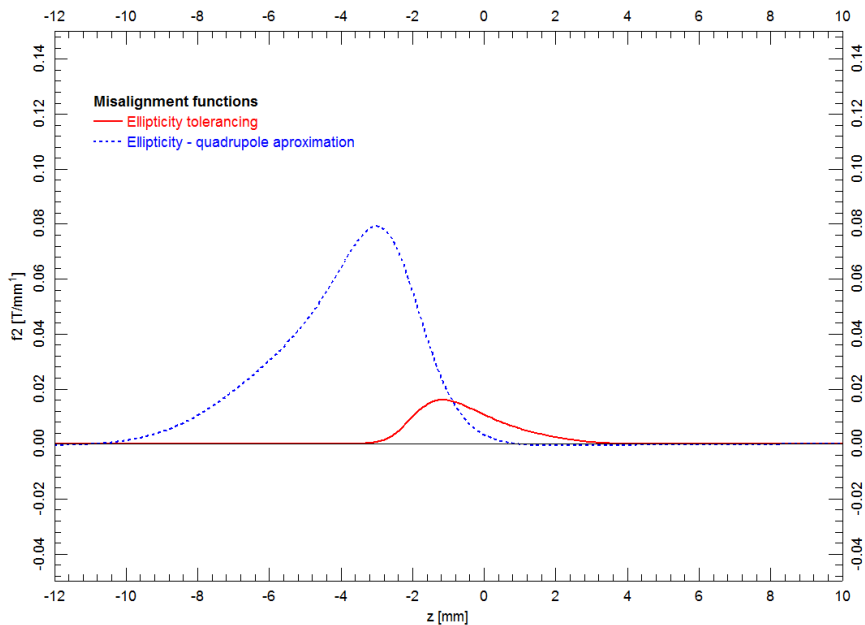


Fig. 4.8: Calculation of the axial function for ellipticity in Region D using EOD 4.001 tolerancing plugin (red line) and the quadrupole approximation (dashed blue line).

The dependency of modulus of 2-fold astigmatism $|C_{1,2}^D|$ on ellipticity for Region D is shown in Fig. 4.9. Linear trend line is plotted with following parameters with 95% confidence bands:

$$|C_{1,2}^D| = k_D \epsilon_D + K_D = ((1.398 \pm 0.005)\epsilon_D + (0.011 \pm 0.015))\mu\text{m}, \quad (4.4)$$

where $|C_{1,2}^D|$ is the modulus of the astigmatism coefficient caused by ellipticity ϵ_D introduced in Region D, k_D is the slope of the line and K_D is offset constant. K_D is supposed to be zero from the theory.

Region D has much lower influence on 2-astigmatism than Region A. It can be explained by the bigger radial distance of the Region D from the optical axis compared with Region A and different shape of their axial functions.

The ratio $g_{A,D}$ can be expressed from Eq. (4.1) and (4.4) as following:

$$g_{A,D} = \frac{k_A}{k_D} = 1.578. \quad (4.5)$$

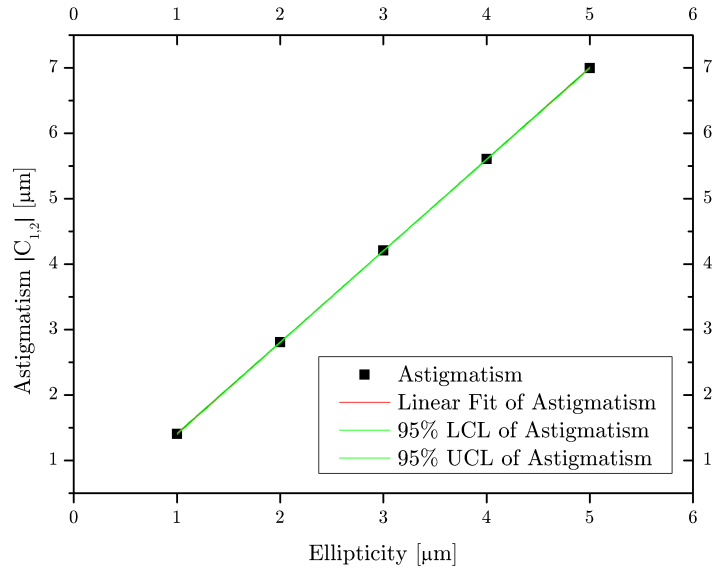


Fig. 4.9: Influence of Region D on the absolute value of the astigmatism coefficient $|C_{1,2}^D|$.

4.4. Combinations of imperfections in different regions

The lens does not suffer from independent mechanical imperfections in general so all combinations of misalignment, tilt and ellipticity were put together to simulate the real mechanical situation.

Possible combinations of misalignment and ellipticity for four regions (A, B, C, D) in the range of $\langle 0; 10 \rangle \mu\text{m}$ with step of $1 \mu\text{m}$ and tilt up to 1 mrad which are standard tolerances of the objective lens poles and their relative orientation from 0 to 90 degrees can easily exceed 10^7 independent calculations. It is not possible to do them all even in time of powerful computers.

So, the careful selection of important combinations was done assuming the worst cases of summation of imperfections in the range of typical values expected in the regions from

4.4. COMBINATIONS OF IMPERFECTIONS IN DIFFERENT REGIONS

manufacturing point of view. The results calculated for these 267 sorted and calculated combinations are shown in Tab. 6.1 in Appendix I.

4.4.1. Mechanical vs. optical mutual region rotation

It is important to highlight that there is a difference between the real mechanical mutual rotation of two regions and their optical rotation. Not only mechanical rotation of regions φ_A , φ_C and φ_D but the rotation of the electron beam Ξ_A , Ξ_C and Ξ_D caused by magnetic field has to be taken into account as it is shown Fig. 4.10.

The coefficient of 2-fold astigmatism of the regions A and C is maximum when $C_{1,2}^A$ and $C_{1,2}^C$ have the same orientation at the image plane (see Fig. 4.11). This is crucial for determining maximum allowable tolerances to reach 100% yield in the real production. $C_{1,2}$ of the particular region can be expressed as a complex number as:

$$C_{1,2} = |C_{1,2}| e^{2i(\Xi+\varphi)}, \quad (4.6)$$

where φ is the mechanical rotation of ellipticity of the region in global coordinates system and Ξ is the rotation of the meridional plane which can be calculated for magnetic lens solving trajectory equation Eq. (2.22) as:

$$\Xi_{A,B,C} = \frac{k}{2} \int_{z_{A,B,C}}^{z_{\text{specimen}}} B(z) dz, \quad (4.7)$$

where $z_{A,B,C}$ and z_{specimen} are the positions of the particular region and the specimen plane - see Fig. 4.10.

To calculate the angle of additional mechanical rotation $\Delta\varphi_C$ of the second region C (see Fig. 4.11) which maximize the astigmatism coefficient is only easy solution of maximization the sum of two complex numbers. It can be expressed as:

$$\Delta\varphi_C = \Xi_A + \varphi_A - \Xi_C - \varphi_C, \quad (4.8)$$

where Ξ_A is rotation of meridional plane from z_A to the specimen plane, φ_A is rotation of ellipticity in Region A, Ξ_C is rotation of meridional plane from z_C to the specimen plane and φ_C is rotation of ellipticity in Region C.

To prove this assumption a collection of 36 combinations of mutual rotations of Region A and C changing only by addition of 5 degrees was calculated (see Fig. 4.11). Looking at this figure we can write:

$$C_{1,2}^{A,C} = C_{1,2}^A + C_{1,2}^C. \quad (4.9)$$

4.4.2. Combined influence of Region A and D

The combination of Region A and D was chosen as the first one by the purpose because their acting region of ellipticity overlap each other. Mechanical angle for maximizing of the combined effect of these two regions $\Delta\varphi_D$ was calculated to 16 degrees with using Eq. 4.8. Ellipticity in Region A was kept at the constant value of 1, 2 and 3 μm respectively and ellipticity in Region D was changed. Their combined influence is shown in Fig 4.12.

Linear trend lines in Fig. 4.12 have following dependencies on ellipticity in Region D in combination with 1 μm in Region A as follows:

$$C_{1,2}^{A=1,D} = k_{A=1,D}\epsilon_D + K_{A=1,D} = ((1.385 \pm 0.006)\epsilon_D + (2.248 \pm 0.023))\mu\text{m}, \quad (4.10)$$

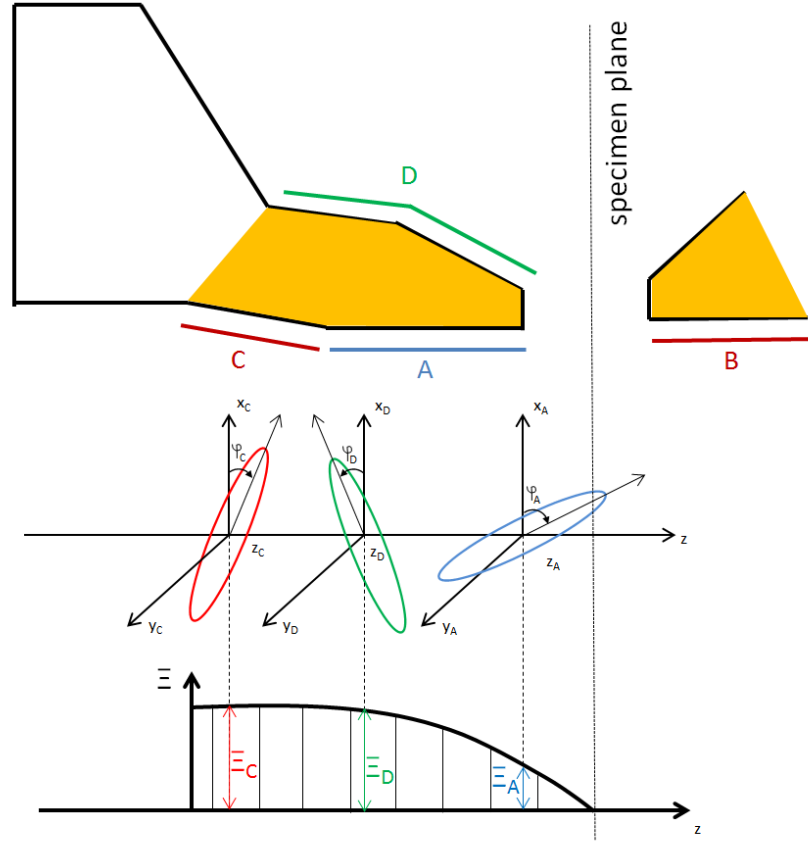


Fig. 4.10: Mechanical positions of Regions A, C and D and the rotation of meridional plane.

in combination with $2 \mu\text{m}$ in Region A as follows

$$C_{1,2}^{A=2,D} = k_{A=2,D}\epsilon_D + K_{A=2,D} = ((1.373 \pm 0.009)\epsilon_D + (4.477 \pm 0.029))\mu\text{m}, \quad (4.11)$$

in combination with $3 \mu\text{m}$ in Region A as follows

$$C_{1,2}^{A=3,D} = k_{A=3,D}\epsilon_D + K_{A=3,D} = ((1.356 \pm 0.011)\epsilon_D + (6.695 \pm 0.036))\mu\text{m}. \quad (4.12)$$

Comparing Eq. (4.1), (4.4), (4.10), (4.11) and (4.12) we can derive the general equation for the maximum total modulus of the combined 2-fold astigmatism aberration coefficient $C_{1,2}^{A,D}$ caused by a combination of ellipticities in Region A and Region D as follows:

$$C_{1,2}^{A,D} = k_A\epsilon_A + k_D\epsilon_D \quad (4.13)$$

with an very good agreement with results calculated with Eq. (4.10), (4.11) and (4.12) (maximum relative error less than 0.8%). Coefficients K_A and K_D are neglected because they are zero.

4.4.3. Cobminded influence of Region A and C

Regions A and C have the different acting area so the mechanical angle difference was expected to be higher compare to Region D. Mechanical angle φ_C maximizing the combined effect of these two regions was calculated to 43 degrees using Eq. 4.8. Ellipticity in

4.4. COMBINATIONS OF IMPERFECTIONS IN DIFFERENT REGIONS

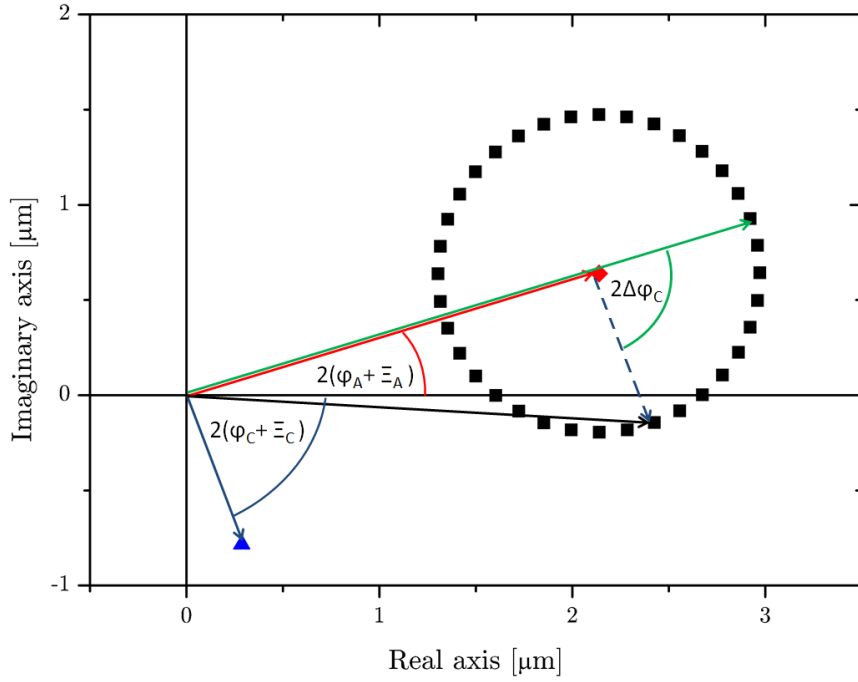


Fig. 4.11: Representation of $C_{1,2}$ for $1 \mu\text{m}$ ellipticity in regions A and C and their combination in the image plane x, y . Red arrow represents $C_{1,2}^{A=1\mu\text{m}}$, blue arrow represents $C_{1,2}^{C=1\mu\text{m}}$, dashed blue arrow represents $C_{1,2}^{C=1\mu\text{m}}$ shifted into position of $C_{1,2}^{A=1\mu\text{m}}$, green arrow represents the maximum $C_{1,2}$ caused by regions A and C, black squares represent $C_{1,2}^{A=1\mu\text{m},C}$, where $\varphi_C \in \langle 0; 180 \rangle$ degrees.

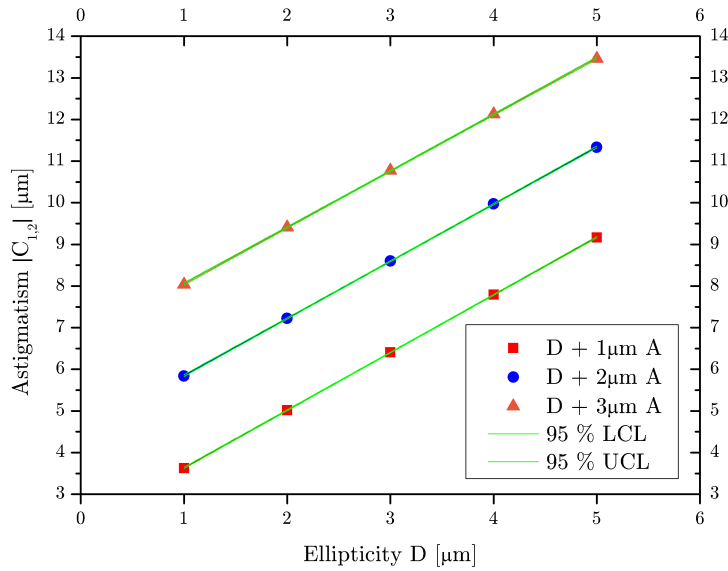


Fig. 4.12: Combined influence of Region A and D ellipticity on absolute value of astigmatism coefficient $|C_{1,2}^{A=1,2,3\mu\text{m},D}|$.

Region A was kept at the constant value of 1, 2 and $3 \mu\text{m}$ respectively and ellipticity in Region C was changed.

4. STUDY OF CONDENSER ASTIGMATISM

All results with respect to the modulus of the astigmatism coefficient $|C_{1,2}^{A,C}|$ are shown in Fig. 4.13 and are summarised in Appendix I section 6.1 calculation lines 18-31 and 40-247.

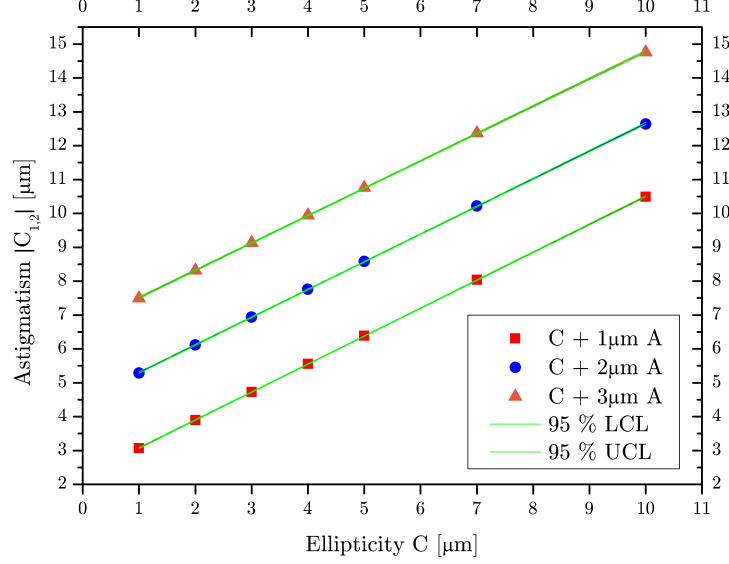


Fig. 4.13: Combined influence of Region A and C ellipticity on the modulus of astigmatism coefficient $|C_{1,2}^{A=1,2,3\mu m,C}|$.

Linear trend lines in Fig. 4.13 have following dependancies on ellipticity in Region C in combination with $1\mu m$ in Region A as follows:

$$|C_{1,2}^{A=1,C}| = k_{A=1,C}\epsilon_C + K_{A=1,C} = ((0.825 \pm 0.005)\epsilon_C + (2.252 \pm 0.023))\mu m, \quad (4.14)$$

in combination with $2\mu m$ in Region A as follows

$$|C_{1,2}^{A=2,C}| = k_{A=2,C}\epsilon_C + K_{A=2,C} = ((0.817 \pm 0.005)\epsilon_C + (4.486 \pm 0.056))\mu m, \quad (4.15)$$

in combination with $3\mu m$ in Region A as follows

$$|C_{1,2}^{A=3,C}| = k_{A=3,C}\epsilon_C + K_{A=3,C} = ((0.808 \pm 0.006)\epsilon_C + (6.705 \pm 0.036))\mu m. \quad (4.16)$$

Comparing Eq. 4.1, 4.2, 4.14, 4.15 and 4.16 we can derive a general equation for total modulus of the combined 2-fold astigmatism aberration coefficient $C_{1,2}^{A,C}$ caused by a combination of ellipticities in Region A and Region C as follows:

$$|C_{1,2}^{A,C}| = k_A\epsilon_A + k_C\epsilon_C. \quad (4.17)$$

with a very good agreement with results calculated with Eq. 4.14, 4.15 and 4.16 (relative error less than 2.8%). Coefficients K_A and K_C were neglected because they are zero.

It was found that misalignment in range below $5\mu m$ in Region A and below $5\mu m$ in Region C respectively and tilt below 1 mrad of Region A and C does not cause any additional contribution to 2-fold astigmatism (see Appendix I section 6.1 calculation lines 39-66). Coma aberration caused by these imperfections is corrected with deflection coils.

4.4.4. Combined influence of Regions A, C and D

Calculation of combined contributions of particular regions has not been done due to its high complexity. Assuming the same behavior of summation of all three regions as for duos Region A and D or Region A and C it can be written the general formula for the astigmatism coefficient $C_{1,2}^{A,C,D}$ caused by ellipticity ϵ_A , ϵ_C and ϵ_D derived from Eq. 4.9 and 4.13 and 4.17 as follows:

$$C_{1,2}^{A,C,D} = C_{1,2}^A + C_{1,2}^C + C_{1,2}^D. \quad (4.18)$$

Modulus of astigmatism coefficient $|C_{1,2}^{A,C,D}|$ for the worst case when coefficients of astigmatism of all regions are in-lined ($\varphi_C = 43$ degrees and $\varphi_D = 16$ degrees) can be calculated with using Eq. 4.1, 4.2 and 4.4 as follows:

$$|C_{1,2}^{A,C,D}| = k_A \epsilon_A + k_C \epsilon_C + k_D \epsilon_D. \quad (4.19)$$

4.5. Measurements on prototype pole pieces

Theoretical influence of different regions was calculated in the previous section. To compare results with real pole piece performances optical and mechanical measurement were performed on 26 prototype pole pieces produced for this study.

Mechanical tolerances were produced in wide range by the purpose to see the influence of different values of geometrical tolerances.

4.5.1. Optical measurement

Tested pole pieces were inserted in standard TEM microscope. Complete optical alignment procedure following the spot optimization process described in the Section 3.3 was done to minimize the influence of other system imperfections.

Correction of 2-fold astigmatism was done by the quadrupole stigmator looking at the spot shape in TEM mode and by final tuning of Ronchigram in HR-STEM (see Fig. 4.14). Ronchigram is the image of the objective back focal plane created by the beam focused to the specimen plane. That is used for final tuning because all aberrations are easier visible. This method enables us to measure stigmator current within reproducibility ± 5 mA.

Stigmator currents are used to describe 2-fold astigmatism. They can be compared with results of calculations because excitations of stigmatators are known as a result of the spot optimization process.

Summarization of optical results is shown in Tab 7.2.

4.5.2. Mechanical tolerance measurement

Outputs of machine measuring mechanical properties of pole piece surfaces are in the machinery standards as described in the Section 2.5. It is crucial to define the geometrical parameter which is in the best agreement with the ellipticity used in our calculation to ease the comparison of measured and calculated values of 2-fold astigmatism effect.

Circularity can be used to describe ellipticity only in one particular cross-section. It can vary over the length of the measured region where circularity $x_1 \neq x_2 \neq x_3$ as shown in Fig. 4.15 a).

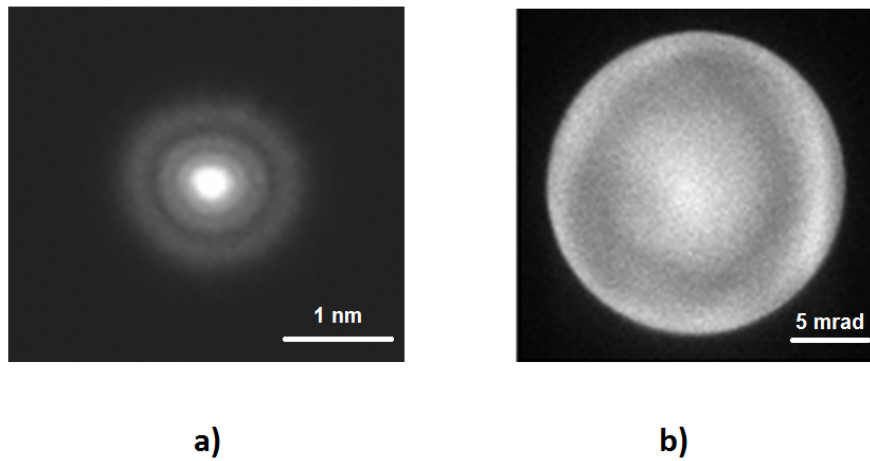


Fig. 4.14: Well corrected 2-fold astigmatism in a) TEM and b) in HR-STEM (Ronchigram).

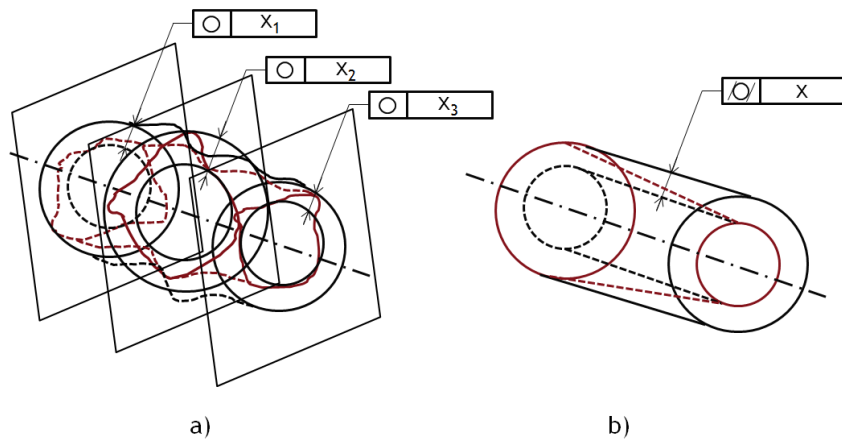


Fig. 4.15: Mechanical tolerancing description of ellipticity with help of a) circularity, b) cylindricity.

The cylindricity can be used as a better approximation but still not perfect. Cylindricity describes the integral value of imperfection and does not care about its shape. So, it can happen that the circularity of the region in any cross-section plane is zero and the cylindricity is high. It can be caused by the small diameter at the beginning of the measured region and big one at the end as shown in Fig. 4.15 b).

Runout and total runout cannot be used as well because they combine ellipticity with misalignment and tilt together. Last two imperfections do not have any influence on 2-fold astigmatism.

None of standard mechanical tolerancing method is suitable to describe ellipticity used in calculations misto is not optimal for us. So new method of mechanical properties of pole piece surface was developed. Measured region was measured at three equidistant

4.6. COMPARISON OF CALCULATED AND MEASURED VALUES

cross-section planes for circularity (see Fig. 4.15 a)) and these results were averaged to so called representative circularity as:

$$x_r = \frac{x_1 + x_2 + x_3}{3}. \quad (4.20)$$

This approach was chosen after discussions with skilled craftsmen managing measuring machines to describe the real mechanical imperfection shape as close as possible to the term of ellipticity established in EOD.

Mechanical measurements of 26 tested upper pole pieces were done with two measuring machines to minimize a systematic error:

- CIP (accuracy $(0.8 + L/200)\mu\text{m}$),
- Mahr MMQ 400 (accuracy $(20 + L/1000)\text{nm}$),

where L is the size of the measured parameter.

Complete set of measured data is listed in Appendix II section 7.1 Tab. 7.1 and 7.2. As it was mentioned in Section 4.2 only ellipticity has influence on 2-fold astigmatism. Important role on the total value of astigmatism have mutual angles of different regions. Unfortunately, mechanical measurement did not provide an information about mutual angles of regions A, C and D.

4.6. Comparison of calculated and measured values

To compare calculated and measured results the comparison of stigmator current was chosen.

Only the maximum modulus value $|C_{1,2}^{A,C,D}|$ of 2-fold astigmatism can be calculated from Eq. 4.19 using measured data because the mutual rotation data cannot be determined by measurement. Values of circularity in Region A, C and D were used for this calculation from Tab. 7.1. Expected value of 2-fold astigmatism then covers the worst situation when all regions contribute to the positive summation of their 2-fold astigmatism.

Stigmator current $I_{A,C,D}$ needed to eliminate astigmatism $|C_{1,2}^{A,C,D}|$ caused by mechanical imperfections was then calculated for each pole piece with ellipticities in its regions A,C and D according Eq. (4.19). This enables direct comparison of stigmator current found by experiment with prediction calculated from mechanical imperfections measurement of the same pole piece. Results of such comparison are shown in Fig. 4.6. All data points above the red line satisfy misto fit with the theory of the linear summation of particular region influence on 2-fold astigmatism defined by Eq. (4.19) because calculated stigmator current is the worst possible estimation. Red line represents the agreement of calculated value of stigmator current with measured under an assumption of maximal positive contribution to 2-fold astigmatism of all regions. Because of the random direction of mechanical imperfections of each region and their mutual angles the measured stigmator current is expected to be smaller than calculated.

It can be seen that only 4 from 26 data points do not agree with our assumptions. This can be explained by measuring error during mechanical or optical measurement or by material inhomogeneity which was not taken into account.

To investigate if it is really necessary to use the model describing the combined influence of Region A, C and D particular stigmator current calculation for each region

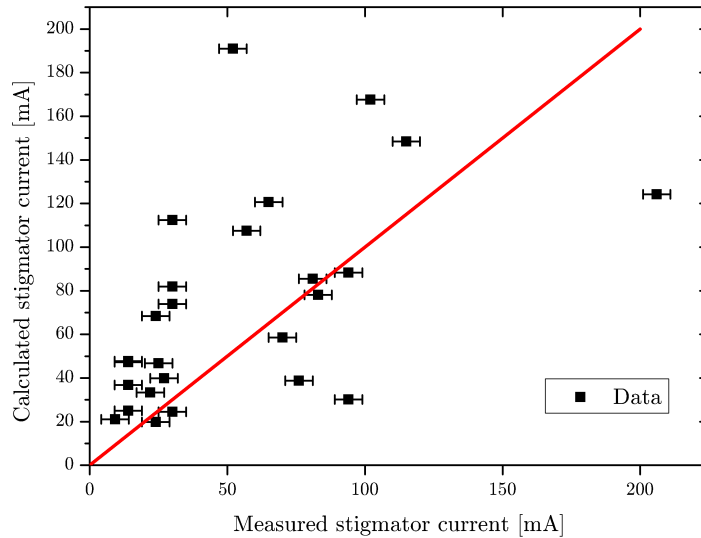


Fig. 4.16: Comparison of condenser stigmators current calculation and measurements for combined influence of Regions A, C and D. Red line represents the situation when the measured stigmator current is the same as stigmator current expected for the worst combination of mechanical imperfections of given pole piece from theory. Data points error bars are given by optical measuring accuracy ± 5 mA.

individually was done using Eq. 4.1, 4.2 and 4.4. These results are shown in Fig. 4.17, 4.18 and 4.19. It can be seen that none of these regions itself can describe the measured stigmator current values. The model combining influences of Regions A, C and D is thus necessary.

4.7. Influence of other mechanical imperfections

The influence of ellipticity on 2-fold astigmatism is obvious and is described in sections above.

Given theory tells us that misalignment and tilt (concentricity and perpendicularity in mechanical terminology) do not have any influence on astigmatism.

The measurement of circularity including its directionality was not done because it is impossible in our setup. So, it cannot be claimed that the discrepancies between measured and calculated values of stigmator currents in 16 cases are caused only by vector summation of ellipticities in regions without any proof.

To investigate possible influence of misalignment and tilt on 2-fold astigmatism the residual stigmator current I_{res} is introduced as:

$$I_{\text{res}} = I_{\text{calc}} - I_{\text{meas}}, \quad (4.21)$$

where I_{calc} is the calculated stigmator current and I_{meas} is the measured stigmator current.

Dependencies of the residual current on concentricity and perpendicularity are shown in Fig. 4.20 and 4.21.

There is not significant dependence of residual stigmator current on concentricity and perpendicularity. The distribution of points is random in both graphs. These results confirm that misalignment and tilt do not have influence on 2-fold astigmatism.

4.7. INFLUENCE OF OTHER MECHANICAL IMPERFECTIONS

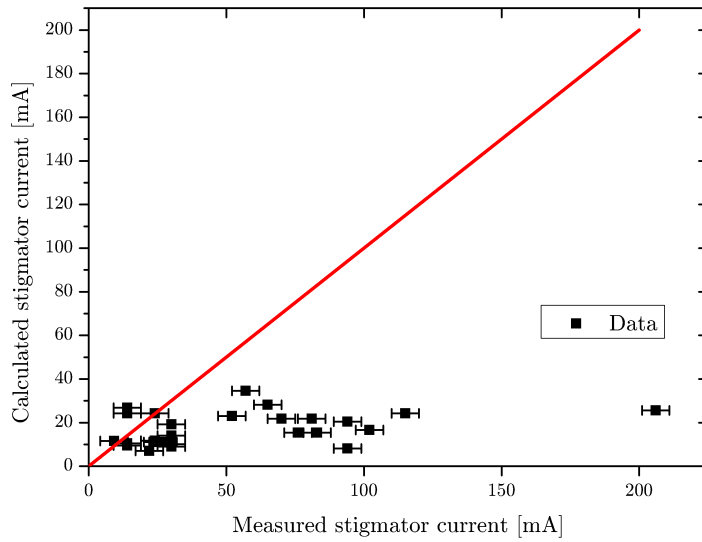


Fig. 4.17: Comparison of condenser stigmators current calculation and measurements for particular influence of Region A. Red line represents the situation when the measured stigmator current is the same as stigmator current expected for the worst combination of mechanical imperfections of given pole piece from theory. Data points error bars are given by optical measuring accuracy ± 5 mA.

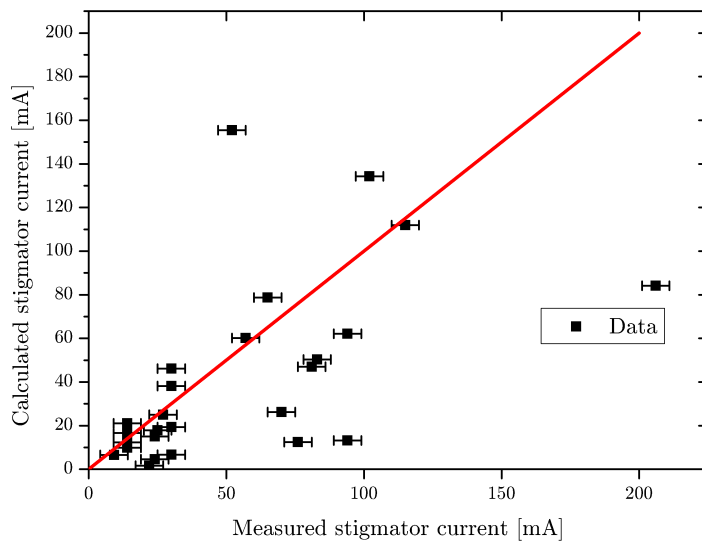


Fig. 4.18: Comparison of condenser stigmators current calculation and measurements for particular influence of Region C. Red line represents the situation when the measured stigmator current is the same as stigmator current expected for the worst combination of mechanical imperfections of given pole piece from theory. Data points error bars are given by optical measuring accuracy ± 5 mA.

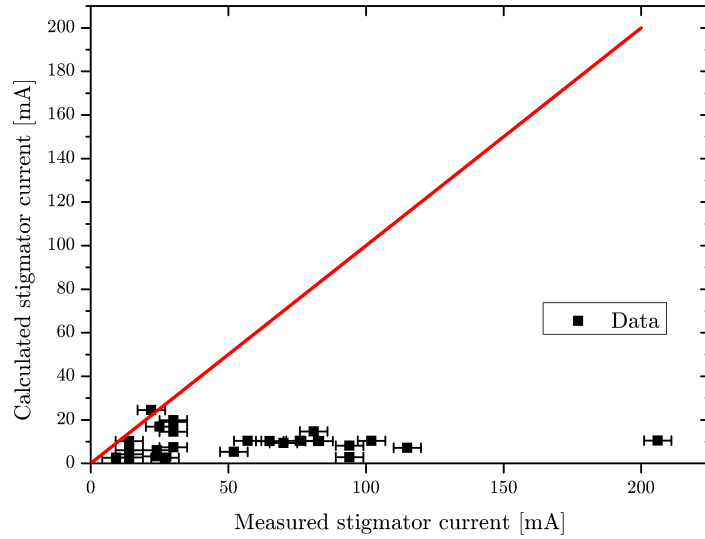


Fig. 4.19: Comparison of condenser stigmators current calculation and measurements for particular influence of Region D. Red line represents the situation when the measured stigmator current is the same as stigmator current expected for the worst combination of mechanical imperfections of given pole piece from theory. Data points error bars are given by optical measuring accuracy ± 5 mA.

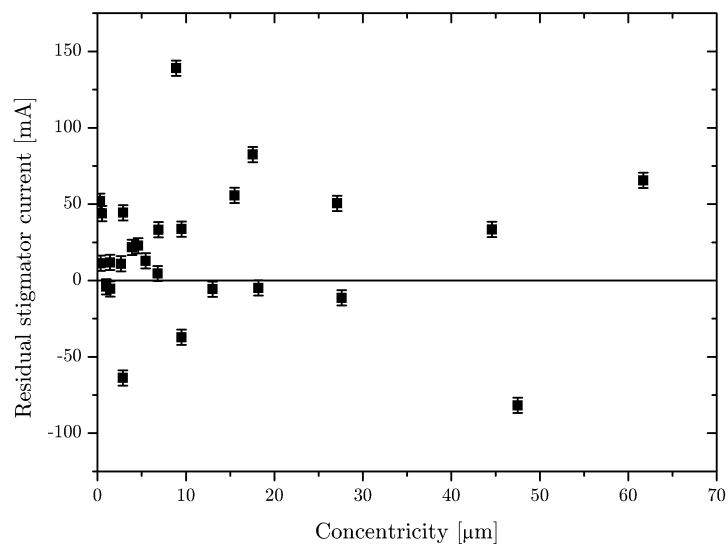


Fig. 4.20: Dependence of the residual stigmator current on concentricity between Region A and C.

4.7. INFLUENCE OF OTHER MECHANICAL IMPERFECTIONS

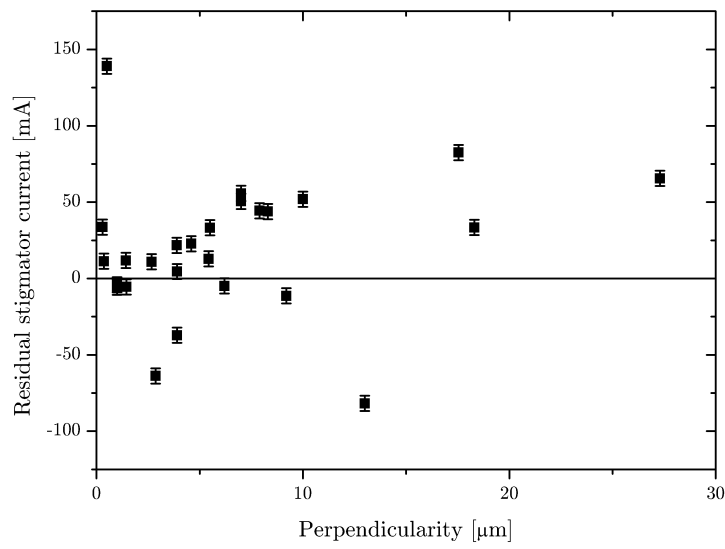


Fig. 4.21: Dependence of the residual stigmator current on perpendicularity between Region A and C.

Chapter 5

Conclusion

200 keV TEM microscope without spherical correction with resolution 0.2nm in HR-STEM was studied for 2-fold astigmatism in this work. Four pairs of saddle deflection coils and two quadrupole stigmators were used to correct aberrations.

Calculation in EOD 4.001 showed and defined critical regions of the upper pole piece of the objective lens whose mechanical imperfections have the significant influence on the condenser 2-fold astigmatism which is limiting factor to obtain desired resolution.

Newly introduced tolerancing plugin was used to investigate an influence of mechanical imperfections of the particular region and also combinations of different regions. Ellipticity, misalignment and tilt were introduced in four pole piece regions in typical values derived from their mechanical accuracies ($\langle 0; 10 \rangle \mu\text{m}$ for ellipticity, $\langle 0; 5 \rangle \mu\text{m}$ for misalignment and $\langle 0; 1 \rangle \text{mrad}$ for tilt) to express real mechanical imperfections.

Analysis of misalignment and tilt in typical geometrical tolerances below $5 \mu\text{m}$ and 1 mrad respectively showed that they do not have significant influence on 2-fold astigmatism and coma arising from these imperfections can be corrected by deflection coils.

3-fold astigmatism and other higher order aberrations were not studied because their influence on spot size is insignificant with comparison of 2-fold astigmatism.

Calculations of 2-fold astigmatism induced by ellipticity of individual regions and their combinations were done. They showed that the linear summation of influences of particular regions can be used for description of the combined influence of all regions for ellipticities smaller than $5 \mu\text{m}$ in Region A and D and $10 \mu\text{m}$ in Region C.

The theory estimating the worst possible value of 2-fold astigmatism for given mechanical tolerances of each region was compared with the experimental results on the batch of 26 prototype pole pieces made specially for this study. All pole pieces were measured for the studied geometrical tolerances and then inserted in TEM microscope to measure their 2-fold astigmatism expressed as the current of stigmators.

The best expression translating measured geometrical tolerances into ellipticity used in simulation model was found as the average of three circularities measured in equidistant distances over the studied region. Theoretically calculated stigmator current agreed with measured values in 22 from 26 cases.

This work gives the tool for designer to detect regions whose mechanical imperfections which have the significant influence to objective lens performance. Also tolerances needed to be prescribed to these regions can be determined.

5.1. Publication

The article "Calculation of the performance of magnetic lenses with limited machining precision" will be published in Ultramicroscopy Volume 137 in February 2014.

References

- [1] Zlámal, J., Lencová, B. *Development of the program EOD for design in electron and ion microscopy*, Nuclear Instruments and Methods in Physics Research A 645, 2011, p. 278–282
- [2] Wikipedia article, *Matter wave*, [http : //en.wikipedia.org/wiki/Matterwave](http://en.wikipedia.org/wiki/Matterwave), 11.12.2013
- [3] Karlík, M., *Transmisní elektronová mikroskopie: pohled do nitra materiálu*, Čs. čas.fyz. 55, 2005, p. 457–464
- [4] Dahmen, et al., *An update on the TEAM project—first results from the TEAM 0.5 microscope, and its future development.*, In Proc. 14th European Microscopy Congress, Aachen, Germany, vol. 1 (eds M. Luysberg, K. Tillmann and T. Weirich), Berlin, Germany: Springer, 2008, p. 3–4
- [5] Nebesářová, J., *Elektronová mikroskopie pro biology*, p. e-book, downloadable from: <<http://www.paru.cas.cz/lem/book/Podkap/1.0.html>>, 23.4.2008
- [6] Barth, J. E., Kruit, P., *Addition of different contributions to the charged particle probe size*, Optik 101, No.3, Wissenschaftliche Verlagsgesellschaft mbH, Stuttgart, 1996, p. 101–109
- [7] Mory, C. P., *Etude theorique et experimentale de la formation de l'image en microscopie and electronique a balayage par transmission*, PhD. thesis, Paris, 1985
- [8] Reichelt, R., *Science of Microscopy*, chapter *Scanning Electron Microscopy*, edited by: Hawkes, P. W. and Spence, J. C. H., Springer Science+Bussines Media, LLC, New York, 2007, p. 137–191. ISBN 0-387-25296-7
- [9] Hawkes, P. W., *Magnetic Electron Lenses*, Springer-Verlag, Berlin Heidelberg New York, 1982, p. 26–50, ISBN 3-540-10296-5
- [10] Hawkes, P. W., Kasper, E., *Principles of Electron Optics*, vol. 1, Academic Press Limited, London, 1996 ISBN 0-12-333341-5
- [11] Oral, M. *Určení přesných trajektorií nabitých částic a vad soustav v částicové optice*, [PhD thesis], Brno: MU, FU, 2009, p. 11–18
- [12] Lenc, M., Lencová, B., *Metody analýzy povrchu, Elektronová mikroskopie a difrakce*, chapter *Optické prvky elektronových mikroskopu*, edited by: Eckertová, L. and Frank, L., Academia, Praha, 1995, p. 20–89

REFERENCES

- [13] Lencová, B., *Částicová optika*, students learning text, p. 1–14, downloadable from: <http://www.isibrno.cz/~bohunka/co2004.pdf>, 28.4.2008
- [14] Hulínský, V., Jurek, K., *Zkoumání látek elektronovým paprskem*, SNTL - Nakladatelství technické, literatury, Praha, 1982, p. 111–258. ISBN 04-817-83
- [15] Lencová, B., Lenc, M., *Accurate computation of higher multipole components of electrostatic and magnetic deflectors with the first order FEM*, Proc. SPIE 2858, 1996, p. 58–67.
- [16] Orloff, J., *Charged Particle Optics*, CRC Press, Boca Raton, 2009, p. 249-252, 292-294 and 605-614, ISBN-13:978-1-4200-4554-3
- [17] Barthel, J., *Ultra-Precise Measurement of Optical Aberrations for Sub-Ångström Transmission Electron Microscopy*, PhD. thesis, Leipzig, 2007, p. 43–45
- [18] Munro, E., *Finite-difference programs for computing tolerances for electrostatic lenses*, J. Vac. Sci. Technol. A, Volume 243, 1988, p. 941–948.
- [19] Sturrock, P. A., *the aberration of magnetic electron lenses due to asymmetries*, Philos. Trans. R. Soc. Lond. A, Vol. 243, 1951, p. 387–429.
- [20] Sháněl, O., Zlámal, J., Oral, M., *Calculation of the performance of magnetic lenses with limited machining precision*, Ultramicroscopy 137, 2014, p. 1–6
- [21] Svoboda, P., Brandejs, J., Prokeš, F., *Základy konstruování*, Akademické, nakladatelství CERM s.r.o., Brno, 2003, p. 60–71, ISBN 80-7204-306-4
- [22] Oral, M., B. Lencová, B., *Calculation of aberration coefficients by ray tracing*, Ultramicroscopy 109, 2009, p. 1365–1373.
- [23] Komrska, J., *Fourierovské metody v teorii difrakce a ve strukturní analýze*, downloadable from <http://physics.fme.vutbr.cz/~komrska/Eng/KapF01.pdf>, 27.10.2013
- [24] *Example 2D FFT (MATLAB)*, downloadable from <http://blakertools.blogspot.cz/2012/06/testing-1-2-3.html>, 27.10.2013

Chapter 6

Appendix I

6.1. Simulation results

Following tables contain data of calculated combinations of tolerances of regions A, C and D and results of the spot optimization. Meaning of tables columns is:

- **Calc. number** - order number of tolerances combination
- **RegD elip.** - ellipticity of Region D
- **RegA elip.** - ellipticity of Region A
- **RegA elip. angle** - angle α_A of ellipticity of Region A
- **RegA mis.** - misalignment of Region A
- **RegC elip.** - ellipticity of Region C
- **RegC elip. angle** - angle α_C of ellipticity of Region C
- **RegC mis.** - misalignment of Region C
- **RegC tilt** - tilt of Region C
- **Obj. cur.** - objective lens excitation (maximal excitation is 12086 Ampere turns)
- **Up. X defl.** - upper X deflection coil excitation
- **Up. Y defl.** - upper Y deflection coil excitation
- **Low. X defl.** - upper X deflection coil excitation
- **Low. Y defl.** - upper Y deflection coil excitation
- **Stig. X** - stigmator X excitation
- **Stig. Y** - stigmator Y excitation
- **RSS stig. cur.** - total stigmator excitation $RSS_{stig.cur.} = [(Stig.X)^2 + (Stig.Y)^2]^{1/2}$
- **$C_{1,2}$** - coefficient of 2-fold astigmatism
- **$|C_{1,2}|$** - modulus of coefficient of 2-fold astigmatism

6.1. SIMULATION RESULTS

Calc. number	RegD elip.[μm]	RegA elip.[μm]	RegA elip. angle[degree]	RegA mis.[μm]
1	1	0	0	0
2	1	1	0	0
3	1	2	0	0
4	1	3	0	0
5	1	5	0	0
6	1	1	0	1
7	1	1	0	2
8	1	1	0	3
9	1	1	0	4
10	1	1	0	5
11	1	2	0	1
12	1	2	0	2
13	1	2	0	3
14	1	2	0	4
15	1	2	0	5
16	1	1	0	1
17	1	1	0	1
18	1	1	0	1
19	1	1	0	1
20	1	1	0	1
21	1	1	0	1
22	1	1	0	1
23	1	1	0	1
24	1	1	0	1
25	1	1	0	1
26	1	1	0	1
27	1	1	0	1
28	1	1	0	1
29	1	1	0	1
30	1	1	0	1
31	1	1	0	1
32	1	1	0	1
33	1	1	0	1
34	1	1	0	1
35	1	1	0	1
36	1	1	0	1
37	1	1	0	1
38	1	1	0	1
39	1	1	0	1
40	1	1	0	1

Tab. 6.1: Calculated condenser stigmator currents depends on mechanical imperfections - part I.

Calc. number	RegD elip.[μm]	RegA elip.[μm]	RegA elip. angle[degree]	RegA mis.[μm]
41	1	1	0	1
42	1	1	0	1
43	1	1	0	1
44	1	1	0	1
45	1	1	0	1
46	1	1	0	1
47	1	1	0	1
48	1	1	0	1
49	1	1	0	1
50	1	1	0	1
51	1	1	0	1
52	1	1	0	1
53	1	1	0	1
54	1	1	0	1
55	1	1	0	1
56	1	1	0	1
57	1	1	0	1
58	1	1	0	1
59	1	1	0	1
60	1	1	0	1
61	1	1	0	1
62	1	1	0	1
63	1	1	0	1
64	1	1	0	1
65	1	1	0	1
66	1	1	0	1
67	0	0	0	0
68	0	0	0	0
69	0	0	0	0
70	0	0	0	0
71	0	0	0	0
72	0	0	0	0
73	0	0	0	0
74	0	2	0	0
75	0	2	0	0
76	0	2	0	0
77	0	2	0	0
78	0	2	0	0
79	0	2	0	0
80	0	2	0	0

Tab. 6.2: Calculated condenser stigmator currents depends on mechanical imperfections - part II.

6.1. SIMULATION RESULTS

Calc. number	RegD elip.[μm]	RegA elip.[μm]	RegA elip. angle[degree]	RegA mis.[μm]
81	0	3	0	0
82	0	3	0	0
83	0	3	0	0
84	0	3	0	0
85	0	3	0	0
86	0	3	0	0
87	0	3	0	0
88	1	0	0	0
89	0	1	0	0
90	0	1	0	0
91	0	1	0	0
92	0	1	0	0
93	0	1	0	0
94	0	1	0	0
95	0	1	0	0
96	0	2	0	0
97	0	2	0	0
98	0	2	0	0
99	0	2	0	0
100	0	2	0	0
101	0	2	0	0
102	0	2	0	0
103	0	3	0	0
104	0	3	0	0
105	0	3	0	0
106	0	3	0	0
107	0	3	0	0
108	0	3	0	0
109	0	3	0	0
110	1	0	0	0
111	0	1	0	0
112	0	1	0	0
113	0	1	0	0
114	0	1	0	0
115	0	1	0	0
116	0	1	0	0
117	0	1	0	0
118	0	2	0	0
119	0	2	0	0
120	0	2	0	0

Tab. 6.3: Calculated condenser stigmator currents depends on mechanical imperfections - part III.

Calc. number	RegD elip.[μm]	RegA elip.[μm]	RegA elip. angle[degree]	RegA mis.[μm]
121	0	2	0	0
122	0	2	0	0
123	0	2	0	0
124	0	2	0	0
125	0	3	0	0
126	0	3	0	0
127	0	3	0	0
128	0	3	0	0
129	0	3	0	0
130	0	3	0	0
131	0	3	0	0
132	1	1	0	0
133	2	1	0	0
134	3	1	0	0
135	4	1	0	0
136	5	1	0	0
137	1	2	0	0
138	2	2	0	0
139	3	2	0	0
140	4	2	0	0
141	5	2	0	0
142	1	3	0	0
143	2	3	0	0
144	3	3	0	0
145	4	3	0	0
146	5	3	0	0
147	1	4	0	0
148	2	4	0	0
149	3	4	0	0
150	4	4	0	0
151	5	4	0	0
152	1	5	0	0
153	2	5	0	0
154	3	5	0	0
155	4	5	0	0
156	5	5	0	0
157	1	0	0	0
158	2	0	0	0
159	3	0	0	0
160	4	0	0	0

Tab. 6.4: Calculated condenser stigmator currents depends on mechanical imperfections - part IV.

6.1. SIMULATION RESULTS

Calc. number	RegD elip. [μm]	RegA elip. [μm]	RegA elip. angle [degree]	RegA mis. [μm]
161	5	0	0	0
162	0	0	0	0
163	0	0	0	0
164	0	0	0	0
165	0	0	0	0
166	0	0	0	0
167	0	0	0	0
168	0	0	0	0
169	1	0	0	0
170	0	1	0	0
171	0	1	0	0
172	0	1	0	0
173	0	1	0	0
174	0	1	0	0
175	0	1	0	0
176	0	1	0	0
177	0	2	0	0
178	0	2	0	0
179	0	2	0	0
180	0	2	0	0
181	0	2	0	0
182	0	2	0	0
183	0	2	0	0
184	0	3	0	0
185	0	3	0	0
186	0	3	0	0
187	0	3	0	0
188	0	3	0	0
189	0	3	0	0
190	0	3	0	0
191	0	1	0	0
192	0	1	0	0
193	0	1	0	0
194	0	1	0	0
195	0	1	0	0
196	0	1	0	0
197	0	1	0	0
198	0	1	0	0
199	0	1	0	0
200	0	1	0	0

Tab. 6.5: Calculated condenser stigmator currents depends on mechanical imperfections - part V.

Calc. number	RegD elip.[μm]	RegA elip.[μm]	RegA elip. angle[degree]	RegA mis.[μm]
201	0	1	0	0
202	0	1	0	0
203	0	1	0	0
204	0	1	0	0
205	0	1	0	0
206	0	1	0	0
207	0	1	0	0
208	0	1	0	0
209	0	1	0	0
210	0	1	0	0
211	0	1	0	0
212	0	1	0	0
213	0	1	0	0
214	0	1	0	0
215	0	1	0	0
216	0	1	0	0
217	0	1	0	0
218	0	1	0	0
219	0	1	0	0
220	0	1	0	0
221	0	1	0	0
222	0	1	0	0
223	0	1	0	0
224	0	1	0	0
225	0	1	0	0
226	0	1	0	0
227	0	1	0	0
228	0	1	0	0
229	0	1	0	0
230	0	1	0	0
231	0	1	0	0
232	0	1	0	0
233	0	1	0	0
234	0	2	0	0
235	0	2	0	0
236	0	2	0	0
237	0	2	0	0
238	0	2	0	0
239	0	2	0	0
240	0	2	0	0

Tab. 6.6: Calculated condenser stigmator currents depends on mechanical imperfections - part VI.

6.1. SIMULATION RESULTS

Calc. number	RegD elip.[μm]	RegA elip.[μm]	RegA elip. angle[degree]	RegA mis.[μm]
241	0	3	0	0
242	0	3	0	0
243	0	3	0	0
244	0	3	0	0
245	0	3	0	0
246	0	3	0	0
247	0	3	0	0
248	1	0	15	0
249	2	0	16	0
250	3	0	16	0
251	4	0	16	0
252	5	0	16	0
253	1	1	16	0
254	2	1	16	0
255	3	1	16	0
256	4	1	16	0
257	5	1	16	0
258	1	1	-15	0
259	1	2	16	0
260	2	2	16	0
261	3	2	16	0
262	4	2	16	0
263	5	2	16	0
264	1	3	16	0
265	2	3	16	0
266	3	3	16	0
267	4	3	16	0
268	5	3	16	0
269	1	1	-10	0
270	1	1	-5	0
271	1	1	5	0
272	1	1	10	0
273	1	1	15	0
274	1	1	25	0
275	1	1	30	0
276	1	1	35	0
277	1	1	40	0
278	1	1	45	0
279	1	1	50	0

Tab. 6.7: Calculated condenser stigmator currents depends on mechanical imperfections - part VII.

Calc. number	RegC elip.[μm]	RegA elip. angle[deg]	RegC mis.[μm]	RegC mis.[deg]
1	0	0	0	0
2	0	0	0	0
3	0	0	0	0
4	0	0	0	0
5	0	0	0	0
6	0	0	0	0
7	0	0	0	0
8	0	0	0	0
9	0	0	0	0
10	0	0	0	0
11	0	0	0	0
12	0	0	0	0
13	0	0	0	0
14	0	0	0	0
15	0	0	0	0
16	0	0	0	0
17	0	0	0	0
18	1	0	0	0
19	2	0	0	0
20	3	0	0	0
21	4	0	0	0
22	5	0	0	0
23	7	0	0	0
24	10	0	0	0
25	1	90	0	0
26	2	90	0	0
27	3	90	0	0
28	4	90	0	0
29	5	90	0	0
30	7	90	0	0
31	10	90	0	0
32	0	0	1	0
33	0	0	2	0
34	0	0	3	0
35	0	0	4	0
36	0	0	5	0
37	0	0	7	0
38	0	0	10	0
39	2	0	1	0
40	2	0	2	0

Tab. 6.8: Calculated condenser stigmator currents depends on mechanical imperfections - part VIII.

6.1. SIMULATION RESULTS

Calc. number	RegC elip. [μm]	RegA elip. angle [deg]	RegC mis. [μm]	RegC mis. [deg]
41	2	0	3	0
42	2	0	4	0
43	2	0	5	0
44	2	0	7	0
45	2	0	10	0
46	5	0	1	0
47	5	0	2	0
48	5	0	3	0
49	5	0	4	0
50	5	0	5	0
51	5	0	7	0
52	5	0	10	0
53	2	0	1	0
54	2	0	2	0
55	2	0	3	0
56	2	0	4	0
57	2	0	5	0
58	2	0	7	0
59	2	0	10	0
60	5	0	1	0
61	5	0	2	0
62	5	0	3	0
63	5	0	4	0
64	5	0	5	0
65	5	0	7	0
66	5	0	10	0
67	1	0	0	0
68	2	0	0	0
69	3	0	0	0
70	4	0	0	0
71	5	0	0	0
72	7	0	0	0
73	10	0	0	0
74	1	0	0	0
75	2	0	0	0
76	3	0	0	0
77	4	0	0	0
78	5	0	0	0
79	7	0	0	0
80	10	0	0	0

Tab. 6.9: Calculated condenser stigmator currents depends on mechanical imperfections - part IX.

Calc. number	RegC elip.[μm]	RegA elip. angle[deg]	RegC mis.[μm]	RegC mis.[deg]
81	1	0	0	0
82	2	0	0	0
83	3	0	0	0
84	4	0	0	0
85	5	0	0	0
86	7	0	0	0
87	10	0	0	0
88	0	-26	0	0
89	1	-26	0	0
90	2	-26	0	0
91	3	-26	0	0
92	4	-26	0	0
93	5	-26	0	0
94	7	-26	0	0
95	10	-26	0	0
96	1	-26	0	0
97	2	-26	0	0
98	3	-26	0	0
99	4	-26	0	0
100	5	-26	0	0
101	7	-26	0	0
102	10	-26	0	0
103	1	-26	0	0
104	2	-26	0	0
105	3	-26	0	0
106	4	-26	0	0
107	5	-26	0	0
108	7	-26	0	0
109	10	-26	0	0
110	0	-116	0	0
111	1	-116	0	0
112	2	-116	0	0
113	3	-116	0	0
114	4	-116	0	0
115	5	-116	0	0
116	7	-116	0	0
117	10	-116	0	0
118	1	-116	0	0
119	2	-116	0	0
120	3	-116	0	0

Tab. 6.10: Calculated condenser stigmator currents depends on mechanical imperfections - part X.

6.1. SIMULATION RESULTS

Calc. number	RegC elip. [μm]	RegA elip. angle [deg]	RegC mis. [μm]	RegC mis. [deg]
121	4	-116	0	0
122	5	-116	0	0
123	7	-116	0	0
124	10	-116	0	0
125	1	-116	0	0
126	2	-116	0	0
127	3	-116	0	0
128	4	-116	0	0
129	5	-116	0	0
130	7	-116	0	0
131	10	-116	0	0
132	0	0	0	0
133	0	0	0	0
134	0	0	0	0
135	0	0	0	0
136	0	0	0	0
137	0	0	0	0
138	0	0	0	0
139	0	0	0	0
140	0	0	0	0
141	0	0	0	0
142	0	0	0	0
143	0	0	0	0
144	0	0	0	0
145	0	0	0	0
146	0	0	0	0
147	0	0	0	0
148	0	0	0	0
149	0	0	0	0
150	0	0	0	0
151	0	0	0	0
152	0	0	0	0
153	0	0	0	0
154	0	0	0	0
155	0	0	0	0
156	0	0	0	0
157	0	0	0	0
158	0	0	0	0
159	0	0	0	0
160	0	0	0	0

Tab. 6.11: Calculated condenser stigmator currents depends on mechanical imperfections - part XI.

Calc. number	RegC elip.[μm]	RegA elip. angle[deg]	RegC mis.[μm]	RegC mis.[deg]
161	0	0	0	0
162	1	0	0	0
163	2	0	0	0
164	3	0	0	0
165	4	0	0	0
166	5	0	0	0
167	7	0	0	0
168	10	0	0	0
169	0	-15	0	0
170	1	-15	0	0
171	2	-15	0	0
172	3	-15	0	0
173	4	-15	0	0
174	5	-15	0	0
175	7	-15	0	0
176	10	-15	0	0
177	1	-15	0	0
178	2	-15	0	0
179	3	-15	0	0
180	4	-15	0	0
181	5	-15	0	0
182	7	-15	0	0
183	10	-15	0	0
184	1	-15	0	0
185	2	-15	0	0
186	3	-15	0	0
187	4	-15	0	0
188	5	-15	0	0
189	7	-15	0	0
190	10	-15	0	0
191	1	5	0	0
192	1	10	0	0
193	1	15	0	0
194	1	20	0	0
195	1	25	0	0
196	1	30	0	0
197	1	35	0	0
198	1	40	0	0
199	1	45	0	0
200	1	50	0	0

Tab. 6.12: Calculated condenser stigmator currents depends on mechanical imperfections - part XII.

6.1. SIMULATION RESULTS

Calc. number	RegC elip. [μm]	RegA elip. angle [deg]	RegC mis. [μm]	RegC mis. [deg]
201	1	55	0	0
202	1	60	0	0
203	1	65	0	0
204	1	70	0	0
205	1	75	0	0
206	1	80	0	0
207	1	85	0	0
208	1	90	0	0
209	1	95	0	0
210	1	100	0	0
211	1	105	0	0
212	1	110	0	0
213	1	115	0	0
214	1	120	0	0
215	1	125	0	0
216	1	130	0	0
217	1	135	0	0
218	1	140	0	0
219	1	145	0	0
220	1	150	0	0
221	1	155	0	0
222	1	160	0	0
223	1	165	0	0
224	1	170	0	0
225	1	175	0	0
226	1	180	0	0
227	1	43	0	0
228	2	43	0	0
229	3	43	0	0
230	4	43	0	0
231	5	43	0	0
232	7	43	0	0
233	10	43	0	0
234	1	43	0	0
235	2	43	0	0
236	3	43	0	0
237	4	43	0	0
238	5	43	0	0
239	7	43	0	0
240	10	43	0	0

Tab. 6.13: Calculated condenser stigmator currents depends on mechanical imperfections - part XIII.

Calc. number	RegC elip.[μm]	RegA elip. angle[deg]	RegC mis.[μm]	RegC mis.[deg]
241	1	43	0	0
242	2	43	0	0
243	3	43	0	0
244	4	43	0	0
245	5	43	0	0
246	7	43	0	0
247	10	43	0	0
248	0	0	0	0
249	0	0	0	0
250	0	0	0	0
251	0	0	0	0
252	0	0	0	0
253	0	0	0	0
254	0	0	0	0
255	0	0	0	0
256	0	0	0	0
257	0	0	0	0
258	0	0	0	0
259	0	0	0	0
260	0	0	0	0
261	0	0	0	0
262	0	0	0	0
263	0	0	0	0
264	0	0	0	0
265	0	0	0	0
266	0	0	0	0
267	0	0	0	0
268	0	0	0	0
269	0	0	0	0
270	0	0	0	0
271	0	0	0	0
272	0	0	0	0
273	0	0	0	0
274	0	0	0	0
275	0	0	0	0
276	0	0	0	0
277	0	0	0	0
278	0	0	0	0
279	0	0	0	0

Tab. 6.14: Calculated condenser stigmator currents depends on mechanical imperfections - part XIV.

6.1. SIMULATION RESULTS

Calc. number	RegC tilt [mrad]	Obj. cur. [Max exc.]	Up. X defl[A]	Up. Y defl.[A]
1	0	0.99987	0.000000	0.000000
2	0	0.99986	0.000002	-0.000003
3	0	0.99981	0.000000	0.000000
4	0	0.99973	0.000000	0.000000
5	0	0.99948	0.000001	-0.000002
6	0	0.99986	0.009008	-0.010527
7	0	0.99986	0.018011	-0.021045
8	0	0.99986	0.027018	-0.031569
9	0	0.99986	0.036028	-0.042099
10	0	0.99985	0.045047	-0.052643
11	0	0.99981	0.009001	-0.010515
12	0	0.99981	0.018016	-0.021052
13	0	0.99981	0.027031	-0.031589
14	0	0.99981	0.036054	-0.042140
15	0	0.99981	0.045081	-0.052696
16	0	0.99986	0.009008	-0.010527
17	0	0.99985	0.078946	-0.091654
18	0	0.99984	0.079037	-0.091758
19	0	0.99984	0.079129	-0.091863
20	0	0.99983	0.079220	-0.091969
21	0	0.99981	0.079307	-0.092066
22	0	0.99979	0.079398	-0.092171
23	0	0.99974	0.079580	-0.092380
24	0	0.99964	0.079838	-0.092669
25	0	0.99985	0.078853	-0.091546
26	0	0.99984	0.078779	-0.091468
27	0	0.99983	0.078698	-0.091379
28	0	0.99982	0.078613	-0.091284
29	0	0.99980	0.078525	-0.091185
30	0	0.99975	0.078352	-0.090990
31	0	0.99966	0.078094	-0.090698
32	0	0.99985	0.083713	-0.097014
33	0	0.99985	0.088484	-0.102382
34	0	0.99985	0.093243	-0.107728
35	0	0.99984	0.098021	-0.113107
36	0	0.99984	0.102792	-0.118474
37	0	0.99984	0.112329	-0.129200
38	0	0.99984	0.126650	-0.145315
39	0	0.99984	0.083897	-0.097226
40	0	0.99984	0.088667	-0.102593

Tab. 6.15: Calculated condenser stigmator currents depends on mechanical imperfections - part XV.

Calc. number	RegC tilt [mrad]	Obj. cur. [Max exc.]	Up. X defl.[A]	Up. Y defl.[A]
41	0	0.99984	0.093444	-0.107969
42	0	0.99984	0.098213	-0.113333
43	0	0.99983	0.102977	-0.118689
44	0	0.99983	0.112517	-0.129421
45	0	0.99983	0.126824	-0.145515
46	0	0.99979	0.084164	-0.097531
47	0	0.99979	0.088932	-0.102894
48	0	0.99979	0.093698	-0.108254
49	0	0.99979	0.098469	-0.113622
50	0	0.99979	0.103236	-0.118984
51	0	0.99979	0.112772	-0.129711
52	0	0.99979	0.127075	-0.145799
53	1	0.99983	0.114849	-0.132303
54	1	0.99983	0.119620	-0.137670
55	1	0.99983	0.124390	-0.143035
56	1	0.99983	0.129150	-0.148385
57	1	0.99983	0.133929	-0.153766
58	1	0.99983	0.143465	-0.164491
59	1	0.99983	0.157775	-0.180590
60	1	0.99979	0.115105	-0.132592
61	1	0.99979	0.119875	-0.137959
62	1	0.99979	0.124644	-0.143324
63	1	0.99979	0.129413	-0.148688
64	1	0.99979	0.134182	-0.154055
65	1	0.99979	0.143720	-0.164784
66	1	0.99978	0.158018	-0.180865
67	0	0.99987	0.000000	0.000000
68	0	0.99987	0.000000	0.000000
69	0	0.99986	0.000002	-0.000003
70	0	0.99984	0.000002	-0.000002
71	0	0.99982	0.000002	-0.000004
72	0	0.99978	0.000002	-0.000004
73	0	0.99968	0.000000	0.000000
74	0	0.99981	0.000000	0.000001
75	0	0.99980	0.000000	0.000000
76	0	0.99979	0.000000	0.000000
77	0	0.99977	-0.000001	0.000002
78	0	0.99975	0.000000	0.000000
79	0	0.99970	0.000000	0.000000
80	0	0.99960	0.000000	0.000001

Tab. 6.16: Calculated condenser stigmator currents depends on mechanical imperfections - part XVI.

6.1. SIMULATION RESULTS

Calc. number	RegC tilt [mrad]	Obj. cur. [Max exc.]	Up. X defl[A]	Up. Y defl.[A]
81	0	0.99973	0.000001	-0.000002
82	0	0.99972	0.000001	-0.000001
83	0	0.99971	0.000000	0.000000
84	0	0.99969	0.000000	0.000000
85	0	0.99967	0.000001	-0.000002
86	0	0.99962	0.000000	0.000000
87	0	0.99952	0.000000	0.000000
88	0	0.99987	0.000000	0.000000
89	0	0.99985	0.000000	0.000000
90	0	0.99983	0.000000	0.000000
91	0	0.99981	0.000000	0.000000
92	0	0.99979	0.000002	-0.000003
93	0	0.99976	0.000001	-0.000001
94	0	0.99970	0.000000	0.000000
95	0	0.99957	0.000000	0.000000
96	0	0.99979	0.000000	0.000001
97	0	0.99977	0.000001	-0.000001
98	0	0.99974	0.000001	-0.000001
99	0	0.99971	0.000000	0.000000
100	0	0.99967	-0.000001	0.000002
101	0	0.99959	0.000000	0.000000
102	0	0.99944	0.000000	0.000000
103	0	0.99970	0.000001	-0.000002
104	0	0.99967	0.000000	0.000001
105	0	0.99964	0.000000	0.000001
106	0	0.99960	0.000000	0.000000
107	0	0.99955	-0.000001	0.000001
108	0	0.99945	0.000000	0.000000
109	0	0.99928	0.000000	0.000000
110	0	0.99987	0.000000	0.000000
111	0	0.99986	0.000000	0.000000
112	0	0.99987	0.000001	-0.000002
113	0	0.99987	0.000000	0.000000
114	0	0.99986	0.000002	-0.000003
115	0	0.99985	-0.000001	0.000001
116	0	0.99982	0.000002	-0.000004
117	0	0.99975	-0.000001	0.000002
118	0	0.99983	0.000000	0.000000
119	0	0.99984	-0.000002	0.000003
120	0	0.99985	-0.000001	0.000002

Tab. 6.17: Calculated condenser stigmator currents depends on mechanical imperfections - part XVII.

Calc. number	RegC tilt [mrad]	Obj. cur. [Max exc.]	Up. X defl.[A]	Up. Y defl.[A]
121	0	0.99985	0.000000	0.000000
122	0	0.99985	0.000001	-0.000001
123	0	0.99984	0.000000	0.000000
124	0	0.99979	0.000001	-0.000001
125	0	0.99976	0.000000	0.000000
126	0	0.99978	0.000001	-0.000002
127	0	0.99979	0.000002	-0.000003
128	0	0.99981	0.000000	0.000000
129	0	0.99982	-0.000001	0.000001
130	0	0.99982	0.000001	-0.000002
131	0	0.99980	0.000000	0.000000
132	0	0.99983	-0.000001	0.000002
133	0	0.99980	0.000001	-0.000001
134	0	0.99975	0.000000	0.000000
135	0	0.99970	0.000000	0.000001
136	0	0.99962	0.000002	-0.000004
137	0	0.99977	-0.000001	0.000001
138	0	0.99972	0.000000	0.000000
139	0	0.99966	0.000000	0.000000
140	0	0.99958	-0.000001	0.000002
141	0	0.99950	-0.000002	0.000003
142	0	0.99968	-0.000002	0.000003
143	0	0.99961	0.000000	0.000000
144	0	0.99953	0.000000	-0.000001
145	0	0.99944	0.000001	-0.000001
146	0	0.99934	0.000000	0.000000
147	0	0.99955	0.000001	-0.000001
148	0	0.99947	-0.000002	0.000003
149	0	0.99937	0.000000	0.000000
150	0	1.00005	0.000000	0.000000
151	0	0.99981	0.000000	0.000000
152	0	0.99940	0.000000	0.000001
153	0	0.99930	0.000000	0.000000
154	0	0.99919	-0.000002	0.000003
155	0	0.99907	-0.000001	0.000002
156	0	0.99894	0.000000	0.000000
157	0	0.99987	0.000000	0.000001
158	0	0.99985	0.000000	0.000000
159	0	0.99982	0.000001	-0.000002
160	0	0.99978	-0.000001	0.000002

Tab. 6.18: Calculated condenser stigmator currents depends on mechanical imperfections - part XVIII.

6.1. SIMULATION RESULTS

Calc. number	RegC tilt [mrad]	Obj. cur. [Max exc.]	Up. X defl[A]	Up. Y defl.[A]
161	0	0.99972	0.000000	0.000000
162	0	0.99987	0.000000	0.000000
163	0	0.99987	0.000001	-0.000001
164	0	0.99986	-0.000004	0.000007
165	0	0.99984	-0.000002	0.000003
166	0	0.99982	0.000002	-0.000004
167	0	0.99978	0.000001	-0.000002
168	0	0.99968	0.000000	0.000001
169	0	0.99987	0.000001	-0.000001
170	0	0.99985	0.000002	-0.000003
171	0	0.99984	0.000001	-0.000001
172	0	0.99982	-0.000001	0.000002
173	0	0.99980	0.000000	0.000000
174	0	0.99978	0.000002	-0.000004
175	0	0.99972	0.000000	0.000000
176	0	0.99960	-0.000001	0.000002
177	0	0.99980	0.000002	-0.000004
178	0	0.99978	0.000001	-0.000001
179	0	0.99976	-0.000001	0.000001
180	0	0.99973	0.000000	-0.000001
181	0	0.99970	0.000000	0.000000
182	0	0.99963	0.000000	0.000000
183	0	0.99950	0.000001	-0.000001
184	0	0.99971	-0.000001	0.000001
185	0	0.99969	0.000000	0.000000
186	0	0.99966	0.000000	0.000000
187	0	0.99963	0.000000	0.000000
188	0	0.99960	0.000000	0.000000
189	0	0.99951	-0.000001	0.000002
190	0	0.99936	0.000000	0.000000
191	0	0.99986	0.000000	0.000001
192	0	0.99986	0.000000	0.000001
193	0	0.99986	0.000000	0.000000
194	0	0.99986	0.000001	-0.000002
195	0	0.99986	0.000000	0.000000
196	0	0.99986	-0.000001	0.000001
197	0	0.99987	0.000000	0.000000
198	0	0.99987	-0.000001	0.000002
199	0	0.99987	0.000002	-0.000003
200	0	0.99987	0.000000	0.000000

Tab. 6.19: Calculated condenser stigmator currents depends on mechanical imperfections - part XIX.

Calc. number	RegC tilt [mrad]	Obj. cur. [Max exc.]	Up. X defl.[A]	Up. Y defl.[A]
201	0	0.99987	0.000000	0.000000
202	0	0.99987	0.000000	0.000000
203	0	0.99986	-0.000001	0.000001
204	0	0.99986	0.000000	0.000000
205	0	0.99986	0.000000	0.000000
206	0	0.99986	0.000002	-0.000004
207	0	0.99986	-0.000001	0.000001
208	0	0.99986	0.000002	-0.000003
209	0	0.99985	-0.000003	0.000005
210	0	0.99985	-0.000001	0.000002
211	0	0.99985	0.000002	-0.000004
212	0	0.99985	0.000000	-0.000001
213	0	0.99985	0.000003	-0.000005
214	0	0.99985	-0.000001	0.000001
215	0	0.99985	0.000000	0.000000
216	0	0.99985	0.000000	0.000000
217	0	0.99985	0.000000	0.000000
218	0	0.99985	0.000000	0.000000
219	0	0.99985	0.000000	0.000000
220	0	0.99985	0.000000	0.000000
221	0	0.99985	0.000000	0.000000
222	0	0.99985	0.000004	-0.000006
223	0	0.99985	0.000003	-0.000004
224	0	0.99985	-0.000001	0.000001
225	0	0.99985	-0.000001	0.000001
226	0	0.99985	0.000002	-0.000003
227	0	0.99985	0.000000	0.000000
228	0	0.99983	0.000000	0.000000
229	0	0.99981	0.000000	0.000000
230	0	0.99978	0.000001	-0.000002
231	0	0.99975	0.000001	-0.000001
232	0	0.99969	-0.000001	0.000002
233	0	0.99955	0.000000	0.000000
234	0	0.99979	-0.000001	0.000002
235	0	0.99976	-0.000001	0.000002
236	0	0.99973	0.000000	0.000000
237	0	0.99969	0.000000	0.000000
238	0	0.99966	-0.000002	0.000003
239	0	0.99957	-0.000001	0.000001
240	0	0.99940	0.000001	-0.000001

Tab. 6.20: Calculated condenser stigmator currents depends on mechanical imperfections - part XX.

6.1. SIMULATION RESULTS

Calc. number	RegC tilt [mrad]	Obj. cur. [Max exc.]	Up. X defl[A]	Up. Y defl.[A]
241	0	0.99970	0.000000	0.000000
242	0	0.99966	-0.000001	0.000001
243	0	0.99962	-0.000001	0.000001
244	0	0.99957	0.000001	-0.000002
245	0	0.99953	0.000000	0.000000
246	0	0.99942	0.000000	0.000000
247	0	0.99922	0.000002	-0.000003
248	0	0.99987	0.000001	-0.000001
249	0	0.99985	-0.000001	0.000001
250	0	0.99982	0.000000	-0.000001
251	0	0.99978	0.000001	-0.000002
252	0	0.99972	0.000000	0.000000
253	0	0.99983	0.000000	0.000000
254	0	0.99980	0.000000	-0.000001
255	0	0.99975	0.000001	-0.000001
256	0	0.99969	0.000000	0.000000
257	0	0.99961	0.000002	-0.000003
258	0	0.99984	0.000000	0.000000
259	0	0.99977	0.000000	0.000000
260	0	0.99971	0.000000	0.000000
261	0	0.99964	0.000000	0.000000
262	0	0.99956	0.000002	-0.000003
263	0	0.99947	0.000000	0.000000
264	0	0.99967	0.000000	0.000000
265	0	0.99959	0.000001	-0.000002
266	0	0.99951	0.000000	0.000000
267	0	0.99941	0.000000	0.000000
268	0	0.99930	0.000000	0.000000
269	0	0.99984	0.000000	0.000001
270	0	0.99984	0.000000	0.000000
271	0	0.99983	0.000000	0.000000
272	0	0.99983	0.000000	0.000000
273	0	0.99983	0.000000	0.000000
274	0	0.99983	0.000000	0.000000
275	0	0.99983	0.000000	0.000000
276	0	0.99984	-0.000001	0.000001
277	0	0.99984	0.000000	0.000000
278	0	0.99984	0.000000	0.000001
279	0	0.99984	-0.000002	0.000004

Tab. 6.21: Calculated condenser stigmator currents depends on mechanical imperfections - part XXI.

Calc. number	Low. X defl.[A]	Low. Y defl.[A]	Stig. X[A]	Stig. Y[A]
1	0.000000	0.000000	0.000003	0.000002
2	-0.000003	0.000004	-0.003692	-0.012396
3	0.000001	-0.000002	-0.007371	-0.024749
4	0.000000	0.000000	-0.011023	-0.037051
5	0.000000	0.000000	-0.018198	-0.061296
6	-0.017121	0.019492	-0.003689	-0.012401
7	-0.034243	0.038984	-0.003687	-0.012401
8	-0.051360	0.058469	-0.003686	-0.012401
9	-0.068487	0.077971	-0.003677	-0.012404
10	-0.085608	0.097462	-0.003668	-0.012410
11	-0.017123	0.019490	-0.007368	-0.024761
12	-0.034254	0.038992	-0.007367	-0.024761
13	-0.051387	0.058495	-0.007362	-0.024766
14	-0.068528	0.078013	-0.007357	-0.024771
15	-0.085669	0.097531	-0.007347	-0.024771
16	-0.017121	0.019492	-0.003689	-0.012401
17	-0.148895	0.169366	-0.003634	-0.012443
18	-0.148980	0.169457	0.000914	-0.014100
19	-0.149048	0.169524	0.005455	-0.015765
20	-0.149140	0.169626	0.009994	-0.017429
21	-0.149221	0.169712	0.014529	-0.019079
22	-0.149295	0.169788	0.019060	-0.020737
23	-0.149471	0.169981	0.028100	-0.024022
24	-0.149668	0.170173	0.041575	-0.028915
25	-0.148794	0.169249	-0.008178	-0.010776
26	-0.148704	0.169151	-0.012724	-0.009107
27	-0.148634	0.169082	-0.017260	-0.007437
28	-0.148553	0.168996	-0.021794	-0.005768
29	-0.148477	0.168918	-0.026320	-0.004104
30	-0.148304	0.168731	-0.035353	-0.000773
31	-0.148060	0.168475	-0.048809	0.004205
32	-0.149803	0.170323	-0.003630	-0.012434
33	-0.150702	0.171268	-0.003631	-0.012432
34	-0.151620	0.172240	-0.003626	-0.012429
35	-0.152524	0.173191	-0.003627	-0.012423
36	-0.153424	0.174137	-0.003622	-0.012418
37	-0.155240	0.176053	-0.003615	-0.012407
38	-0.157965	0.178927	-0.003605	-0.012390
39	-0.149970	0.170502	0.005453	-0.015760
40	-0.150872	0.171450	0.005454	-0.015754

Tab. 6.22: Calculated condenser stigmator currents depends on mechanical imperfections - part XXII.

6.1. SIMULATION RESULTS

Calc. number	Low. X defl.[A]	Low. Y defl.[A]	Stig. X[A]	Stig. Y[A]
41	-0.151782	0.172411	0.005466	-0.015752
42	-0.152700	0.173383	0.005464	-0.015752
43	-0.153602	0.174332	0.005467	-0.015747
44	-0.155420	0.176250	0.005475	-0.015739
45	-0.158162	0.179150	0.005482	-0.015718
46	-0.150211	0.170757	0.019064	-0.020728
47	-0.151114	0.171707	0.019065	-0.020727
48	-0.152028	0.172673	0.019073	-0.020720
49	-0.152935	0.173629	0.019075	-0.020719
50	-0.153848	0.174592	0.019076	-0.020711
51	-0.155663	0.176506	0.019082	-0.020703
52	-0.158384	0.179373	0.019093	-0.020689
53	-0.158236	0.179389	0.005481	-0.015739
54	-0.159127	0.180320	0.005480	-0.015737
55	-0.160051	0.181303	0.005486	-0.015730
56	-0.160952	0.182249	0.005487	-0.015724
57	-0.161861	0.183208	0.005494	-0.015719
58	-0.163678	0.185126	0.005498	-0.015706
59	-0.166405	0.188002	0.005509	-0.015687
60	-0.158483	0.179647	0.019089	-0.020708
61	-0.159390	0.180603	0.019086	-0.020702
62	-0.160306	0.181572	0.019089	-0.020694
63	-0.161217	0.182534	0.019094	-0.020694
64	-0.162120	0.183484	0.019096	-0.020683
65	-0.163940	0.185404	0.019104	-0.020670
66	-0.166663	0.188275	0.019114	-0.020652
67	-0.000002	0.000003	0.004550	-0.001667
68	0.000001	-0.000002	0.009096	-0.003331
69	0.000007	-0.000011	0.013638	-0.005000
70	0.000003	-0.000005	0.018172	-0.006661
71	0.000000	0.000000	0.022705	-0.008323
72	-0.000001	0.000001	0.031745	-0.011637
73	0.000000	0.000000	0.045223	-0.016576
74	0.000002	-0.000003	-0.002834	-0.026418
75	0.000000	0.000000	0.001705	-0.028076
76	0.000000	0.000000	0.006241	-0.029730
77	-0.000003	0.000005	0.010778	-0.031378
78	0.000000	0.000000	0.015308	-0.033021
79	-0.000001	0.000001	0.024346	-0.036282
80	0.000001	-0.000001	0.037822	-0.041125

Tab. 6.23: Calculated condenser stigmator currents depends on mechanical imperfections - part XXIII.

Calc. number	Low. X defl.[A]	Low. Y defl.[A]	Stig. X[A]	Stig. Y[A]
81	0.000000	0.000000	-0.006496	-0.038706
82	0.000000	0.000000	-0.001963	-0.040357
83	0.000000	0.000000	0.002570	-0.041997
84	0.000000	0.000000	0.007094	-0.043638
85	0.000001	-0.000001	0.011614	-0.045267
86	0.000000	0.000000	0.020640	-0.048504
87	0.000000	0.000000	0.034100	-0.053287
88	0.000000	0.000000	0.000263	0.000088
89	-0.000002	0.000003	-0.002205	-0.016997
90	0.000000	0.000000	-0.000715	-0.021594
91	0.000000	0.000000	0.000768	-0.026180
92	-0.000001	0.000002	0.002250	-0.030765
93	0.000000	0.000000	0.003732	-0.035338
94	0.000000	0.000000	0.006686	-0.044438
95	0.000000	0.000000	0.011088	-0.057982
96	0.000002	-0.000004	-0.005881	-0.029335
97	0.000002	-0.000003	-0.004394	-0.033907
98	0.000004	-0.000006	-0.002902	-0.038472
99	0.000000	0.000000	-0.001417	-0.043022
100	-0.000001	0.000001	0.000063	-0.047564
101	0.000000	0.000000	0.003024	-0.056590
102	0.000000	0.000000	0.007428	-0.069987
103	0.000000	0.000000	-0.009530	-0.041597
104	-0.000001	0.000002	-0.008037	-0.046139
105	-0.000001	0.000002	-0.006546	-0.050668
106	0.000000	0.000000	-0.005060	-0.055174
107	-0.000001	0.000001	-0.003568	-0.059668
108	0.000000	0.000000	-0.000607	-0.068598
109	0.000003	-0.000004	0.003810	-0.081834
110	0.000000	0.000000	0.000263	0.000088
111	0.000000	0.000000	-0.005179	-0.007790
112	0.000000	-0.000001	-0.006663	-0.003176
113	0.000000	0.000000	-0.008150	0.001432
114	-0.000002	0.000002	-0.009638	0.006041
115	-0.000001	0.000001	-0.011113	0.010643
116	0.000002	-0.000004	-0.014072	0.019843
117	-0.000001	0.000001	-0.018484	0.033585
118	0.000000	0.000000	-0.008859	-0.020159
119	-0.000005	0.000008	-0.010350	-0.015565
120	-0.000001	0.000001	-0.011837	-0.010958

Tab. 6.24: Calculated condenser stigmator currents depends on mechanical imperfections - part XXIV.

6.1. SIMULATION RESULTS

Calc. number	Low. X defl.[A]	Low. Y defl.[A]	Stig. X[A]	Stig. Y[A]
121	0.000000	0.000000	-0.013319	-0.006351
122	0.000003	-0.000005	-0.014807	-0.001740
123	0.000002	-0.000003	-0.017768	0.007469
124	0.000000	0.000000	-0.022190	0.021263
125	0.000003	-0.000004	-0.012515	-0.032472
126	0.000002	-0.000003	-0.014008	-0.027897
127	0.000002	-0.000003	-0.015500	-0.023306
128	0.000000	0.000000	-0.016989	-0.018719
129	0.000003	-0.000004	-0.018482	-0.014119
130	0.000003	-0.000004	-0.021450	-0.004916
131	0.000000	0.000000	-0.025886	0.008896
132	0.000001	-0.000002	-0.001708	-0.020280
133	0.000002	-0.000003	0.000273	-0.028148
134	0.000000	0.000000	0.002261	-0.035990
135	-0.000001	0.000002	0.004240	-0.043789
136	-0.000004	0.000005	0.006207	-0.051547
137	0.000002	-0.000002	-0.005381	-0.032601
138	0.000000	0.000000	-0.003392	-0.040426
139	-0.000001	0.000002	-0.001401	-0.048203
140	0.000003	-0.000005	0.000582	-0.055935
141	0.000001	-0.000001	0.002565	-0.063610
142	0.000002	-0.000003	-0.009020	-0.044839
143	0.000002	-0.000003	-0.007022	-0.052594
144	0.000004	-0.000006	-0.005024	-0.060291
145	0.000001	-0.000001	-0.003028	-0.067938
146	-0.000005	0.000007	-0.001041	-0.075516
147	0.000001	-0.000001	-0.012622	-0.056951
148	-0.000001	0.000001	-0.010608	-0.064622
149	0.000000	0.000000	-0.008603	-0.072232
150	0.000000	0.000000	-0.007886	-0.079208
151	-0.000007	0.000011	-0.007619	-0.086468
152	-0.000002	0.000003	-0.016168	-0.068912
153	0.000000	0.000000	-0.014139	-0.076484
154	-0.000007	0.000010	-0.012122	-0.083982
155	-0.000009	0.000012	-0.010095	-0.091407
156	0.000002	-0.000002	-0.008075	-0.098749
157	0.000001	-0.000001	0.001981	-0.007904
158	0.000000	0.000000	0.003963	-0.015798
159	-0.000001	0.000001	0.005945	-0.023680
160	0.000002	-0.000002	0.007918	-0.031531

Tab. 6.25: Calculated condenser stigmator currents depends on mechanical imperfections - part XXV.

Calc. number	Low. X defl.[A]	Low. Y defl.[A]	Stig. X[A]	Stig. Y[A]
161	0.000000	0.000000	0.009886	-0.039355
162	0.000000	0.000000	0.004546	-0.001666
163	-0.000001	0.000001	0.009095	-0.003332
164	-0.000003	0.000005	0.013631	-0.005003
165	-0.000001	0.000001	0.018176	-0.006663
166	-0.000002	0.000003	0.022706	-0.008324
167	-0.000001	0.000002	0.031745	-0.011635
168	0.000002	-0.000003	0.045221	-0.016575
169	0.000000	0.000000	0.000003	0.000002
170	-0.000001	0.000001	-0.000588	-0.016108
171	-0.000002	0.000003	0.002514	-0.019817
172	0.000001	-0.000002	0.005615	-0.023519
173	0.000000	0.000000	0.008710	-0.027217
174	-0.000001	0.000002	0.011805	-0.030900
175	-0.000003	0.000005	0.017967	-0.038249
176	-0.000002	0.000003	0.027155	-0.049181
177	0.000001	-0.000002	-0.004272	-0.028459
178	-0.000001	0.000001	-0.001166	-0.032148
179	0.000000	0.000000	0.001926	-0.035831
180	-0.000002	0.000003	0.005018	-0.039504
181	0.000000	0.000000	0.008113	-0.043168
182	0.000000	0.000000	0.014269	-0.050460
183	0.000002	-0.000002	0.023445	-0.061285
184	0.000001	-0.000002	-0.007924	-0.040728
185	0.000000	0.000000	-0.004830	-0.044394
186	0.000000	0.000000	-0.001734	-0.048056
187	0.000002	-0.000003	0.001356	-0.051697
188	0.000000	0.000000	0.004443	-0.055331
189	0.000001	-0.000002	0.010592	-0.062548
190	0.000000	0.000000	0.019756	-0.073244
191	-0.000002	0.000004	0.001074	-0.013254
192	-0.000002	0.000003	0.001148	-0.012411
193	0.000000	0.000000	0.001078	-0.011567
194	-0.000002	0.000002	0.000858	-0.010747
195	0.000000	0.000000	0.000505	-0.009989
196	0.000003	-0.000005	0.000018	-0.009294
197	0.000002	-0.000003	-0.000572	-0.008700
198	0.000001	-0.000001	-0.001262	-0.008211
199	0.000001	-0.000002	-0.002025	-0.007851
200	0.000001	-0.000002	-0.002845	-0.007631

Tab. 6.26: Calculated condenser stigmator currents depends on mechanical imperfections - part XXVI.

6.1. SIMULATION RESULTS

Calc. number	Low. X defl.[A]	Low. Y defl.[A]	Stig. X[A]	Stig. Y[A]
201	0.000000	0.000000	-0.003683	-0.007555
202	-0.000002	0.000003	-0.004526	-0.007630
203	-0.000001	0.000001	-0.005342	-0.007846
204	0.000000	0.000000	-0.006106	-0.008203
205	0.000000	0.000000	-0.006797	-0.008680
206	-0.000001	0.000001	-0.007394	-0.009278
207	-0.000002	0.000003	-0.007883	-0.009965
208	-0.000002	0.000002	-0.008240	-0.010732
209	0.000000	0.000000	-0.008457	-0.011543
210	0.000000	0.000000	-0.008534	-0.012385
211	-0.000001	0.000002	-0.008462	-0.013222
212	-0.000001	0.000002	-0.008244	-0.014039
213	0.000001	-0.000002	-0.007887	-0.014803
214	0.000001	-0.000001	-0.007405	-0.015493
215	0.000000	0.000000	-0.006812	-0.016089
216	0.000000	0.000000	-0.006123	-0.016577
217	0.000000	0.000000	-0.005359	-0.016935
218	0.000000	0.000000	-0.004545	-0.017156
219	0.000000	0.000000	-0.003701	-0.017231
220	0.000000	0.000000	-0.002861	-0.017163
221	0.000000	0.000000	-0.002045	-0.016944
222	-0.000002	0.000003	-0.001281	-0.016592
223	0.000001	-0.000001	-0.000588	-0.016108
224	0.000002	-0.000003	0.000010	-0.015512
225	0.000001	-0.000002	0.000496	-0.014824
226	-0.000003	0.000004	0.000853	-0.014060
227	0.000000	0.000000	-0.005359	-0.016935
228	0.000000	0.000000	-0.007021	-0.021468
229	0.000000	0.000000	-0.008678	-0.025994
230	0.000001	-0.000002	-0.010335	-0.030511
231	0.000003	-0.000004	-0.011982	-0.035018
232	0.000000	0.000000	-0.015272	-0.043993
233	0.000000	0.000000	-0.020162	-0.057335
234	0.000001	-0.000001	-0.009032	-0.029279
235	0.000000	0.000000	-0.010685	-0.033783
236	0.000000	0.000000	-0.012331	-0.038283
237	0.000000	0.000000	-0.013971	-0.042763
238	0.000002	-0.000003	-0.015610	-0.047231
239	0.000004	-0.000006	-0.018865	-0.056119
240	0.000004	-0.000006	-0.023690	-0.069308

Tab. 6.27: Calculated condenser stigmator currents depends on mechanical imperfections - part XXVII.

Calc. number	Low. X defl.[A]	Low. Y defl.[A]	Stig. X[A]	Stig. Y[A]
241	0.000000	0.000000	-0.012669	-0.041533
242	-0.000004	0.000006	-0.014310	-0.046004
243	-0.000003	0.000004	-0.015942	-0.050459
244	0.000000	0.000001	-0.017568	-0.054897
245	-0.000003	0.000004	-0.019186	-0.059320
246	0.000000	0.000000	-0.022394	-0.068102
247	-0.000001	0.000001	-0.027157	-0.081103
248	-0.000001	0.000001	0.002249	-0.007820
249	-0.000001	0.000002	0.004496	-0.015629
250	0.000002	-0.000003	0.006735	-0.023416
251	-0.000001	0.000002	0.008975	-0.031186
252	0.000000	0.000000	0.011201	-0.038919
253	0.000004	-0.000006	0.005244	-0.020380
254	0.000001	-0.000002	0.007483	-0.028154
255	0.000005	-0.000007	0.009722	-0.035906
256	0.000000	0.000000	0.011943	-0.043609
257	0.000002	-0.000003	0.014162	-0.051273
258	0.000001	-0.000002	-0.007140	-0.016696
259	0.000000	0.000000	0.008228	-0.032879
260	0.000000	0.000000	0.010460	-0.040599
261	0.000002	-0.000002	0.012683	-0.048283
262	0.000002	-0.000003	0.014890	-0.055913
263	0.000000	0.000000	0.017095	-0.063486
264	-0.000005	0.000007	0.011200	-0.045289
265	0.000003	-0.000005	0.013417	-0.052936
266	0.000000	0.000000	0.015624	-0.060530
267	0.000000	0.000000	0.017814	-0.068059
268	-0.000003	0.000005	0.019999	-0.075520
269	-0.000001	0.000002	-0.005456	-0.018190
270	0.000000	0.000000	-0.003538	-0.019371
271	0.000000	0.000000	0.000767	-0.020647
272	-0.000001	0.000001	0.003014	-0.020706
273	0.000004	-0.000006	0.005244	-0.020380
274	0.000000	0.000000	0.009361	-0.018596
275	0.000000	0.000000	0.011129	-0.017197
276	0.000000	0.000000	0.012621	-0.015515
277	0.000000	0.000000	0.013801	-0.013594
278	-0.000002	0.000003	0.014632	-0.011500
279	0.000000	0.000000	0.015084	-0.009296

Tab. 6.28: Calculated condenser stigmator currents depends on mechanical imperfections - part XXVIII.

6.1. SIMULATION RESULTS

Calc. number	RSS stig. cur.[A]	$C_{1,2}[\mu\text{m}]$	$ C_{1,2} [\mu\text{m}]$
1	4.04E-06	0.00 + 0.00 i	0.00
2	1.29E-02	2.14 + 0.64 i	2.23
3	2.58E-02	4.27 + 1.28 i	4.46
4	3.87E-02	6.39 + 1.91 i	6.67
5	6.39E-02	10.57 + 3.15 i	11.03
6	1.29E-02	2.14 + 0.64 i	2.23
7	1.29E-02	2.14 + 0.64 i	2.23
8	1.29E-02	2.14 + 0.64 i	2.23
9	1.29E-02	2.14 + 0.64 i	2.23
10	1.29E-02	2.14 + 0.64 i	2.23
11	2.58E-02	4.27 + 1.28 i	4.46
12	2.58E-02	4.27 + 1.28 i	4.46
13	2.58E-02	4.27 + 1.27 i	4.46
14	2.58E-02	4.27 + 1.27 i	4.46
15	2.58E-02	4.27 + 1.27 i	4.46
16	1.29E-02	2.14 + 0.64 i	2.23
17	1.30E-02	2.15 + 0.63 i	2.24
18	1.41E-02	2.43 - 0.15 i	2.44
19	1.67E-02	2.72 -0.94 i	2.87
20	2.01E-02	3.00 -1.72 i	3.46
21	2.40E-02	3.29 -2.50 i	4.13
22	2.82E-02	3.57 - 3.28 i	4.85
23	3.70E-02	4.14 - 4.84 i	6.37
24	5.06E-02	4.98 - 7.16 i	8.72
25	1.35E-02	1.86 + 1.41 i	2.34
26	1.56E-02	1.57 + 2.20 i	2.70
27	1.88E-02	1.29 + 2.98 i	3.24
28	2.25E-02	1.00 + 3.76 i	3.89
29	2.66E-02	0.71 + 4.54 i	4.60
30	3.54E-02	0.14 + 6.10 i	6.10
31	4.90E-02	-0.71 + 8.42 i	8.45
32	1.30E-02	2.14 + 0.63 i	2.24
33	1.30E-02	2.14 + 0.63 i	2.24
34	1.29E-02	2.14 + 0.63 i	2.23
35	1.29E-02	2.14 + 0.63 i	2.23
36	1.29E-02	2.14 + 0.63 i	2.23
37	1.29E-02	2.14 + 0.63 i	2.23
38	1.29E-02	2.14 + 0.62 i	2.23
39	1.67E-02	2.72 - 0.94 i	2.87
40	1.67E-02	2.72 - 0.94 i	2.87

Tab. 6.29: Calculated condenser stigmator currents depends on mechanical imperfections - part XXIX.

Calc. number	RSS stig. cur. [A]	$C_{1,2}[\mu\text{m}]$	$ C_{1,2} [\mu\text{m}]$
41	1.67E-02	2.72 - 0.94 i	2.87
42	1.67E-02	2.72 - 0.94 i	2.87
43	1.67E-02	2.71 - 0.94 i	2.87
44	1.67E-02	2.71 - 0.94 i	2.87
45	1.66E-02	2.71 - 0.94 i	2.87
46	2.82E-02	3.57 - 3.28 i	4.85
47	2.82E-02	3.57 - 3.28 i	4.85
48	2.82E-02	3.57 - 3.28 i	4.85
49	2.82E-02	3.57 - 3.28 i	4.85
50	2.82E-02	3.57 - 3.29 i	4.85
51	2.82E-02	3.57 - 3.29 i	4.85
52	2.82E-02	3.56 - 3.29 i	4.85
53	1.67E-02	2.71 - 0.94 i	2.87
54	1.67E-02	2.71 - 0.94 i	2.87
55	1.67E-02	2.71 - 0.94 i	2.87
56	1.67E-02	2.71 - 0.94 i	2.87
57	1.67E-02	2.71 - 0.94 i	2.87
58	1.66E-02	2.71 - 0.94 i	2.87
59	1.66E-02	2.70 - 0.95 i	2.86
60	2.82E-02	3.57 - 3.29 i	4.85
61	2.82E-02	3.57 - 3.29 i	4.85
62	2.82E-02	3.56 - 3.29 i	4.85
63	2.82E-02	3.56 - 3.29 i	4.85
64	2.82E-02	3.56 - 3.29 i	4.85
65	2.81E-02	3.56 - 3.29 i	4.85
66	2.81E-02	3.56 - 3.29 i	4.85
67	4.85E-03	0.29 - 0.78 i	0.83
68	9.69E-03	0.57 - 1.57 i	1.67
69	1.45E-02	0.86 - 2.35 i	2.50
70	1.94E-02	1.14 - 3.13 i	3.33
71	2.42E-02	1.43 - 3.91 i	4.17
72	3.38E-02	2.00 - 5.47 i	5.83
73	4.82E-02	2.85 - 7.79 i	8.30
74	2.66E-02	4.56 + 0.49 i	4.58
75	2.81E-02	4.84 - 0.29 i	4.85
76	3.04E-02	5.13 - 1.07 i	5.24
77	3.32E-02	5.41 - 1.85 i	5.72
78	3.64E-02	5.69 - 2.63 i	6.27
79	4.37E-02	6.25 - 4.19 i	7.53
80	5.59E-02	7.08 -6.51 i	9.62

Tab. 6.30: Calculated condenser stigmator currents depends on mechanical imperfections - part XXX.

6.1. SIMULATION RESULTS

Calc. number	RSS stig. cur.[A]	$C_{1,2}[\mu\text{m}]$	$ C_{1,2} [\mu\text{m}]$
81	3.92E-02	6.68 + 1.13 i	6.77
82	4.04E-02	6.96 + 0.35 i	6.97
83	4.21E-02	7.24 -0.43 i	7.25
84	4.42E-02	7.52 - 1.21 i	7.62
85	4.67E-02	7.80 -1.99 i	8.05
86	5.27E-02	8.36 -3.55 i	9.08
87	6.33E-02	9.18 -5.87 i	10.90
88	2.77E-04	-0.02 - 0.05 i	0.05
89	1.71E-02	2.93 + 0.38 i	2.96
90	2.16E-02	3.72 + 0.13 i	3.73
91	2.62E-02	4.51 - 0.13 i	4.52
92	3.08E-02	5.30 -0.38 i	5.32
93	3.55E-02	6.09 -0.64 i	6.13
94	4.49E-02	7.66 - 1.14 i	7.75
95	5.90E-02	10.00 - 1.90 i	10.18
96	2.99E-02	5.06 + 1.02 i	5.16
97	3.42E-02	5.85 + 0.77 i	5.90
98	3.86E-02	6.63 + 0.51 i	6.65
99	4.30E-02	7.42 + 0.25 i	7.42
100	4.76E-02	8.20 + 0.00 i	8.20
101	5.67E-02	9.76 - 0.51 i	9.77
102	7.04E-02	12.07 - 1.27 i	12.13
103	4.27E-02	7.18 + 1.65 i	7.36
104	4.68E-02	7.96 + 1.40 i	8.08
105	5.11E-02	8.74 + 1.14 i	8.81
106	5.54E-02	9.52 + 0.88 i	9.56
107	5.98E-02	10.29 + 0.63 i	10.31
108	6.86E-02	11.83 + 0.12 i	11.83
109	8.19E-02	14.11 - 0.64 i	14.13
110	2.77E-04	-0.02 - 0.05 i	0.05
111	9.35E-03	1.34 + 0.89 i	1.62
112	7.38E-03	0.55 + 1.15 i	1.27
113	8.27E-03	-0.25 + 1.41 i	1.43
114	1.14E-02	- 1.04 + 1.66 i	1.96
115	1.54E-02	-1.83 + 1.91 i	2.65
116	2.43E-02	-3.42 + 2.42 i	4.19
117	3.83E-02	-5.79 + 3.18 i	6.60
118	2.20E-02	3.48 + 1.53 i	3.80
119	1.87E-02	2.69 + 1.79 i	3.23
120	1.61E-02	1.89 + 2.04 i	2.79

Tab. 6.31: Calculated condenser stigmator currents depends on mechanical imperfections - part XXXI.

Calc. number	RSS stig. cur.[A]	$C_{1,2}[\mu\text{m}]$	$ C_{1,2} [\mu\text{m}]$
121	1.48E-02	1.10 + 2.30 i	2.55
122	1.49E-02	0.30 + 2.55 i	2.57
123	1.93E-02	-1.28 + 3.06 i	3.32
124	3.07E-02	-3.66 + 3.82 i	5.29
125	3.48E-02	5.60 + 2.17 i	6.01
126	3.12E-02	4.81 + 2.42 i	5.39
127	2.80E-02	4.02 + 2.68 i	4.83
128	2.53E-02	3.23 + 2.93 i	4.36
129	2.33E-02	2.44 + 3.19 i	4.02
130	2.20E-02	0.85 + 3.70 i	3.80
131	2.74E-02	-1.53 + 4.46 i	4.72
132	2.04E-02	3.50 + 0.30 i	3.51
133	2.81E-02	4.85 - 0.04 i	4.85
134	3.61E-02	6.21 - 0.38 i	6.22
135	4.40E-02	7.55 - 0.72 i	7.58
136	5.19E-02	8.89 - 1.06 i	8.95
137	3.30E-02	5.62 + 0.94 i	5.70
138	4.06E-02	6.97 + 0.59 i	7.00
139	4.82E-02	8.31 + 0.25 i	8.32
140	5.59E-02	9.65 - 0.09 i	9.65
141	6.37E-02	10.97 - 0.43 i	10.98
142	4.57E-02	7.73 + 1.57 i	7.89
143	5.31E-02	9.07 + 1.22 i	9.15
144	6.05E-02	10.40 + 0.88 i	10.44
145	6.80E-02	11.72 + 0.54 i	11.73
146	7.55E-02	13.02 + 0.20 i	13.02
147	5.83E-02	9.82 + 2.19 i	10.06
148	6.55E-02	11.15 + 1.84 i	11.30
149	7.27E-02	12.46 + 1.50 i	12.55
150	7.96E-02	13.66 + 1.38 i	13.73
151	8.68E-02	14.91 + 1.33 i	14.97
152	7.08E-02	11.89 + 2.80 i	12.21
153	7.78E-02	13.19 + 2.45 i	13.42
154	8.49E-02	14.48 + 2.11 i	14.64
155	9.20E-02	15.77 + 1.76 i	15.86
156	9.91E-02	17.03 + 1.41 i	17.09
157	8.15E-03	1.36 - 0.34 i	1.40
158	1.63E-02	2.72 - 0.68 i	2.81
159	2.44E-02	4.08 - 1.02 i	4.21
160	3.25E-02	5.44 - 1.36 i	5.60

Tab. 6.32: Calculated condenser stigmator currents depends on mechanical imperfections - part XXXII.

6.1. SIMULATION RESULTS

Calc. number	RSS stig. cur.[A]	$C_{1,2}[\mu\text{m}]$	$ C_{1,2} [\mu\text{m}]$
161	4.06E-02	6.78 - 1.70 i	6.99
162	4.84E-03	0.29 - 0.78 i	0.83
163	9.69E-03	0.57 - 1.57 i	1.67
164	1.45E-02	0.86 - 2.35 i	2.50
165	1.94E-02	1.15 - 3.13 i	3.34
166	2.42E-02	1.43 - 3.91 i	4.17
167	3.38E-02	2.00 - 5.47 i	5.83
168	4.82E-02	2.85 - 7.79 i	8.30
169	4.04E-06	0.00 + 0.00 i	0.00
170	1.61E-02	2.78 + 0.10 i	2.78
171	2.00E-02	3.42 - 0.43 i	3.44
172	2.42E-02	4.05 - 0.96 i	4.17
173	2.86E-02	4.69 - 1.50 i	4.92
174	3.31E-02	5.33 - 2.03 i	5.70
175	4.23E-02	6.59 - 3.09 i	7.28
176	5.62E-02	8.48 -4.67 i	9.68
177	2.88E-02	4.91 + 0.74 i	4.96
178	3.22E-02	5.54 + 0.21 i	5.55
179	3.59E-02	6.18 - 0.32 i	6.19
180	3.98E-02	6.81 - 0.86 i	6.86
181	4.39E-02	7.44 - 1.39 i	7.57
182	5.24E-02	8.70 - 2.45 i	9.04
183	6.56E-02	10.56 - 4.03 i	11.31
184	4.15E-02	7.03 + 1.38 i	7.16
185	4.47E-02	7.66 + 0.84 i	7.70
186	4.81E-02	8.29 + 0.31 i	8.29
187	5.17E-02	8.91 - 0.22 i	8.92
188	5.55E-02	9.54 - 0.75 i	9.57
189	6.34E-02	10.78 - 1.81 i	10.94
190	7.59E-02	12.63 - 3.39 i	13.07
191	1.33E-02	2.29 -0.18 i	2.29
192	1.25E-02	2.14 - 0.20 i	2.15
193	1.16E-02	1.99 - 0.18 i	2.00
194	1.08E-02	1.85 - 0.15 i	1.86
195	1.00E-02	1.72 - 0.08 i	1.72
196	9.29E-03	1.60 + 0.00 i	1.60
197	8.72E-03	1.50 + 0.10 i	1.50
198	8.31E-03	1.42 + 0.22 i	1.43
199	8.11E-03	1.35 + 0.35 i	1.40
200	8.14E-03	1.32 + 0.49 i	1.41

Tab. 6.33: Calculated condenser stigmator currents depends on mechanical imperfections - part XXXIII.

Calc. number	RSS stig. cur.[A]	$C_{1,2}[\mu\text{m}]$	$ C_{1,2} [\mu\text{m}]$
201	8.40E-03	1.30 + 0.64 i	1.45
202	8.87E-03	1.32 + 0.78 i	1.53
203	9.49E-03	1.35 + 0.92 i	1.64
204	1.02E-02	1.42 + 1.05 i	1.77
205	1.10E-02	1.50 + 1.17 i	1.90
206	1.19E-02	1.60 + 1.28 i	2.05
207	1.27E-02	1.72 + 1.36 i	2.19
208	1.35E-02	1.85 + 1.42 i	2.34
209	1.43E-02	1.99 + 1.46 i	2.47
210	1.50E-02	2.14 + 1.47 i	2.60
211	1.57E-02	2.28 + 1.46 i	2.71
212	1.63E-02	2.42 + 1.42 i	2.81
213	1.68E-02	2.55 + 1.36 i	2.90
214	1.72E-02	2.67 + 1.28 i	2.96
215	1.75E-02	2.78 + 1.18 i	3.02
216	1.77E-02	2.86 + 1.06 i	3.05
217	1.78E-02	2.92 + 0.93 i	3.07
218	1.77E-02	2.96 + 0.79 i	3.06
219	1.76E-02	2.97 + 0.64 i	3.04
220	1.74E-02	2.96 + 0.50 i	3.00
221	1.71E-02	2.92 + 0.36 i	2.94
222	1.66E-02	2.86 + 0.22 i	2.87
223	1.61E-02	2.78 + 0.10 i	2.78
224	1.55E-02	2.68 + 0.00 i	2.68
225	1.48E-02	2.56 -0.08 i	2.56
226	1.41E-02	2.42 - 0.14 i	2.43
227	1.78E-02	2.92 + 0.93 i	3.07
228	2.26E-02	3.70 + 1.22 i	3.90
229	2.74E-02	4.48 + 1.50 i	4.73
230	3.22E-02	5.26 + 1.79 i	5.56
231	3.70E-02	6.04 + 2.07 i	6.39
232	4.66E-02	7.59 + 2.64 i	8.04
233	6.08E-02	9.89 + 3.49 i	10.49
234	3.06E-02	5.05 + 1.56 i	5.29
235	3.54E-02	5.83 + 1.85 i	6.11
236	4.02E-02	6.60 + 2.13 i	6.94
237	4.50E-02	7.38 + 2.42 i	7.76
238	4.97E-02	8.15 + 2.70 i	8.58
239	5.92E-02	9.68 + 3.27 i	10.22
240	7.32E-02	11.96 + 4.10 i	12.64

Tab. 6.34: Calculated condenser stigmator currents depends on mechanical imperfections - part XXXIV.

6.1. SIMULATION RESULTS

Calc. number	RSS stig. cur.[A]	$C_{1,2}[\mu\text{m}]$	$ C_{1,2} [\mu\text{m}]$
241	4.34E-02	7.17 + 2.19 i	7.49
242	4.82E-02	7.94 + 2.48 i	8.31
243	5.29E-02	8.70 + 2.76 i	9.13
244	5.76E-02	9.47 + 3.04 i	9.95
245	6.23E-02	10.23 + 3.32 i	10.76
246	7.17E-02	11.75 + 3.88 i	12.37
247	8.55E-02	13.99 + 4.70 i	14.76
248	8.14E-03	1.35 -0.39 i	1.40
249	1.63E-02	2.69 - 0.77 i	2.80
250	2.44E-02	4.04 - 1.16 i	4.20
251	3.25E-02	5.38 - 1.54 i	5.59
252	4.05E-02	6.71 - 1.92 i	6.98
253	2.10E-02	3.51 - 0.90 i	3.63
254	2.91E-02	4.85 - 1.28 i	5.02
255	3.72E-02	6.19 - 1.67 i	6.41
256	4.52E-02	7.52 - 2.05 i	7.79
257	5.32E-02	8.84 -2.43 i	9.17
258	1.82E-02	2.88 + 1.23 i	3.13
259	3.39E-02	5.67 - 1.41 i	5.84
260	4.19E-02	7.00 - 1.79 i	7.23
261	4.99E-02	8.32 - 2.18 i	8.60
262	5.79E-02	9.64 - 2.56 i	9.97
263	6.57E-02	10.94 - 2.93 i	11.33
264	4.67E-02	7.81 - 1.92 i	8.04
265	5.46E-02	9.13 - 2.30 i	9.41
266	6.25E-02	10.43 - 2.68 i	10.77
267	7.04E-02	11.73 - 3.06 i	12.12
268	7.81E-02	13.02 - 3.43 i	13.46
269	1.90E-02	3.14 + 0.94 i	3.28
270	1.97E-02	3.34 + 0.61 i	3.40
271	2.07E-02	3.56 - 0.13 i	3.56
272	2.09E-02	3.57 - 0.52 i	3.61
273	2.10E-02	3.51 -0.90 i	3.63
274	2.08E-02	3.20 - 1.61 i	3.59
275	2.05E-02	2.96 - 1.92 i	3.53
276	2.00E-02	2.67 - 2.17 i	3.44
277	1.94E-02	2.34 - 2.38 i	3.34
278	1.86E-02	1.98 - 2.52 i	3.21
279	1.77E-02	1.60 - 2.60 i	3.05

Tab. 6.35: Calculated condenser stigmator currents depends on mechanical imperfections - part XXXV.

Chapter 7

Appendix II

7.1. Measured data

Following tables contain data of measured mechanical imperfections of 26 prototype pole pieces and the result of the measurement of the stigmators current in TEM. Meaning of tables columns is:

- **Serial number** - order number of pole piece
- **Circularity A** - representative circularity of Region A
- **Circularity D** - representative circularity of Region D
- **Circularity C** - representative circularity of Region C
- **Perpendicularity AC** - perpendicularity of Region C measured with datum axis of Region A
- **Concentricity AC** - concentricity of regions C measured with datum axis of Region A
- **2-fold astig.** - 2-fold astigmatism expressed as current of the stigmators

7.1. MEASURED DATA

Serial number of pole piece	Circularity A [μm]	Circularity D [μm]	Circularity C [μm]
1	1.70	1.16	5.70
2	2.10	1.27	2.10
3	2.20	1.26	17.10
4	1.90	0.88	24.30
5	2.70	1.28	13.00
6	2.00	1.30	18.30
7	1.30	1.28	29.20
8	1.20	1.27	10.90
9	1.20	1.28	2.70
10	1.70	1.81	10.20
11	1.10	2.45	8.30
12	1.50	1.80	10.00
13	1.60	0.35	13.50
14	1.80	0.65	33.80
15	1.90	0.75	3.60
16	0.92	0.41	0.99
17	0.82	0.52	4.59
18	0.64	1.01	2.87
19	0.79	0.91	1.45
20	0.87	2.09	3.89
21	0.55	3.03	0.36
22	0.87	0.32	5.44
23	0.91	0.32	1.42
24	0.74	0.33	2.67
25	0.70	2.35	17.54
26	1.90	0.75	7.90

Tab. 7.1: Measured mechanical imperfections of prototype pole pieces.

Serial number of pole piece	Perpendicularity AC [μm]	Concentricity AC [μm]	2-fold astig. [mA]
1	9.20	27.60	70
2	5.50	6.90	14
3	7.00	15.50	65
4	18.30	44.60	115
5	7.00	27.10	57
6	13.00	47.50	206
7	27.30	61.70	102
8	6.20	18.20	83
9	3.90	9.50	76
10	3.90	6.80	81
11	8.30	0.50	30
12	10.00	0.30	30
13	1.00	13.00	94
14	0.50	8.90	52
15	0.30	9.50	14
16	0.99	0.99	24
17	4.59	4.59	14
18	2.87	2.87	94
19	1.45	1.45	30
20	3.89	3.89	25
21	0.36	0.36	22
22	5.44	5.44	27
23	1.42	1.42	9
24	2.67	2.67	14
25	17.54	17.54	30
26	7.90	2.90	24

Tab. 7.2: Measured condenser stigmator currents and mechanical imperfections of prototypes pole pieces.